Basel 2015

June 4–6, 2015 · Congress Center Basel

Swiss Congress of Radiology
Schweizerischer Radiologiekongress
Congrès Suisse de Radiologie

ONLINE ABSTRACT BOOK

of the Swiss Congress of Radiology

www.radiologiekongress.ch

TABLE OF CONTENTS

Dear Delegates and Visitors of the Swiss Congress of Radiology 2015, Dear Colleagues!

The Swiss Society of Radiology (SGR-SSR) and the Swiss Society of Nuclear Medicine (SGNM-SSMN) are delighted about the high quality and the great amount of abstracts which were submitted for presentation at the annual Swiss Congress of Radiology. The continuous excellent work of all authors is highly appreciated as it makes the congress a very prestigious scientific meeting.

This **"Online Abstract Book of the Swiss Congress of Radiology"** is the 5th issue which is solely published online. It represents a cost efficient, durable and platform independent documentation of scientific abstracts, integration of the abstract data into both the Society's and Congress' web page as well as permanent accessibility all over the world.

The **"Online Abstract Book of the Swiss Congress of Radiology"** will permanently be accessible on both the Society's and Congress' web page at **www.sgr-ssr.ch** and **www.radiologiekongress.ch**. It includes all the abstracts of the scientific talks and posters presented at the annual Swiss Congress of Radiology in Basel.

Proper citation of scientific abstracts is however important, especially in case of online-only web publications. The Swiss Society of Radiology thereof recommends the use of the following structure to cite abstracts from the new **"Online Abstract Book of the Swiss Congress of Radiology"**:

"Author1 A, Author2 B, ..., Author last X. Title of the abstract (abstr.).
Swiss Congress of Radiology 2015, Basel. Online Abstract Book, www.radiologiekongress.ch"

We look forward to welcoming you to the Swiss Congress of Radiology 2015 in Basel.

PD Dr. G. ANDREISEK, MBA
Member Scientific Committee SGR-SSR

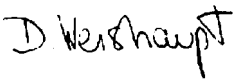

Prof. Dr. D. WEISHAUPT
President Scientific Committee SGR-SSR

SWISS CONGRESS OF RADIOLOGY 2015, BASEL

Congress President

E. Merkle, Basel

SGR-SSR Executive Board

PRESIDENT
T. Jung, Zurich

PAST PRESIDENT
S. Duewell, Frauenfeld

SECRETARY
U. Wolfensberger, Horgen

TREASURER
T. Roeren, Aarau

ASSESSORS
H. Alkadhi, Zurich
C. Becker, Geneva
C. H. Benoit, Zurich
H. M. Hoogewoud, Fribourg
R. Kubik, Baden
D. Weishaupt, Zurich

SGR-SSR Scientific Committee

PRESIDENT
D. Weishaupt, Zurich

MEMBERS
G. Andreisek, Zurich
M. Anooshiravani-Dumont, Geneva
M. Becker, Geneva
G. Bongartz, Basel
J. Bremerich, Basel
K. O. Loevblad, Geneva
R. Meuli, Lausanne
P. A. Poletti, Geneva
S. Schmidt, Lausanne
H. Thoeny, Bern

REPRESENTATIVE SGPR-SSRP
G. Eich, Aarau

REPRESENTATIVE SSVIR
S. D. Qanadli, Lausanne

SGR-SSR Office

SGR-SSR Secretariat
Christoph Lüssi
Moosstrasse 2
3073 Gümligen
Switzerland
Phone +41 31 301 22 55
Fax +41 31 952 76 83
E-Mail info@sgr-ssr.ch
Website www.sgr-ssr.ch

Congress Management

c/o Education Congress Research GmbH
Wolfgang Duchek/Patricia Leeb/Angelika Schwingshackl
Neutorgasse 9
1010 Vienna
Austria
Phone +43 1 5350599
Fax +43 1 5334064448
E-Mail info@radiologiekongress.ch
Website www.radiologiekongress.ch

Abstract Reviewing Panel SGR-SSR

G. Andreisek, Zurich
L. Alamo, Lausanne
M. Anooshiravani-Dumont, Geneva
M. Becker, Geneva
G. Bongartz, Basel
J. Bremerich, Basel
K. O. Loevblad, Geneva
R. Meuli, Lausanne
P. A. Poletti, Geneva
S. D. Qanadli, Lausanne
S. Schmidt, Lausanne
J. Schneider, Basel
H. Thoeny, Bern
D. Weishaupt, Zurich

Abstract Reviewing Panel SGNM-SSMN

F. Forrer, Basel
L. Giovanella, Bellinzona
P. Kaufmann, Zurich
P. Koch, Zurich
T. Krause, Bern
E. Nitzsche, Baden
J. Prior, Lausanne
O. Ratib, Geneva
R. Schibli, Villigen
K. Strobel, Lucerne
D. Wild, Basel
M. Wissmeyer, Geneva

Poster Jury

P. Bize, Lausanne
A. Cornelius, Aarau
Z. Szücs, Biel
N. Farshad, Zurich
J. Hohmann, Basel
L. Kara, Zurich
S. Leschka, St. Gallen
A. Platon, Geneva
S. Terraz, Geneva
R. Wolf, Bern

SS101

MR-based attenuation correction for cardiac FDG-PET on a hybrid PET/MR scanner: Comparison with standard CT attenuation correction

J. Vontobel, R. Liga, M. Possner, O.F. Clerc, F. Mikulicic, P. Veit-Haibach, E. ter Voert, T. A. Fuchs, R. Buechel, P. A. Kaufmann; Zurich/CH

Purpose: The aim of this study was to evaluate the feasibility of attenuation correction (AC) for cardiac FDG-PET using MR-based attenuation maps.
Methods and Materials: We included 23 Patients with no known cardiac history undergoing whole-body FDG PET/CT imaging for oncologic indications on a PET/CT scanner using time-of-flight (TOF) and subsequent whole-body PET/MR imaging on an investigational hybrid PET/MR scanner Data sets from PET/MR (with and without TOF) were reconstructed using MR AC and semi-quantitative segmental (20 segment model) myocardial tracer uptake (percent of maximum) was compared to PET/CT which was reconstructed using CT AC and served as standard of reference.
Results: Excellent correlations were found for regional uptake values between PET/CT and PET/MR with TOF (n=460 segments in 23 patients; r=0.913; p<0.0001) with narrow Bland-Altman limits of agreement (-8.5% to +12.6%). Correlation coefficients were slightly lower between PET/CT and PET/MR without TOF (n=460 segments in 23 patients; r=0.851; p<0.0001) with broader Bland-Altman limits of agreement (-12.5% to +15.0%). PET/MR with and without TOF showed minimal underestimation of tracer uptake (-2.08% and -1.29% respectively), compared to PET/CT.
Conclusion: Relative myocardial FDG uptake obtained from MR-based AC FDG-PET is highly comparable to standard CT-based attenuation corrected FDG-PET, suggesting interchangeability of both AC techniques.

SS102

Hybrid PET/MRI: An algorithm to reduce metal artifacts from dental implants on dixon-based attenuation correction maps using a MAVRIC sequence

I. A. Burger, M. Wurnig, A. Becker, D. Kenkel, G. Delso, P. Veit-Haibach, A. Boss; Zurich/CH

Purpose: It was the aim of this study to implement an algorithm, directly modifying a Dixon-based magnetic resonance imaging (MRI) dataset acquired for attenuation correction in hybrid PET/MRI with a Multi-Acquisition Variable Resonance Image Combination (MAVRIC) sequence to reduce metal artifacts.
Methods and Materials: A cohort of eight patients referred for a clinically indicated oncology examination were scanned within a tri-modality PET/CT-MR setup. MAVRIC and Dixon sequences were automatically co-registrated and a newly developed correction algorithm was applied to generate µMaps from the Dixon only dataset using the MAVRIC sequence to reduce the signal void artefact. With histogram analysis the mean values for noise, fat and water were determined for each scan. These values served to determine the thresholds to determine the attenuation value for each voxel. The artefact sizes were measured on and compared between uncorrected Dixon-based and MAVRIC-corrected µMaps.
Results: The algorithm could be successfully applied in all patients with a short computing time for the algorithm of 78±5 seconds. There was a significant reduction in mean artifact size of 70.5% between uncorrected and corrected µMaps from 697±589 mm2 to 202±119 mm2 (p=0.016).
Conclusion: We showed that a semi-automatic algorithm can be used to correct Dixon based µMaps using a MAVRIC sequence with a substantial reduction of the artifact size.

SS103

Non-contrast-enhanced perfusion imaging of the lung using Fourier Decomposition Magnetic Resonance Imaging (FD MRI): Assessment of feasibility in patients with COPD in correlation with Single Photon Emission Computed Tomography/Computed Tomography

G. Sommer, M. Wiese, G. Nicolas, D. Lardinois, J. Bremerich, O. Bieri, G. Bauman; Basel/CH

Purpose: To evaluate the clinical feasibility and diagnostic capabilitiy of Fourier Decomposition MRI [Bauman G et al., Radiology 2011] combined with ultra-fast bSSFP (ufSSFP) [Bieri O, MRM 2014] for assessment of regional lung perfusion in patients with COPD.
Methods and Materials: This pilot study was performed in four patients (2 female, 2 male, age 53-69y) with COPD (±lung cancer) and markedly reduced pulmonary function (FEV1<80%) who underwent perfusion scintigraphy and SPECT/CT of the lung with 99mTc-MAA for clinical indications. Examinations were performed at 1.5T using 2D coronal and sagittal ufSSFP-acquisitions during free breathing (TE/TR=0.6/1.4ms, FA=65°, slice thickness=12mm, FOV=(450mm)2, matrix=1282, parallel imaging factor 2). Total acquisition time was 10min. SPECT/CT images of the chest acquired within a narrow time frame to MRI (0-7 days) were available for comparison. Image interpretation included assessment of image quality and a comparison of findings in MRI and SPECT/CT.
Results: The ufSSFP-based FD MRI sequence provided good image quality in all patients. There was good visual correlation between the distribution patterns of lung perfusion observed on the FD MRI perfusion weighted maps and 99mTc-MAA SPECT/CT. Limitations of the FD MRI technique, however, are seen in the lung regions adjacent to the heart and mediastinum due to artifacts from cardiac pulsation.
Conclusion: The combination of FD MRI and ufSSFP represents a promising technique for non-contrast-enhanced assessment of lung perfusion at 1.5T even in patients with rarefied lung parenchyma such as in COPD. The quantitative potential of this method for estimating the likely postoperative pulmonary reserve in comparison with SPECT/CT remains to be investigated.

SS104

Evaluation of DWI-derived measures of perfusion and tissue microstructure in hepatic metastases from neuroendocrine tumors before and 48 hours after metabolic therapy with 90Y-DOTATOC

B. Stieltjes, O. C. Maas, T. Haas, J. Bremerich, D. Wild, G. Sommer; Basel/CH

Purpose: To evaluate if DWI-derived quantitative parameters show a distinct pattern of response in hepatic metastases from neuroendocrine tumors (NETs) treated with 90Y-DOTATOC, 48h after therapy initialization.
Methods and Materials: Thirty-four hepatic metastases were evaluated in 13 patients with NETs of gastrointestinal or pancreatic origin. MRI was performed before (t0) and 48h after initialization of therapy (t1). MRI included a multi-b-value DWI-sequence; perfusion- and microstructural parameters (f and D respectively) were extracted from the complete tumor volume and their change from t0 to t1 was quantified. Furthermore, total tumor volume was measured and compared between the two time-points.
Results: Group comparisons did not reveal a significant difference in f and D from t0 to t1 (f=9.8 vs 10.0%, D=0.98 vs 1.11*10-3mm2/s). However, 14/34 lesions showed a clear increase and 17/34 showed a clear decrease (>30%) in f. Only 8/34 showed a significant change in D (decrease in 2, increase in 6 lesions). Only three lesions did not show any significant change from t0 to t1. Volumetrically, as expected, none of the lesions showed a significant change within this time-frame.
Conclusion: In this initial evaluation, two distinct responses to therapy, either a large increase or decrease in perfusion fraction f, were noted in the majority of the NET lesions (92%). In our ongoing prospective longitudinal study, we will utilize long term measures of therapy response including RECIST, volumetric-, and SPECT assessment to further our understanding of these changes and to evaluate the potential clinical impact of DWI in terms of early response monitoring.

SS105

Whole-body diffusion imaging applying simultaneous multi-slice excitation: Initial experience and feasibility

D. Kenkel[1], M. Wurnig[1], L. Filli[1], E. J. Ulbrich[1], T. Beck[2], V. M. Runge[1], A. Boss[1]; [1]Zurich/CH, [2]Erlangen/DE

Purpose: The aim of this study was to perform a fast protocol for whole-body diffusion weighted imaging (WB-DWI) with nearly identical image quality compared to a conventional WB-DWI protocol with a significant reduction of the measurement time by using a slice accelerated multiband echo-planar sequence.
Methods and Materials: A WB-DWI was optimized and tested using a single-shot echo-planar imaging sequence capable of simultaneous slice excitation and acquisition, and compared to a conventional WB-DWI protocol serving as the reference standard for WB-DWI on a 3T MR scanner. Eight healthy volunteers and one oncologic patient were included in the study. Quantitative analysis was carried out by calculating the apparent diffusion coefficient (ADC) and the coefficient of variation (CV) in different organs. We assessed the image quality by two independent radiologists with a 4-point Likert scale.
Results: The scan time of the WB-DWI measurement was reduced by up to 36% with the multiband protocol. Both protocols showed comparable image quality and no statistically significant differences in the reader scores. Further, there were no significant differences of the ADC values of the examined organs, except of the ADC values of brain tissue, which were slightly higher in the multiband protocol.
Conclusion: With our study we demonstrated that multiband DWI sequences can be applied to WB-DWI protocols with the potential to greatly reduce the required measurement time, which is substantially increasing clinical applicability.

SS106

Iodine concentration as a perfusion marker in oncology: Elucidation and correlation using volume perfusion CT

W. Thaiss[1], U. Haberland[3], K. Nikolaou[1], M. Horger[1], A. Sauter[3]; [1]Tübingen/DE, [2]Forchheim/DE, [3]Basel/CH

Purpose: To objectify the value of iodine concentration (IC), derived from computed tomography acquired with a tube voltage of 80 kVp, as a surrogate for tumor perfusion in HCC and lymphoma by comparing iodine-related attenuation with Volume Perfusion CT (VPCT) parameters.
Methods and Materials: VPCT parameters of 30 HCC and 30 lymphoma lesions were correlated with tumoral IC at 5 time points after the aortic peak enhancement (APE).
Results: The following parameters were acquired for HCC: blood flow (BF) 52.7 ± 17.0 mL/100 mL/min, blood volume (BV) 12.6 ± 4.3 mL/100 mL, arterial liver perfusion (ALP) 44.4 ± 12.8 mL/100mL/min. Lesion IC 7 sec after APE was 133.4 ± 57.3 mg/100 mL.
Lymphoma showed a BF of 36.8 ± 13.4 mL/100 mL/min, BV of 8.8 ± 2.8 mL/100 mL, flow extraction product (Ktrans) of 24.7 ± 8.4 mL/100 mL/min and IC of 118.2 ± 64.5 mg/ 100 mL 3.5 sec after APE.
Of all investigated time points, strongest correlations exist for BF and ALP with IC in HCC 7 sec after APE (r = 0.71 and r = 0.84) and 3.5 sec after APE in lymphoma lesions (r = 0.77).
Conclusion: We identified a substantial, time-dependent agreement between VPCT-derived flow values and iodine concentrations in HCC and lymphoma. Thus, CT-derived iodine concentrations 7 sec after APE in HCC and 3.5 sec in lymphoma may now be used as surrogate markers for perfusion.

SS107

The additional value of SPECT/CT in the assessment of necrotic bone fragments in patients with non-union after traumatic fractures

U . Bhure[1], H. S. Grünig[2], A. Zander[2] , J. Mühlebach[2], M. Pérez Lago[2], H.-R. Zenklusen[2], K. Strobel[2]; [1]Mumbai/IN, [2]Lucerne/CH

Purpose: To evaluate the additional value of SPECT/CT in the assessment of necrotic bone fragments in patients with non-union after traumatic fractures of the extremities.
Methods and Materials: Planar scintigraphy and SPECT/CT images were performed in 21 patients (9 female, 12 male, mean age 5,14 years, range 25-75 years) with suspicion for necrotic bone fragments in non healing fractures of the extremities (12 femur, 5 tibia, 3 humerus, 1 radius). Planar images (PI) and SPECT/CT images were compared regarding the presence of necrotic fragments. Necrotic fragments were diagnosed in bone areas with missing radionuclide uptake. Operation with histological reference standard was –so far- available in 7 patients and sufficient clinical follow up without operation in 6 patients.
Results: Necrotic fragments were diagnosed with PI in 6 of 21 patients (29%) and with SPECT/CT in 11 (52%) patients. Mean size of necrotic fragments was 4 cm (range 1-10 cm). Sensitivity and specificity for the diagnosis of necrotic fragments was 50% / 71% with PI and 100%/71% for SPECT/CT.
Conclusion: SPECT/CT is a valuable tool and more sensitive than planar imaging regarding the diagnosis of necrotic fragments in in patients with non-union after traumatic fractures of the extremities.

SS108

The additional value of intraarticular contrast in SPECT/CT of the knee and ankle

H. S. Grünig[2], U. Bhure[1], A. Zander[2], U. Müller[2], M. Pérez Lago[2], K. Strobel[2]; [1]Mumbai/IN, [2]Lucerne/CH

Purpose: To evaluate the additional value of intraarticular contrast (SPECT/CT arthrography) in painful ankle and knee joints.
Methods and Materials: Arthrography was performed under fluoroscopic guidance followed by SPECT/CT in 11 knee and 13 ankle joints in 22 patients (mean age 36 years, range 16-72 years). Additional findings obtained by the intraarticular contrast were evaluated.
Results: SPECT/CT arthrography was feasible without complications in all patients. SPECT/CT showed active lesions in 22 (92%) joints. In 20 joints (83%) additional lesions were diagnosed, owed to the use of intraarticular contrast: 19 cartilage lesions and 4 intraarticular loose bodies.
Conclusion: Intraarticular application of contrast prior to SPECT/CT (so called SPECT/CT arthrography) is feasible and detects a significant number of cartilage lesions and loose bodies in painful ankle and knee joints.

SS109

The value of SPECT/CT in carpal boss

U. Bhure[1], A. Zander[2], U. Hug[2], H. S. Grünig[2], M. D. S. Perez Lago[2], K. Strobel[2]; [1]Mumbai/IN, [2]Lucerne/CH

Purpose: To assess the value of SPECT/CT in carpal boss.
Methods and Materials: In 24 wrists with carpal boss (CB) (18 right sided, 6 left sided) of 21 patients planar and SPECT/CT images were performed. 3 patients had bilateral CB. Grade of uptake (0=no, 1=low, 2=moderate, 3=high) on planar images (PI) and SPECT/CT was assessed and compared with CT findings and clinical symptoms. Clinical follow-up was available in 17 patients.
Results: CB affected CMC II joint in 4 wrists, CMC III in 12 and both joints in 3 wrists. 12 CB (50%) were active on planar images, 18 (75%) on SPECT/CT. Of 17 symptomatic CB 10 (59%) were active, 7 were inactive on planar images and 14 (82%) were active (mean grade 1,9; range 1-3) and 3 were inactive on SPECT/CT. Of 7 asymptomatic CB 2 were active and 5 were inactive on planar images; 4 were active (mean grade 1,25; range 1-2) and 3 were inactive on SPECT/CT. CT alone showed CB in all patients and an accessory ossicle (os styloideum) in 8 wrists. MR imaging was available in 7 patients and positive for CB in 5 (71% sensitivity). X-rays were available in 17 patients and positive in 10 (59%). in 8 patients infiltration of CB with corticosteroids was performed and CB resection in 4 patients.
Conclusion: SPECT/CT provides important morphologic and metabolic information for the evaluation of carpal boss.

SS110

Quantitative shear wave ultrasound elastography of the supraspinatus muscle in relation to tendon integrity and muscle quality

A. Rosskopf, C. Ehrmann, F. M. Buck, C. Gerber, C. W. A. Pfirrmann; Zurich/CH

Purpose: To evaluate the reliability of ultrasound elastography in the supraspinatus (SSP) muscle, define normal shear wave velocity (SWV) values, and assess muscle stiffness in symptomatic patients with correlation to tendon integrity and muscle quality.
Methods and Materials: SSP-SWV was prospectively assessed in 22 asymptomatic volunteers (mean age 53.8 years; 11 female) by two independent examiners using Virtual Touch Tissue Imaging Quantification(VTIQ; Siemens) for evaluation of test-retest and inter-examiner reliability. Forty-four patients (mean age 51.9 years; 22 female) were prospectively included: SWV in the SSP muscle was assessed using VTIQ and compared to tendon integrity, tendon retraction, fatty muscle infiltration, and muscle volume atrophy on MR images of the same day.
Results: Test-retest-reliability for total mean shear wave velocity (MTSWV) was good for Examiner 1(ICC=0.70;0.30-0.87) and 2(ICC=0.80;0.53-0.92). Inter-examiner-reliability was excellent(ICC=0.89;0.64-0.96).MTSWV in asymptomatic volunteers(3.0m/sec±0.5) was higher than in patients(2.5m/sec±0.5;p=0.001). A significant difference in MTSWV was found in muscles with partial tendon tears compared to full thickness tears(p=0.042). A significant difference between MTSWV and degree of tendon retraction(p=0.047) was found. Fatty infiltration:Goutallier 0=43.2%(2.7 m/sec±0.4),I=20.5%(2.5m/sec±0.4),II=13.6%(2.4m/sec±0.4),III=15.9%(2.2m/sec±0.5),IV=6.8% (2.4m/sec±0.3). A negative correlation was found for MTSWV (r=-0.39/p=0.008) and a positive Tangent sign (n=10).
Conclusion: VTIQ is a reproducible technique for assessment of the SSP muscle stiffness. Normal SSP-SWV is 3.0±0.5m/sec. In patients the SWV decreases with increasing fat content of the SSP muscle (Goutallier 0-III).

SS111

Quantification of early fatty infiltration of the rotator cuff muscles: Comparison of multi-echo dixon with single-voxel MR spectroscopy

C. Agten, A. Rosskopf, C. Gerber, C. W. A. Pfirrmann; Zurich/CH

Purpose: To evaluate quantification of early infiltration in the supraspinatus muscle with magnetic resonance (MR) imaging using a T2*-corrected multi-echo 3D gradient echo Dixon-based sequence (multi-echo Dixon) in comparison to a Proton-MR-spectroscopy.
Methods and Materials: This study was approved by our local ethics committee and informed consent was obtained. Fifty patients and 10 healthy volunteers with good supraspinatus muscle quality on 1.5T MR imaging were included. Fat percentage (FP) in the supraspinatus muscle was quantified using a multi-echo Dixon compared to single-voxel MR spectroscopy as reference standard. In 18 subjects the multi-echo Dixon was repeated to assess test-retest reliability. Measurements based on multi-echo Dixon were performed by two independent readers by placing region-of-interests in the supraspinatus muscle corresponding to the MR-spectroscopy voxel. Intraclass correlation coefficients (ICC) were used for statistical analysis.
Results: In the 18 subjects for test-retest analysis, mean FP (±standard deviation) were 3.3±1.1 and 3.2±1.1 for reader 1, 3.4±1.6 and 3.3±1.3 for reader 2 (first and second multi-echo Dixon), and 2.9±1.4 for MR-spectroscopy. Test-retest reliability was substantial for reader 1 (ICC=0.757) and almost perfect for reader 2 (ICC=0.873). Inter-reader reliability for multi-echo was almost perfect (ICC=0.893, P<.0005). Mean FP in all 60 subjects with multi-echo Dixon was 3.5±1.6 for reader 1, 3.7±1.8 for reader 2, and 2.8±1.4 with MR spectroscopy. Correlation between multi-echo Dixon and MR spectroscopy was good (ICC =0.645, P<.0005).
Conclusion: The multi-echo Dixon sequence is a reliable method and comparable to MR-spectroscopy for quantification of low levels of fatty infiltration in the supraspinatus muscle.

SS112

Simultaneous multi-slice echo planar imaging with blipped CAIPIRINHA: A promising technique for accelerated diffusion tensor imaging of skeletal muscle

L. Filli, M. Piccirelli, D. Kenkel, R. Guggenberger, G. Andreisek, V. M. Runge, A. Boss; Zurich/CH

Purpose: To investigate the feasibility of accelerated diffusion tensor imaging (DTI) of skeletal muscle using simultaneous multi-slice echo planar imaging (EPI) with blipped "Controlled Aliasing in Parallel Imaging Results in Higher Acceleration" (CAIPIRINHA) unaliasing.
Methods and Materials: After institutional review board approval, the lower leg muscles of eight healthy volunteers (mean age and SD, 29.4±2.9 years) were examined in a clinical 3.0T MR scanner (Skyra, Siemens) using a 16-channel knee coil. EPI was performed at a b-value of 500 s/mm2 without slice acceleration (conventional DTI) as well as with two- and three-fold acceleration. Fractional anisotropy (FA) and mean diffusivity (MD) were measured in all three acquisitions. Fiber tracking performance was compared between the acquisitions regarding number of tracks, average track length, and anatomical precision using multivariate ANOVA and Mann-Whitney-U tests.
Results: Acquisition time was 7:24min for conventional DTI, 3:53min for two-fold and 2:38min for three-fold acceleration. Overall FA and MD values ranged from 0.220-0.378 and 1.595-1.829 mm2/s, respectively. Two-fold acceleration yielded similar FA and MD values (p≥0.901) and fiber tracking performance compared with conventional DTI. Three-fold acceleration resulted in comparable MD (p=0.199) but higher FA values (p=0.006) and significantly impaired fiber tracking in the soleus and tibialis anterior muscles (number of tracks, p<0.001; anatomical precision, p≤0.005).
Conclusion: Simultaneous multi-slice EPI with blipped CAIPIRINHA can remarkably reduce acquisition time in DTI of skeletal muscle with similar image quality and quantification accuracy of diffusion parameters. This may increase the clinical applicability of muscle DTI.

SS113

MR imaging of the temporomandibular joint at 7.0 Tesla: A feasibility study using novel high permittivity dielectric pads

A. Manoliu, G. Spinner, M. Wyss, S. Erni, D. Ettlin, D. Nanz, E. J. Ulbrich, L. M. Gallo, G. Andreisek; Zurich/CH

Purpose: MR imaging of the temporomandibular joint (TMJ) at 7.0T using a clinically feasible setting has not been shown before. Purpose was to quantitatively and qualitatively evaluate the use of high-permittivity dielectric pads for enabling clinical MR imaging of the TMJ at 7.0T.
Methods and Materials: IRB approved study with written informed consent. 10 volunteers were imaged at 7.0 T (Achieva, Philips) using a commercially available 32-channel head coil with and without high-permittivity dielectric pads containing barium titanate in deuterated suspension. Imaging protocol consisted of coronar and oblique sagittal PDw-TSE sequences. For quantitative evaluation, voxel-wise B1-maps and signal-to-noise-ratio-maps (SNR) were calculated using Matlab routines (Natick, USA). Manual segmentation was performed to extract the corresponding SNR-values according to the anatomical location of the TMJ. For qualitative evaluation, MR images were assessed by two readers in consensus for image quality and visibility of relevant anatomical structures using 5-point-Lickert-scales. Assessments performed with and without pads were compared using t-tests.
Results: The quantitative analysis showed significantly higher B1+ and SNR for the scans performed with dielectric pads compared to those without pads (p<0.05). The qualitative analysis showed significantly better image quality and better visibility of the articular disc as well as for the surrounding anatomic structures when using the dielectric pads (p<0.05, corrected for multiple comparisons). In particular, in most volunteers, many anatomic structures were not visible without pads.
Conclusion: The application of high-permittivity dielectric pads improves the B1+ field and the SNR and consecutively enables clinical MR imaging of the TMJ at 7.0T.

SS114

Whole-body diffusion tensor imaging (DTI)

D. Kenkel[1], J. von Spiczak[1], M. Wurnig[1], L. Filli[1], G. Steidle[2], M. Wyss[1], A. Boss[1]; [1]Zurich/CH, [2]Tübingen/DE

Purpose: The aim of this study was to show the technical feasibility of whole-body DTI and report initial experiences.

Methods and Materials: A whole-body DTI protocol was implemented on a 3 T whole-body MR scanner, and whole-body DTI acquisitions were performed on 12 healthy individuals. A region-of-interest (RoI) analysis was used to compute mean values and standard deviations of mean diffusivity (MD) and the principal diffusivities (Eigenvalues λ_{1-3} of the diffusion tensor) in different organs/body regions. Image quality was assessed by two independent radiologists on a 4-point Likert scale (1 (excellent depiction of organs), 2 (good depiction), 3 (fair depiction), 4 (poor depiction)) and ICC was calculated.

Results: Mean scan time was 79.2 minutes. Parametrical maps of DTI parameters could be obtained for all subjects with a good to fair image quality (MD Reader 1 (R1): 2.7±0.5 Reader 2 (R2): 2.5±0.5, λ_1 R1:2.7±0.5 R2:2.6±0.5,λ_2 R1: 2.5±0.5 R2: 2.5±0.5, λ_3 R1:2.6±0.5 R2:2.7±0.5). Interreader agreement regarding the image quality of the parametrical maps was substantial to almost perfect (ICC of MD: 0.83, λ_1: 0.91, λ_2:0.79, λ_3: 0.91). There was no significant difference concerning the reader (P=0.16) and the type of parametrical map (P=0.82). In the RoI analysis mean MD as well as the principle diffusivities in the examined organs were consistent with previously performed studies, which focused on single organs.

Conclusion: Whole body DTI is a feasible examination, and for instance might be used as an ol for the assessment of changes in muscle microstructure in systemic myopathies.

SS115

Usefulness of multi acquisition variable resonance image combination (MAVRIC) and slice phase encoding for metal artifact correction (SEMAC) in different implant materials

N. A. Farshad-Amacker, L. Jud, L. Filli, R. Lüchinger, D. Nanz, S. Kozerke, V. Runge, G. Andreisek; Zurich/CH

Purpose: To evaluate the usefulness of MAVRIC and SEMAC for MR imaging of various orthopedic implant materials.

Methods and Materials: Prospective study on three samples (identical rods with artificial notches and grooves) made from different orthopedic implant materials: stainless steel, cobalt-chromium-molybdenum and titanium. Samples were inserted into a phantom filled with barium-sulfate solution and placed into a clinical 3.0T scanner (Achieva, Philips). Standard T1-weighted, T2-weighted, and PD-weighted fast spin-echo (FSE) sequences were performed without, as well as with MAVRIC or SEMAC at different parameter settings ("weak", "moderate", and "strong" artifact suppression). MAVRIC and SEMAC were vendor-specific "Work-in-Progress (WIP)" software packages. Two blinded readers independently measured the artifact diameters at three predefined locations. Artifacts between the different sequences and techniques were compared using t-test ($p<0.05$ indicated statistical significance). Intraclass-Correlation-Coefficients (ICC) were calculated for interreader agreement.

Results: ICCs were 0.72-0.98. Stainless steel caused the greatest artifacts, followed by cobalt-chromium-molybdenum, and titanium, regardless to the applied sequence and imaging technique. MAVRIC significantly reduced the artifacts of stainless steel (p=0.03), but there was no incremental improvement from "weak" towards the "strong" parameter settings (p=0.27). SEMAC reduced steel artifacts, but only when the "strong" parameter settings were used (p=0.03). Both, MAVRIC and SEMAC showed inconsistent artifact modifications in cobalt-chromium-molybdenum and titanium.

Conclusion: MAVRIC and SEMAC with appropriate parameter settings reduced artifacts from stainless steel, but their application in cobalt-chromium-molybdenum and titanium showed no benefit.

SS116

Gouty arthritis: Effect of dual-energy CT on diagnostic thinking and therapeutic decision making

T. Finkenstaedt, I.-A. Manoliu, M. Toniolo, T. Frauenfelder, G. Andreisek, B. Michel, K. Higashigaito, R. Guggenberger, H. Alkadhi; Zurich/CH

Purpose: To determine the effect of dual-energy computed tomography (DECT) on diagnostic thinking and therapeutic decision making in patients with known or suspected gout.

Methods and Materials: This IRB approved retrospective study included 43 patients (9 female, mean age 61.1±12.2 years) with known (n=20) or suspected (n=23) gout showing periarticular soft tissue deposits who underwent DECT (80/140kVp) with two material decomposition of the extremities (n=53), hip (n=1), and spine (n=1). Two readers blinded to clinical data independently evaluated DECT images for presence of urate crystal deposits. Clinical diagnosis, suspected location of urate crystal deposits, diagnostic thinking, and therapeutic decisions were noted before and after DECT by another, blinded physician.

Results: Interreader agreement for detection of soft tissue and urate crystal deposits with DECT were excellent (κ=1.0 and 0.94, respectively). 26/43 patients (60%) with periarticular soft tissue deposits were positive for urate according to DECT. After DECT, the clinical diagnosis of gouty arthritis was revoked in 17 of 43 (40%) patients, whereas the diagnosis was maintained in 16/43 (37%) patients. In 4/43 (9%) patients DECT revealed urate deposits at another, clinically not suspected location, and in 6/43 (14%) patients at the clinically suspected plus additional location. In 23/43 (53%) of patients, a change in treatment resulted after DECT. Changes in diagnostic thinking occurred more frequently in patients with suspected gout ($p<0.001$), whereas changes in therapeutic decision making were more frequent in patients with known gout (p=0.014).

Conclusion: In patients with known or suspected gout, DECT has a remarkable effect on diagnostic thinking and therapeutic decision making.

SS117

C-arm flat panel CT arthrography of the shoulder

R. Guggenberger, E. J. Ulbrich, T. Dietrich, T. Pfammatter, H. Alkadhi, G. Andreisek; Zurich/CH

Purpose: To assess diagnostic performance and radiation dose of flexible C-arm flat panel CT (FPCT) arthrography of the shoulder using MR arthrography as standard of reference.

Methods and Materials: IRB approved study. Informed consent provided 30 patients referred for MR arthrography underwent either standard (5s) or prototypic (20s) C-arm FPCT arthrography of the shoulder. Fluoroscopic guided contrast injection and volume tomography was performed in an angiographic C-arm FPCT unit and followed immediately by MR imaging at 1.5 T. On FPCT acquisitions image quality, artifacts and depiction quality of joint tissues were quantitatively and qualitatively rated and findings compared to MR imaging by two blinded radiologists. Radiation dose was assessed using Rando-Alderson phantoms and thermoluminescence dosimetry.

Results: Kappa values for interreader agreements of qualitative ratings ranged between 0.65-0.87. Image quality and artifacts were significantly lower, depiction quality of joint bone, cartilage and labrum higher in 20s FPCT compared to 5s FPCT acquisitions ($p<0.05$ each).

Soft tissue was equally poor depicted in both acquisitions (p=0.67). FPCT and MR imaging findings were highly concordant for joint bone, cartilage or labral pathologies while poor for rotator cuff disease. Effective radiation dose was significantly lower in 5s FPCT (0.6 mSv) compared to MDCT (1.7 mSv) and 20s FPCT (6.2 mSv) acquisitions ($p<0.01$).

Conclusion: C-arm FPCT arthrography of the soulder is feasible with good diagnostic performance for joint bone, cartilage and labral disease but poor for rotator cuff pathologies compared to MR arthrography. Radiation dose for 5s FPCT protocol is inferior to a standard MDCT scan protocol.

SS118

Upright CT of the knee: The effect of weight-bearing on joint alignment

A. Hirschmann[1], F. M. Buck[2], S. F. Fucentese[2], C. W. Pfirrmann[2]; [1]Basel/CH, [2]Zurich/CH

Purpose: To prospectively compare patellofemoral and femorotibial alignment in supine non weight-bearing (NWBCT) and upright weight-bearing CT (WBCT) and assess the differences in joint alignment.

Methods and Materials: NWBCT and WBCT scans of the knee were obtained in 26 patients (mean age, 57.0 ± 15.9 years; range, 21-81) using MDCT for NWBCT and cone-beam extremity-CT for WBCT. Two musculoskeletal radiologists independently quantified joint alignment by measuring femorotibial rotation, tibial tuberosity-trochlear groove distance (TTTG), lateral patellar tilt angle, lateral patellar shift, medial and lateral femorotibial joint space widths. Significant differences between NWBCT and WBCT were sought using Wilcoxon signed-rank test (P-value <0.05).

Results: Significant differences were found for femorotibial rotation (femorotibial rotation changed from NWBCT mean 2.7° ± 5.1 (reader 1) / 2.6° ± 5.6 (reader 2) external rotation to WBCT 0.4° ± 7.7/0.2° ± 7.5 internal rotation; P=0.009/P=0.004), TTTG (decrease from NWBCT (13.8mm ±5.1/13.9mm ±3.9) to WBCT (10.5 mm ± 5.0/10.9 mm ± 5.2; P=0.008/P=0.002), lateral patellar tilt angle (decrease from NWBCT (15.6° ± 6.7/16.9° ± 7.4) to WBCT (12.5° ± 7.7/15.0° ± 6.2; P=0.011/P=0.188). The medial femorotibial joint space decreased from NWBCT (3.9mm ±1.4/4.5mm ±1.3) to WBCT (2.9 mm ± 2.2/3.5 mm ± 2.2; P=0.003/P=0.004). Interreader agreement ranged from 0.52-0.97.

Conclusion: Knee joint alignment changes significantly in the upright weight-bearing position using CT when compared to supine non weight-bearing CT.

SS119

Treatment of distal anterior cerebral artery aneurysms using minimally porous endoluminal devices

D. W. Zumofen[1], E. Nossek[2], C. Stippich[1]; [1]Basel/CH, [2]New York/US

Purpose: Coil-embolization of wide-neck aneurysms often requires adjunct devices such as balloons- or stents. However, the use of adjunct devices is limited in the distal ACA due to the small diameter of the parent artery.
Methods and Materials: We have treated four unruptured distal ACA aneurysms by endoluminal reconstruction using the PED.
Results: Three aneurysms were of saccular configuration, and were judged inappropriate for classic surgical or endovascular strategies based on their geometry. The fourth was of fusiform shape, and had previously aborted clip reconstruction. The mean diameter of the ACA immediately distal to the AcomA was 2.6mm (1.7-3.7mm). The diameter tapered to 1.9mm (0.9-2.6mm) distal to the take-off of the pericallosal artery. A single PED was the sole treatment in three cases. Two telescoped PEDs were used in the fourth case. There were no new neurological deficits or radiographic evidence of ischemia. There was no artery occlusion of either of the parent vessel or of the associated branch vessel, which was covered in all cases. One patient showed immediate complete aneurysm occlusion confirmed on 3-month follow-up MRA. Two patients showed significant angiographic reduction of intra-aneurysmal flow immediately following PED deployment, resulting in complete angiographic aneurysm occlusion at 1year. The remaining patient showed immediate intra-aneurysmal contrast-stasis following PED deployment. This patient has not reached yet his fist angiographic follow-up interval.
Conclusion: Endoluminal reconstruction is a safe and effective treatment alternative for a carefully selected subset of distal ACA aneurysms. We advocate that the current generation of PED can be safely deployed in vessel smaller than 2mm.

SS120

A 12 year experience in standardised presurgical fMRI

A. Tyndall, J. Reinhardt, L. Mariani, C. Stippich; Basel/CH

Purpose: The long-term feasibility, robustness, artifacts, technical and patient dependent limitations of standardised presurgical fMRI were assessed in a cohort of 491 patients scheduled for tumor or epilepsy surgery overseeing 12 years and different MR-scanner platforms at 1.5T and 3.0T.
Methods and Materials: Success rates of task performance and BOLD-activation were determined for motor and somatosensory somatotopic mapping, language localisation and lateralisation. Prerequisites for imaging success, problems and failures were systematically analysed. Data from different MR-scanners were compared.
Results: Of 2346 attempted paradigms (1031 motor, 1220 speech, 95 somatosensory), 2316 (98.7%) were successfully performed. 100 paradigms (4.3%) were repetition runs. In technically failed cases, 23 were speech, 6 motor and 2 sensory paradigms. Most relevant causes of procedural failure for motor paradigms were non-compliance and technical issues. For speech paradigms, most failures were noted in overt paradigms. Pre-scan patient training, direct monitoring for correct task performance and immediate repetition runs helped reduce drop outs. Average significant BOLD-activation was higher for motor than language paradigms (95.8% vs. 81.6%). Almost all speech paradigms showed significantly better activation rates for all areas at 3T compared to 1.5T, which was not the case for motor paradigms.
Conclusion: Standardised presurgical fMRI of motor, somatosensory and language function proved to be very robust in routine neuroimaging across different MR-scanner platforms of 1.5T and 3.0T. Speech paradigms performed less well in terms of compliance and significant BOLD-activation, and benefitted most from higher magnetic fields and repetition runs.

SS121

Localisation and timing of auditory activity demonstrated by fMRI / MEG co-registration

J. Reinhardt[1], J. Benner[1], M. Wengenroth[2], C. Stippich[1], P. Schneider[2], M. Blatow[1]; [1]Basel/CH, [2]Heidelberg/DE

Purpose: It is generally assumed that human auditory cortex (AC) follows the core-belt-parabelt organization found in non-human primates. We hypothesized that investigation of individual structure-function relationships may lead a way to achieve spatial and temporal segregation of human auditory regions.
Methods and Materials: Therefore we used fMRI with passive auditory stimulation in musicians (n=23) and conducted region-of-interest (ROI)-based analyses of functional activations rendered onto 3D-surface reconstructions of AC in individual subjects. BOLD activations were consistently identified in four distinct ROIs within AC, namely: medial Heschl's Gyrus (HG), posterior-lateral HG, anterior-lateral HG and Planum Temporale (PT). Next, we used MEG with a passive listening protocol analogous to the fMRI experiment. We employed a combined fit-seeding model with co-registration of fMRI and MEG data and analysed onset latencies of auditory responses at the locations of every ROI.
Results: Response onsets were measured at ~20 ms in medial HG, at ~30 ms in posterior-lateral HG, and at ~60 ms in anterior-lateral HG and PT.
Conclusion: Our results show that auditory information processing goes first along the medio-lateral (core-belt) axis of HG and then follows anterior-posterior (belt-parabelt) axis to PT and anterior HG, which reflects precisely the prediction from non-human studies.

SS122

Estimating the impact of brain tumors on the structural connectome by lesion simulation in healthy subjects

E. H. J. Nijhuis, A. Bink, C. Stippich; Basel/CH

Purpose: Estimating the loss in structural connectivity following brain lesions, such as tumors, is technically difficult due the absence of measurements prior to the infliction. Here we use a lesion simulation approach on brain tumors to estimate and display topographically the loss of long distance white matter connectivity on the neocortical surface.
Methods and Materials: Non-malignant and malignant primary intraaxial brain neoplasms from twenty patients were segmented semi-automatically using contrast enhanced T1 images with the FSL and ITKsnap software packages. The brain tumors were then mapped within 50 extensively imaged subjects from the human connectome project. The differences in neocortical network connectivity with and without lesion were estimated using graph theoretical measures and displayed topographically with heat maps on the neocortical surface.
Results: The surface maps resulting from the lesion simulation provide a complimentary assessment on how a particular tumor affects the overall network connectivity within a patient. Areas with higher connectivity decrease are visualized with a warmer contrast on the overlapping heat map. Typically displayed is the loss of intra- as well as interhemispheric connectivity.
Conclusion: Our initial results show that lesion simulation techniques could provide a useful tool for retrospective and prospective clinical connectivity research in brain tumors. As for this method only minimal patient imaging data is required, its benefits can be further explored with existing clinical magnetic resonance imaging data and protocols.

SS123

Age, gender and emotion: A fMRI-study of emotional picture processing

V. Romer[1], T. Flaisch[2], M. Imhof[2], P. Lipfert[1], H. Schupp[2], B. Ibach[1], K.-U. Wentz[1]; [1]Münsterlingen/CH, [2]Konstanz/DE

Purpose: Emotional cues guide selective attention. Specifically, viewing pleasant and unpleasant as compared to neutral pictures is associated with increased brain activity in extra-striate visual cortical Regions, as well as limbic core structures such as the amygdala. Previous research largely relied on studying younger participants. However, ample evidence has demonstrated age-related modulations for numerous psychological processes.
Methods and Materials: Using functional magnetic resonance imaging the present study explored the neural processing of emotional images in younger and older participants. Towards this end, participants passively viewed pictures of varying emotional content. Pleasant picture categories included erotic scenes and images of elderly romantic couples. Unpleasant picture categories were comprised by scenes of death and sickness and inter-personal violence and physical injury, respectively. The neutral control condition was comprised by images of people in neutral everyday situations.
Results: Across all participants, preliminary analysis confirmed emotionally increased activation in large cortical and sub-cortical networks, including extra-striate visual cortex and amygdala. Region-of-interest analyses of the bilateral amygdala revealed selectively diminished responding of older participants to the unpleasant violence and injury picture category. Likewise, men showed greater activations to erotica than women. In extra-striate visual areas, older participants responded less to erotica, as well as violence scenes, but this was limited to right hemispheric regions. Men and women responded similarly to all categories in these areas.
Conclusion: These preliminary results show that emotion processing is modulated both by age, as well as gender and argue for controlling these factors in neuroscientific studies of emotion.

SS124

Advances in neuroimaging – GRASP sequence at 1.5 T and 3.0 T

A. Bink, T. Schubert, T. Heye, C. Stippich; Basel/CH

Purpose: Report on imaging advantages with the new Golden-angle RAdial Sparse Parallel MRI sequence (GRASP) at 1.5 T and 3.0 T in patients with intracranial, head and neck diseases.
Methods and Materials: The GRASP sequence was implemented on 4 MR scanners (Prisma, Skyra, Verio and Espree, Siemens Medical Solutions, Erlangen, Germany). Sequence parameters: TR/TE 4.42/2.13 msec, flip angle 12.0 degrees, slice thickness 2 mm, image matrix 256 x 256 mm, voxel size 2.0 x 1.1 x 1.1 mm, receiver bandwidth 400 Hz/voxel, 6/8 slice partial Fourier, temporal resolution 2.3 s, TA 4:02 min. Contrastenhanced GRASP was acquired in patients with suspicion of tumors and vascular pathologies. Two neuroradiologists analysed and compared the GRASP to T1w post contrast with respect to delineation of pathologies and artifacts in each patient.
Results: 22 patients were examined with the GRASP. No pathology was observed in 8 patients. 14 patients had the following reports: meningeoma (3x), arteriovenous malformation (1x), aneurysm (1x), pituitary adenoma (1x); pleomorphic adenoma (3x), glomus jugulare paraganglioma (2x), cavernous hemangioma (2x), squamous cell carcinoma (1x). With GRASP arrival of contrast media and distribution over time was well visible with additional high regional resolution. All pathologies could be evaluated in detail. Pulsation artefacts were not observed. Image quality was still good when the patient moved.
Conclusion: With the GRASP sequence all pathologies were identified in detail. Not only high temporal but also high spatial resolution was provided. Even when motion artifacts appeared diagnostic images could be acquired with the GRASP technique.

SS125

Hematocrit and serum hemoglobine do not influence CT perfusion maps in patients with acute ischemic stroke.

G. M. Karwacki[1], M. Benz[1], S. Ulmer[2]; [1]Basel/CH, [2]Zurich/CH

Purpose: CT-Perfusion (CTP) is ubiquitous and used in diversified patient groups (geographically as well as concerning health status). For CTP changes of attenuation of brain over time are measured. To the best of our knowledge there have been no investigations of influence of serum hemoglobin and hematocrit values (which affect attenuation values of blood) on the results of CTP which could potentially affect further therapeutic procedures.
Methods and Materials: CTP were performed at our local ED in patients suspected for suffering from acute ischemic stroke. In total 45 patients (median age 69±13 years, range 40 - 94 years; 24 women,
21 men fulfilled the inclusion criteria: 21 suffered from stroke whereas 24 did not, leading to 69 unaffected hemispheres as proven by follow-up MRI.
Results: There was no significant difference in hemoglobine values between controls and patients suffering from ischemia. There was no significant difference in attenuation values of arterial blood between controls and patients suffering from ischemia. There was a statistically significant correlation between hemoglobin and hematocrit values and attenuation values in the ICA or MCA of the CT. However, there was no statistically significant correlation between CBV or CBF values and attenuation values of the vessels in the CT.
Conclusion: Conditions affecting hematocrit and hemoglobin values (such as dehydration, anaemia, extracranial haemorrhage, myeloproliferative disorders, high altitude training, COPD etc.) do not influence CBV values obtained with CTP. There is no need for hematocrit/hemoglobin adjusted CBV thresholds for defining penumbra and infarct core in stroke patients as well in other clinical CTP applications.

SS126

Prognostic accuracy of CT-Perfusion in acute ischemic stroke compared to 24h MRI and outcome after 3 months

A. E. T. von Hessling, R. Meyer, C. Stippich; Basel/CH

Purpose: To validate our routine CT-Perfusion protocol for its prognostic value for predicted infarct size and clinical outcome after 3 months (mRS) in patients with acute ischemic stroke.
Methods and Materials: CT-Perfusion measurements were acquired immediately after admission of patients for suspected stroke according to our standard protocol. The data of 145 patients were evaluated with the "Neuro Perfusion" Software by Siemens and the suggested thresholds by the vendor. The predicted volumes of infarct core and penumbra were compared with the infarct volume determined by DWI in the routine MRI within 24h and with the mRS at 3 months after symptom onset.
Results: We found a positive correlation of 0.98 between predicted infarct size and grouped modified Ranking Scores (mRS 0, 1-2 and 3-6). The correlation of predicted penumbra to mRS was 0.9, with a better outcome associated with smaller penumbra volumes. In 78% of cases, the infarct core was overestimated by CTP compared to the 24h DWI.
Conclusion: CTP helps in identifying defective perfusion of brain territories in acute ischemic stroke patients, but CTP overestimates the extent of infarct. This should be taken into consideration for treatment decision.

SS127

Comparison of a 32-channel head coil and a 2-channel surface coil for *MR imaging of the temporomandibular joint at 3.0 Tesla*

A. Manoliu, G. Spinner, M. Wyss, S. Erni, D. Ettlin, D. Nanz, E. J. Ulbrich, L. M. Gallo, G. Andreisek; Zurich/CH

Purpose: Surface coils are still standard for imaging the temporomandibular joint (TMJ), but commercially available head coils would be much more user-friendly. Purpose was to quantitatively and qualitatively compare a 32-channel head coil and a standard 2-channel surface coil for MR-imaging of the TMJ at 3.0T.

Methods and Materials: IRB approved study with written informed consent. A spherical phantom and 22 asymptomatic volunteers underwent high-resolution MR-imaging of the TMJ at 3.0T (Ingenia 3.0T, Philips) using a 32-channel head coil (SENSE Head coil 32-elements, Philips) and a 2-channel surface coil (SENSE FlexS, Philips). Imaging protocol included sagittal and coronal fast spin echo sequences. For quantitative analysis, pixel-by-pixel signal-to-noise-ratio (SNR) maps of the phantom were calculated using Matlab routines (Natick, USA). For qualitative analysis, images were evaluated by two independent readers using 5-point Likert scales. Both coils were compared using t-tests.

Results: The quantitative analysis showed significantly higher SNR for the head coil compared to the surface coil (surface coil: mean±SD, 57.18±12.79; head coil: 102.97±17.03; $p<0.001$). For the Qualitative analysis, inter-rater reliability ranged from "substantial" to "almost perfect" (Kappa, 0.804-0.965). Compared to the surface coil, the head coil showed significantly better visibility of anatomical structures of the TMJ, including the temporomandibular disk, bilaminar zone, mandibular fossa, mandibular condyle and pterygoid muscle and better overall image quality ($p<0.05$, corrected for multiple comparisons).

Conclusion: Quantitative and qualitative data show higher SNR and increased visibility of anatomical structures using the 32-channel head coil compared to a standard 2-channel surface coil.

SS128

Non-invasive assessment of fibrosis and inflammation in the whole kidney of CKD patients by diffusion-weighed magnetic resonance imaging with readout-segmented EPI

I. Friedli, L. A. Crowe, L. Berchtold, S. Moll, K. Hadaya, C. Vesin, T. de Perrot, P. Y. Martin, S. de Seigneux, J.-P. Vallee; Geneva/CH

Purpose: Renal fibrosis in chronic kidney disease (CKD) is highly predictive of its evolution. Whole kidney fibrosis and inflammation were non-invasively assessed with readout-segmented diffusion-weighted MRI (RESOLVE[1]) in CKD. An internal validation study was performed using biopsy gold standard.

Methods and Materials: 27 transplanted CKD patients (54±14 years) scheduled for a renal biopsy were scanned at 3T with respiratory-synchronized RESOLVE: 10 b-values (0-900s/mm^2), TR/TE=2600/68ms, resolution=2*2*5mm^3, 6 slices, GRAPPA=3, readout segments=5. Cortex and medulla ROIs were placed after image fusion between diffusion and T1 anatomical reference. Apparent Diffusion Coefficient (ADC [mm^2/s]) was calculated using MATLAB®. A new predictor index, ΔADC was defined as the difference of mean cortical and medullary ADC. This was compared to fibrosis from biopsy using Pearson's correlation. Internal validation used non-parametric Wilcoxon/Bootstrap comparing thresholds (10-80%).

Results: Excellent correlation was found in patients comparing ΔADC to fibrosis (R^2=0.70,p<0.001) and moderate correlation ΔADC to inflammation (R^2=0.32,p=0.002). Moderate correlation was seen for cortical ADC with fibrosis (R^2=0.37), but no significant correlation for medulla with fibrosis (R^2=0.20), nor cortex and medulla with inflammation (R^2=0.024, R^2=0.016). Negative ΔADC value was observed for all patients with > 40% fibrosis. Non-parametric Wilcoxon (1000 bootstraps) confirmed the threshold of 40% fibrosis as the lowest possible detection level with accuracy 0.94 (specificity 100%, sensitivity 90%).

Conclusion: The ΔADC improves fibrosis evaluation in renal transplant patients. A negative ΔADC was found in all patients with more than 40% of fibrosis suggesting the use of this index as predictor for renal fibrosis, confirmed by internal validation.

[1]Porter, Heidemann;Magn.Reson.Med.;2009;62:468-75.

SS129

In-phase/ opposed phase MR analysis of regenerating liver upon common and extensive partial hepatectomy in C57Bl/6 mice

C. Eberhardt, M. Wurnig, A. Wirsching, M. Lesurtel, A. Boss; Zurich/CH

Purpose: Partial hepatectomy (PH) is often the only surgical treatment to cure patients with liver tumors. Although PH is an established clinical procedure, many patients develop postoperative, often fatal complications such as post-hepatectomy liver failure (PLF) in case of extensive liver resection beyond 70% of liver parenchyma. PLF is usually attributed to an inadequate quantity or quality of the remnant liver, termed small-for-size syndrome (SFSS). We strive to provide early discriminators for SFSS and developing PLF using in-phase/ opposed phase MRI for liver fat quantification on a well-established mouse model of common (70% PH) and extensive partial hepatectomy (86% PH), the latter representing the animal model for SFSS.

Methods and Materials: Anesthetized mice (n=14) were measured in a 4.7T small animal MR imager with an ip/op- FLASH imaging sequence (TE=2.2 ms resp. 2.9 ms/ TR= 200 ms, 8 averages) before surgery, then on day 1,2,3,5 and 7 post hepatectomy. The fat quantification was performed with a custom written Matlab script.

Results: The obtained values for the liver fat content were determined to be specific discriminators between the two study groups: 4.33% ± 1.76% for 70% PH and 11.86% ± 6.52% for the 86% PH mice (P<0.05) on day 2 post hepatectomy.

Conclusion: Our results using ip/op MR techniques for water and fat imaging indicate a distinctive time course of lipid accumulation and metabolism within the comparative study groups. This feature of SFSS can be used to evaluate the prospect of liver recovery and is prone to be applicable also in clinical MRI measurements.

SS130

Gd-EOB-DTPA-enhanced liver MRI for prediction of liver growth after portal vein occlusion

B. Barth, M. Fischer, C. S. Reiner; Zurich/CH

Purpose: To evaluate the use of Gd-EOB-DTPA-enhanced magnetic resonance imaging (MRI)-derived fat- and liver function-measurements for prediction of liver growth after portal vein occlusion (PVO) in patients scheduled for major liver resection.

Methods and Materials: Forty-five patients (age 59±13.9y) who underwent Gd-EOB-DTPA-enhanced liver MRI within 24.5±18 days prior to PVO were included in this study. Fat-Signal-Fraction (FSF) and relative liver enhancement (RLE) of the future liver remnant (FLR) were calculated from in- and out-of-phase (n=42) as-well-as from unenhanced T1-weighted, and hepatocyte-phase images (n=35), respectively. Outcome parameters were the degree of hypertrophy (DH) and kinetic growth rate (KGR, volume increase/day) of the FLR post-PVO. Receiver operating characteristics analysis was computed to identify cutoff values for predicting liver growth.

Results: FSF showed significant inverse correlation with DH and KGR of the FLR (r=-0.462 and -0.375, p<0.05), whereas no significant correlation was found for RLE with DH and KGR. Patients with steatosis (FSF>10%; n=12) showed significantly lower DH than those without steatosis (FSF≤10%;n=30, 2.7% vs. 12.6%, p<0.05). FSF was significantly lower in patients with DH>5% (n=28) than with DH≤5% (n=14, 0.021 vs. 0.166, p<0.05). With a cutoff-FSF of 0.4 patients with DH>5% were identified with 100% (28/28;95%CI;98-100%) sensitivity and 100% negative predictive value (3/3;95%CI;83-100%).

Conclusion: Liver fat-content, but not liver function derived from Gd-EOB-DTPA-enhanced MRI is a predictor of liver growth after PVO. Thus, liver MRI could help in identifying patients at risk for insufficient liver growth, which could lead to re-evaluation of the therapeutic strategy.

SS131

Age dependent liver fat quantification on DIXON MR sequences in a healthy population with normal BMI

E. J. Ulbrich[1], M. Fischer[1], I.-A. Manoliu[1], M. Marcon[2], D. Nanz[1], C. S. Reiner[1]; [1]Zurich/CH, [2]Udine/IT

Purpose: To calculate reference standards of age- and sex-dependent normative values of liver fat in healthy volunteers with normal BMI in magnetic resonance imaging.

Methods and Materials: We selected 80 healthy volunteers (40 men, 40 women) with normal BMI (18.5 to 26 kg/m^2) between 20 and 60 years (10 men/10 women per decade). Quantitative magnetic resonance (qMR) imaging was performed in all study participants at 3.0 T (Achieva Philips) by using a multiecho 2-point DIXON (mDIXON) imaging sequence (repetition time msec/echo time msec, 4.2/1.2, 3.1). Mean dual-echo fat-signal fractions (FSF) of the liver were determined in 5 different liver segments (Segment II, III, VI, VII, VIII) from signal intensities of the ROIs (regions of interest) on fat- and water-only images. ANOVA was performed to test FSF differences among age subgroups corrected for BMI (p<0.05, corrected for multiple comparisons). Pearson correlation analysis was performed for several body measurements.

Results: The mean FSF (%) ± standard deviation for women/men in the different age subgroups was: 3.05 ± 0.81/3.9 ± 0.89 (20-29), 3.75 ± 1.10/4.99 ± 1.93 (30-39), 4.75 ± 1.42/5.25 ± 2.39 (40-49) and 4.09 ± 1.36/4.74 ± 1.76 (50-60).

The FSF differences among age subgroups were significant for women in two of 5 different liver segments after correction for multiple comparisons (p-values < 0.01), but was not significant for men for all segments.

Conclusion: The liver fat fraction increased with age with a peak in the fifth decade for both genders and decreased again thereafter. Men had a higher fat fraction than women in all age groups.

SS132

GRASP for dynamic contrast enhanced liver MRI in routine patients under shallow and heavy breathing

C. Zähringer, T. Block, T. Heye, G. Bongartz, C. J. Zech; Basel/CH

Purpose: To test the feasibility and technical performance of a novel free-breathing T1w 3D-sequence for dynamic liver imaging.
Methods and Materials: This study has been approved by the local ethic committee. 27 patients, which were scheduled for liver MRI due to clinical reasons, were examined with a Golden-angle RAdial Sparse Parallel (GRASP) T1w sequence with a retrospective freely selectable temporal resolution during injection of 0.025 µmol gadoxetic acid in shallow free breathing over a period of 4 minutes. Additionally the same sequence was acquired in the hepato-biliary phase 15 minutes post injection and compared to a standard T1w-3D-GRE sequence acquired directly afterwards. Two readers evaluated the image quality in consensus on a 5-point-scale (contour sharpness and visibility of small structures).
Results: All examinations provided diagnostic image quality. Despite free-breathing of the patients the overall image quality of the dynamic phase was very good with a score of 1.5. Lesion delineation and liver edge sharpness were 1.7 and 2.5, respectively. The quality of an optimal arterial and porto-venous phase was also good with scores of 2.0 and 2.1 in the best matching temporal frames, respectively. The direct comparison between the free-breathing GRASP and the standard T1w breath-hold sequence in the hepato-biliary phase yielded better image quality for the GRASP in 11 cases, similar in 7 cases and worse in 6 cases.
Conclusion: With this new sequence free-breathing dynamic liver MRI examinations are feasible with good image quality. This may overcome current limitations of abdominal MRI in patients unable to hold their breath.

SS133

Perfusion computed tomography for detection of hepatocellular carcinoma in patients with liver cirrhosis

M. A. Fischer[1], N. Kartalis[2], A. Grigoriadis[2], L. Loizou[2], P. Stål[2], B. Leidner[2], P. Aspelin[2], T. B. Brismar[2]; [1]Zurich/CH, [2]Stockholm/SE

Purpose: To evaluate the diagnostic performance of dynamic perfusion CT (P-CT) for detection of hepatocellular carcinoma (HCC) in the cirrhotic liver.
Methods and Materials: 26 cirrhotic patients (19men, 69±10years) with suspicion of HCC prospectively underwent perfusion-CT of the liver using the 4D spiral-mode (100/80kV; 150/175mAs/rot) of a dual-source scanner. Two readers assessed (A) arterial liver-perfusion (ALP), portal-venous liver-perfusion (PLP) and hepatic perfusion-index (HPI) maps alone, and (B) side-by-side with maximum-intensity-projections of arterial time-points (art-MIP) for detection of HCC using histopathology and imaging follow-up as standard of reference. Another reader quantitatively assessed perfusion-maps of detected lesions.
Results: A total of 48 HCC in 21/26 (81%) patients with a mean size of 20±10mm were detected by histopathology (9/48, 19%) or imaging follow-up (39/48, 81%). Detection rates (Reader1/Reader2) of HPI maps and side-by-side analysis of HPI combined with arterial MIP were 92/88% and 98/96%, respectively. Positive-predictive values were 60/58% and 68/71%, respectively. A cut-of-value of ≥85% HPI and ≥99% HPI yielded a sensitivity and specificity of 100% respectively, for detection of HCC.
Conclusion: P-CT shows a high sensitivity for detection of HCC in the cirrhotic liver. Quantitative assessment has the potential to reduce false-positive findings improving the specificity of HCC diagnosis.

SS134

CT Imaging of the liiver: Comparison of sinogram-affirmed with advanced modeled iterative reconstructions

F. Morsbach[1], L. Desbiolles[2], S. Leschka[2], H. Alkadhi[1]; [1]Zurich/CH, [2]St. Gallen/CH

Purpose: To investigate image quality of the liver and conspicuity of liver lesions on abdominal computed tomography (CT) images, reconstructed with advanced modeled iterative reconstruction (ADMIRE), sinogram-affirmed IR (SAFIRE) and filtered back projection (FBP).
Methods and Materials: First an abdominal phantom was scanned and images were reconstructed with ADMIRE (strength levels 3-5), SAFIRE (strength levels 3-5), and FBP at a slice thicknesses of 2 mm. Then forty patients (19 female, mean age 63±14 years) with focal liver lesions(cysts,n=20,metastases,n=20) undergoing standard portalvenous phase abdominal CT were included. In the phantom noise texture deviation was calculated. Two readers evaluated subjective image quality in the patient group focusing on image appearance (score 1: no artifacts, 2: minor artifacts, blotchy, plastic-like appearance, 3: major artifacts, blotchy, plastic-like appearane, 4: artifacts making a diagnosis impossible). Readers also rated the conspicuity of lesions (score 1:well-seen lesion, well delineated margin, score 2: well-seen lesion, poorly delineated margin, score 3: subtle lesions, score 4: probably an artifact mimicking a lesion). Attenuation of the liver, subcutaneous fat and image noise was measured.
Results: The image noise deviation was significantly reduced (P<0.001). Readers found significantly reduced artifacts for all strength levels of ADMIRE compared to the respective SAFIRE levels (P<0.001). Lesion conspicuity was rated similarly with ADMIRE and SAFIRE (P>0.05). HU-values of the liver and fat did not vary with reconstruction algorithms (P>0.05). Noise decreased with increasing strength levels compared to FBP (P<0.05), with no differences among corresponding strength levels (P>0.05).
Conclusion: As compared to SAFIRE, ADMIRE improves image quality and reduces artificial image appearance at a similar noise reduction level without impairing lesion conspicuity.

SS135

Assessment of the radiation dose, image quality and iodine quantification with a novel dual-energy technique for single-source abdominal CT

A. Euler, C. Zähringer, G. Stadelmann, M. Benz, S. T. Schindera; Basel/CH

Purpose: To assess the radiation dose, image quality and iodine quantification of a novel dual-energy technique on a single-source CT scanner using a gold and tin filter (TwinBeam Dual-Energy, Siemens).
Methods and Materials: A custom liver phantom and four tubes with varying iodine concentrations (4-10 mg/ml) were placed in water container mimicking an intermediate-sized patient (diameter: 30 cm). The phantoms were scanned on a single-source scanner (SOMATOM Edge, Siemens) with (A) single-energy mode at 120 kVp and 130 ref mAs, (B) dual-energy mode at AuSn120 kVp and 672 ref. mAs (default protocol of the manufacturer) and (C) with a dose-neutral dual-energy mode at AuSn120 kVp and 420 ref. mAs. The radiation dose was assessed by the $CTDI_{vol}$, the image noise was measured and the CNR was calculated. Software provided by the vendor was used for iodine quantification.
Results: The $CTDI_{vol}$ measured 7.0, 11.5, and 7.1 mGy for protocol A, B and C, respectively. The image noise was 30% and 18% lower and the CNR 29% and 8% higher with protocol B and C, respectively, compared to protocol A. The error of measurement for the iodine quantification ranged for protocol B from 16 to 32% and for protocol C from 10 to 16%.
Conclusion: The novel dual-energy technique allows dose-neutral dual-energy on a single-source CT scanner while providing the added value of the dual-energy mode.

SS136

Clinical evaluation of a dose optimized dual-source, dual-energy abdomino-pelvic CT protocol compared with a single-source CT protocol

M. Benz, C. Zähringer, A. Kircher, L. D'Errico, F. Schwartz, M. Kekelidze, A. Euler, G. Bongartz, S. T. Schindera; Basel/CH

Purpose: To compare the objective and subjective image qualities and radiation doses of a default and a dose-optimized dual-energy abdomino-pelvic CT protocol with those of a single-energy protocol.
Methods and Materials: 75 abdomino-pelvic CT scans were performed on a dual-source CT scanner (Somatom Definition Flash, Siemens) as follows: 25 CT scans were performed using a standard dual-energy protocol (tube A, 100 kVp, 230 ref. mAs; tube B, 140 kVp, 178 ref. mAs) (protocol A), 25 CT scans were performed using a dose-optimized dual-energy protocol (tube A, 100 kVp, 150 ref. mAs; tube B, 140 kVp, 116 ref. mAs) (protocol B), and 25 CT scans were performed using a single-energy CT protocol (120 ref. kVp, 150 ref. mAs) (protocol C). For each protocol the radiation dose was assessed by the volume CT dose index (CTDIvol). Quantitative image quality was measured. Six image
quality characteristics were assessed by 5 readers, namely: image noise, image contrast, artifacts, visibility of small structures, image sharpness, and overall diagnostic confidence.
Results: The CTDIvol of protocols A, B, and C was 12.5±1.9, 7.5±1.2, and 6.5±1.7 mGy, respectively ($p<0.001$). The average objective image noise was 6.6±1.2, 7.8±1.4, and 9.6±2.2 HU for protocols A, B, and C, respectively ($p<0.001$). No significant differences in the six subjective image quality parameters were observed between the dose-optimized dual-energy and the single-energy protocol.
Conclusion: Substantial modification of the default dual-source, dual-energy CT protocol is required to obtain radiation doses comparable to those of single-source CT. However, this protocol modification can be achieved while maintaining objective and subjective image quality.

SS137

Can standard CT be replaced by contrast enhanced ultra-low-dose CT with iterative reconstruction for the screening of patients admitted with acute abdominal pain? A comparative study

P.-A. Poletti, M. Becker, C. D. Becker, A. Platon; Geneva/CH

Purpose: To determine whether i.v. contrast-enhanced ultra-low-dose CT with model based iterative reconstruction (LDCT-IR), delivering a dose of radiation <1.5 mSv can be used for the screening of patients admitted with acute abdominal pain.
Methods and Materials: This study was approved by the IRB of our hospital. 151 consecutive patients, in whom a standard contrast enhanced abdominal CT (CECT) was required for acute abdominal pain, were included in the study. CECT series were immediately followed by an LDCT-IR (30 mAs, VEO^R post-processing), while the contrast media was still in the venous compartment. LDCT-IR images were reviewed independently by 2 board certified radiologists, blinded to the results of the standard abdominal CT, considered reference standard. Reviewers did mention the main diagnosis, related to the abdominal pain. Disparities between them were further resolved by consensus.
Results: An abdominal condition was reported at CECT in 121 (80%) patients. The correct diagnosis was made at LDCT-IR in 115 (92%) and mentioned among other differential diagnoses in 4 cases (3%). The correct diagnosis was not made at LDCT-IR in 2 patients with a BMI>30 (symptomatic gallbladder calculus and small precoccygeal abscess). LDCT-IR was falsely reported positive for a diverticulitis in one patient, with a BMI of 31, in whom standard CT was normal. LDCT-IR was 100% sensitive and 100% specific to establish the cause of an abdominal pain in patients with a BMI < 30.
Conclusion: Our data suggest that LDCT-IR can be safely used for the screening of patients with a BMI < 30 admitted with acute abdominal pain.

SS138

Can an algorithm based on US and ultra-low-dose CT be used for the diagnostic management of pregnant women admitted with acute abdominal pain? An observational study

G. Guglielmi, A. Platon, M. Becker, P.-A. Poletti; Geneva/CH

Purpose: To evaluate whether a new diagnostic algorithm integrating ultrasound and ultra- low dose CT with oral contrast media (LDCT) is sufficient for the screening of pregnant women admitted for acute abdominal pain, not suspect of gynecological condition.
Methods and Materials: 64 consecutive pregnant women with acute abdominal pain, in whom a gynecological examination was considered normal, underwent an abdominal ultrasound. When ultrasound was considered unsatisfying for the clinician, a LDCT (25 mAs, 1.2 mSv) was proposed.
The number of further imaging examinations that were obtained after LDCT was recorded along with the patients' clinical follow-up.
Results: Ultrasound was positive in 23 (36%) of the 64 patients, normal in 24 (38%) and indeterminate in 17 (26%). No further examination was required by the clinician after ultrasound in 37 (58%) patients. A LDCT was obtained in 27 (42%) patients: 12 showed a condition, which was successfully treated without further imaging. Eleven LDCT were normal, 4 indeterminate. The outcome of the 11 patients with a normal LDCT was uneventful, without further imaging. Of the 4 patients with
an indeterminate LDCT, 2 underwent a standard dose CT with i.v. contrast media and two underwent a delayed MRI.
Conclusion: An algorithm based on ultrasound and LDCT is sufficient for the clinical management of 94% (60/64) of pregnant woman admitted with acute abdominal pain. It may be useful to reduce the need of standard CT in acute settings, when MRI is not immediately available.

SS139

Systematic radiation dose reduction in cervical spine CT of human cadaveric specimens: How low can we go?

M. Tozakidou[1], C. Reisinger[1], D. Harder[1], J. Lieb[1], G. Stadelmann[1], Z. Szuecs-Farkas[2], S. T. Schindera[1], A. Hirschmann[1]; [1]Basel/CH, [2]Bern/CH

Purpose: Comparing image quality of the cervical spine CT of cadaveric specimens at different radiation dose levels reconstructed with a filtered back projection (FBP) and an iterative reconstruction (IR) algorithm.

Methods and Materials: The cervical spine of four human formalin-fixated cadavers (BMI;30.5kg/m2±5.2;range 24-36) was examined using a 128-MDCT scanner (DefinitionAS/Siemens) at nine different reference mAs levels (45/75/105/135/150/165/195/275/355) and a tube voltage of 120kVp. Data were reconstructed using both FBP and IR (SAFIRE/Siemens/strength 3). Morphological characteristics (vertebra cortex, anterior/posterior vertebra integrity, posterior vertebral alignment) were quantified on a Likert-scale for each cervical segment by four independent radiologists. Subjective image noise was evaluated on a three-point-scale. Objective image noise was measured in air.

Results: As expected IR provided significantly better image quality than FBP; noise increased as radiation dose decreased. Subjective image noise at levels C1-C4 was rated as either "no noise" or as "acceptable noise" in all scans. In contrast, at lower spine levels subjective image noise was not acceptable, even at 355mAs. Shoulder position of all human cadaveric specimens was found to be at level C5. Taking all spinal levels together, scores for morphological characteristics revealed no significant differences between 105 and 355mAs, but were significantly worse in scans at lower tube currents (45/75mAs).

Conclusion: Clinically acceptable image quality of the cervical spine of cadaveric specimen with different body habitus can be achieved with a reference mAs of 105. However, high position of the shoulders is a limiting factor even with high radiation dose; therefore lowering down of both shoulders during acquisition is fundamental.

SS140

The intervertebral disc, the endplates and the vertebral bone marrow as an interacting unit in the process of degeneration of the lumbar spine

N. A. Farshad-Amacker[1], A. P. Hughes[2], R. J. Herzog[2], B. Seifert[2], M. Farshad[1]; [1]Zurich/CH, [2]New York/US

Purpose: Although known that disc degeneration (DD) is somehow associated with vertebral endplate degeneration (EPD), the interaction is not well understood. This study aimed to find segmental risk factors for DD and EPD and to illuminate the interactions of the disc, the endplate and the bone marrow changes in the process of degeneration in a longitudinal study design.

Methods and Materials: 450 lumbar levels in 90 patients, followed up with MRI at least 4 years, were retrospectively graded for DD according to Pfirrmann (PFG), for EPD according to the endplate score (EPS) and according to the presence, extension and type of Modic changes (MC) to find interactions. Clustered stepwise logistic regression and multivariate analysis was applied in nested, matched case-control subgroups to evaluate potential local risk factor for progression of degeneration.

Results: An EPS score of ≥4 was independently predictive for progression of DD (OR=2.32, 95%CI: 1.1-5.0, p=0.03) and MC (OR=5.49, 95%CI: 2.3-13.1, p<0.0001). Progression of DD was significantly accompanied by progression or evolution of MC (OR=12.25, 95%CI: 1.5-100.6, p=0.02) and with progression of EPS (OR=1.71, 95%CI: 1.0-1.1, p=0.01). Once advanced DD has occurred, it becomes predictive for progression in EPS (OR=2.24, 95%CI: 1.23-4.12, p=0007).

Conclusion: The degenerative processes in the disc, endplate and bone marrow are interacting. Endplate erosions are predictive for DD and MC progression. Bone marrow changes are last to occur in the development of segmental degeneration. A new segmental grading system is presented to assess disc, endplate and bone marrow changes as one interacting unit.

SS141

Is there a difference in treatment outcomes between epidural injection patients receiving particulate versus non particulate steroids?

S. Bensler, R. Sutter, C. W. Pfirrmann, C. K. Peterson; Zurich/CH

Purpose: To compare the outcomes of patients having interlaminar epidural injections treated with particulate vs. non particulate steroid.

Methods and Materials: 531 consecutive patients with no significant age or gender differences were treated with CT guided lumbar interlaminar epidural injections with steroid and local anesthetics. 411 patients achieved a particulate steroid i.e. triamcinolone acetonide and the other 120 patients achieved a non-particulate steroid i.e. dexamethasone. Pain level was recorded immediately prior to injection. Pain levels and overall 'improvement' were assessed at 1 day, 1 week and 1 month post-injection. Descriptive and inferential statistics were applied.

Results: A significantly higher proportion of patients receiving particulate steroids reported clinically relevant improvement at both 1 week and 1 month post injection (p = 0.0001). Additionally, patients receiving particulate steroids were significantly less likely to report worsening of their condition at 1 week (p = 0.0001) and 1 month (p = 0.017) The patients receiving the non-particulate steroid had statistically significantly lower NRS change scores compared to those with the particulate steroid (p=0.0001 at 1 week; p=0.0001 at 1 month).

Conclusion: Patients treated with the non-particulate steroid had significantly less pain relief and were much less likely to report clinically relevant overall 'improvement' at 1 week and 1 month and were significantly more likely to report worsening at 1 week and 1 month compared to the group treated with the particulate depo-steroid.

SS142

Bone metastases: A common but uninformative finding?

D. Keskin, E. Paulin; Neuchâtel/CH

Purpose: Bone is a common site for metastatic tumours. In approximately 20% of cases, the primary tumour is unknown.

Our aim is to utilize decision trees to simplify the analysis of bone metastases in the determination of the primary tumour site.

Methods and Materials: More than one hundred patients, with bone metastases of a known primary tumour, underwent imaging in our institution in 2014. Two radiologists retrospectively studied MRI, CT, and radiographs of these cases to classify the type and location of bone lesions with consideration of the patient clinical data and present the information in the form of algorithms for decision making.

Results: By frequency, bone metastases are secondary to prostate tumours (60% of etiologies in men), breast (70% in women), lung, and kidney.

Approximately 75% of metastases are lytic, 10% are mixed, and 15% are sclerotic. If lytic lesions are seen, lung, breast, kidney, and thyroid cancers should be considered. Mixed metastases are also frequently seen in lung and breast cancers. The osteoblastic lesions are mainly related to prostate cancer and carcinoid tumors.

80% of bone metastases are located on the axial skeleton. Acrometastases or cortical lesion are rare and usually secondary to lung, breast, or renal tumours.

Conclusion: Bone metastases are not only frequent findings but are also rich in information about the primary tumour. Such information allows radiologists to provide more relevant diagnostic differentials and to better target examinations that lead to rapidly identify the primary tumor and begin treatment protocols.

SS143

Edema of the cartilage in the lateral facet of the patella a valuable criteria for assessment of patellar instability before and after femoral trochleoplasty

A. L. Falkowski[1], C. Camathias[2], J. A. Jacobson[3], O. Magerkurth[2]; [1]Bruderholz/CH, [2]Basel/CH, [3]Ann Arbor/US

Purpose: To characterize findings of signal intensity of the cartilage of the lateral facet of the patella in patients with known patellar instability before and after trochleoplasty.

Methods and Materials: IRB approval was obtained. Patients with known instability of the patella with pre- and postoperative MR imaging were included. The following measurements and observations were obtained: if present the existence of edema in the cartilage of the lateral facet of the patella; Insall-Salvati index, TTTG, Patella shape (Wiberg) and Trochlea Shape (Hepp). Results before and after surgery, and intra- and interreader agreement were tested by using the paired t-test and Wilcoxon signed rank test.

Results: 22 patients were included in the study. Edema was present in 20 patients before and in 4 after trochleoplasty. Insall-Salvati Index was >= 1.2 (patella alta) in 20. Patella shape (classification of Wiberg) was greater than 2 in 18. Trochlear Shape (Classification of Hepp) greater than 2 was present in 21 before and 7 after trochleoplasty. Mean TTTG before surgery was 14mm and post surgery 10mm. We found statistical significance comparing results before and after surgery for edema (p=0.0132), TTTG (p=0.0002) and trochlear shape (p=0.0001). Regarding intra- and interreader agreement there were no significant differences (p= 0.1130 to >0.9990).

Conclusion: In this study edema of the cartilage in the lateral facet of the patella seems to be a predictor of patellar instability. Even with postoperative artifacts in the trochlea it is possible to assess the patellar cartilage and describe improvement of the femoropatellar articulation after trochleoplasty.

SS144

Osteochondral lesions of the knee joint follow a distinctive pattern: A comparison of MR imaging results and split line maps

A. L. Falkowski[1], C. Camathias[2], J. A. Jacobson[3], O. Magerkurth[2]; [1]Bruderholz/CH, [2]Basel/CH, [3]Ann Arbor/US

Purpose: To characterize findings of osteochondral lesions in the knee joint with regard to shape, orientation of the axes and compare these findings with a split line map of the distal femoral cartilage.

Methods and Materials: IRB approval was obtained. Patients with acute OCDs were included. Following measurements and observations were obtained: location (21 regions based on International Cartilage Repair Society), shape and size of the OCD. Lesions with a ratio of short axis / long axis <0.6 were considered as oval and over 0.6 as round lesions. Orientation of long and short axes were compared to a split line map. Interreader agreement was tested with a paired two tailed t-test.

Results: 56 patients were included in the study. 17 OCDs were located in the medial central portion of the medial femoral condyle (R13 according to ICRS). Location of other lesions were: 4 in R1, 1 in R4 and R7, 4 in R10, 6 in R11, 1 in R12, 5 in R14, 8 in R17, 4 in R19, and 1 in R20. Orientation of long axis correlated with the split line map. In regions R10-R12, lesions were round, whereas they were oval in R4, R7 and R13-R20. Testing for interreader agreement showed no significant difference and a good correlation (p=0.067, r=0.7100).

Conclusion: In this study shape of osteochondral lesions in the knee joint do follow split line maps representing the layered structure of cartilage. We assume that paying attention to orientation of autologous chondral grafts might increase stability at the recipient site and may improve outcome.

SS145

Femoral and tibial torsion measurements in children: Comparison of MR imaging and 3D models based on low-dose biplanar radiographs

A. Rosskopf, L. Ramseier, C. W. A. Pfirrmann, F. M. Buck; Zurich/CH

Purpose: To evaluate reliability and interchangeability of femoral (FT) and tibial torsion (TT) measurements in children using magnetic resonance (MR) imaging compared to measurements on 3D models based on low-dose biplanar radiographs (3DBPR).

Methods and Materials: FT and TT were measured in 30 children (mean age 10.1 years;range 6.2–15.6 years;14 female) using axial MR images of the hip, knee and ankle by two independent readers. They were compared to measurements on 3DBPR of the lower limb by two separate independent readers. Interreader and intermethod agreement was calculated using descriptive statistics, Intraclass correlation coefficient (ICC) and Bland-Altman analysis.

Results: FT/TT was -6°–47°/+1°–44° on MR images and -13°–46°/9°–49° for measurements on 3DBPR. The average difference between the two methods was 4.6°±4.1/6.0°±3.8, respectively. Interreader agreement (ICC) of FT/TT measurements was 0.97/0.96 on MR images and 0.99/0.94 on 3DBPR. Intermethod agreement (ICC) for MR measurements was 0.93(95% confidence interval [CI], 0.88–0.96) for FT and of 0.87(CI, 0.39–0.95) for TT. Mean interreader differences for 3DBPR were 2.1°(0.0°–7.0°) for FT and 3.4°(0.0°–12.0°) for TT. Mean interreader differences at MR were 3.2°(0.1°–8.0°) for FT and 3.5°(0.1°–9.5°) for TT.Bland-Altman plots showed a systematic underestimation of TT on MR measurements compared to BPR of 5°. All but 3/4 measurements of FT/TT were within the 95% limit of agreement.

Conclusion: FT and TT measurements in children using MR images are comparable to measurements on 3DBPR models.

SS146

Muscle and tendon damage after total hip arthroplasty: MRI evaluation of different surgical approaches

C. Agten, R. Sutter, C. Dora, C. W. A. Pfirrmann; Zurich/CH

Purpose: To provide muscle and tendon damage profiles in patients after total hip arthroplasty with a posterior, direct-lateral, antero-lateral, or anterior surgical approach.

Methods and Materials: This retrospective study was approved by the institutional review board and informed consent was waived. 120 patients with MRI of primary total hip arthroplasty (30 patients per approach, 71 females/49 males, mean age 66 years, mean interval after surgery 60 months) were included. Each MRI was assessed by 2 independent readers regarding fatty atrophy of muscles (Goutallier classification) and tendon quality (0=normal, 1=tendinopathy, 2=partial tear, 3= complete avulsion). The transverse area of the tensor fasciae latae muscle (TFL) was measured. TFL was defined as damaged if an area < 3cm^2 or Goutallier grade 3 or 4 was present. Descriptive statistics were applied.

Results: The direct-lateral approach showed highest Goutallier grades and tendon damage for the gluteus minimus muscle (2.07-2.67 and 2.00-2.77 for reader 1 and 2) and tendon (2.30/1.67 for reader 1/2), as well as the lateral portion of the gluteus medius tendon (2.77/2.20 for reader 1/2). The posterior approach showed highest Goutallier grades and tendon damage for the external rotator muscles (1.97-2.67 and 1.57-2.40 for reader 1/2) and tendons (1.41-2.45 and 1.93-2.76 for reader 1/2). The anterior approach showed most damage to the TFL (7/30 and 6/30 for reader 1/2).

Conclusion: Specific muscle and tendon damage profiles are presented for the different THA approaches, as the soft tissue damage around the hip joint strongly depends on the surgical approach.

SS147

Cross sectional area of the rotator cuff muscles in MRI – Is there evidence for a biomechanical balanced shoulder?

S. Bouaicha, K. Slankamenac, B. K. Moor, G. Andreisek, T. Finkenstaedt; Zurich/CH

Purpose: To provide in-vivo evidence for the well known biomechanical concept of transverse and craniocaudal force couples in the shoulder yielded by the rotator cuff muscles (RCM) and the deltoid, the purpose was to quantitatively evaluate the cross sectional areas (CSA) of the RCM as a surrogate marker for muscle strength using MRI.
Methods and Materials: 49 patients (age range, 18-70 years; mean age, 38 years; 39 male) without rotator cuff tears were included in this retrospective study. CSA measurements were performed on 1.5 Tesla MR-arthrographic shoulder studies of the four rotator cuff muscles and three different measurement sites of the deltoid. Spearman's correlation for the corresponding CSA of the force couple was calculated.
Results: The mean CSA of the supraspinatus was 757 mm^2 and 974 mm^2 for the infraspinatus muscle. The mean CSA of the subscapularis was calculated 1914 mm^2 and 431 mm^2 for the teres minor. The three measurements of the deltoid revealed a CSA of 3016 mm^2 for the upper-, 4021 mm^2 for the lower edge and 3800 mm^2 for the middle of the glenoid. Spearman's correlation of the transverse force couple (subscapularis/infraspinatus) showed a moderate positive correlation of 0.503 ($p=0.0002$) and a strong positive correlation of the craniocaudal force couple (supraspinatus/deltoid) ranging from 0.625 - 0.676 ($p<0.001$).
Conclusion: Significant correlation of the CSA of the RCM forming the transverse (subscapularis/infraspinatus) and craniocaudal (supraspinatus/deltoid) force couple measured on MR-arthrography support the biomechanical concept of a dynamically balanced shoulder in patients with an intact rotator cuff.

SS148

Comparison of optimized high-resolution MR imaging of the temporomandibular joint at 1.5T and 3.0T using an optimized high-resolution protocol

A. Manoliu, G. Spinner, M. Wyss, S. Erni, D. Ettlin, D. Nanz, E. J. Ulbrich, L. M. Gallo, G. Andreisek; Zurich/CH

Purpose: Current literature describes MR imaging of the temporomandibular joint (TMJ) at 1.5T as standard, however, little is known about 3.0T imaging. Purpose was to quantitatively and qualitatively compare TMJ imaging at 1.5T and 3.0T using an optimized high-resolution protocol.
Methods and Materials: IRB approved study with written informed consent. A spherical phantom and 12 asymptomatic volunteers underwent MR imaging of the TMJ at 1.5T and 3.0T (Achieva 1.5T/Ingenia 3.0T, Philips) using identical 2- channel surface coils (SENSE FlexS, Philips). Image protocol included sagittal and coronal fast spin echo sequences. Acquisition parameters were kept identical except for higher spatial resolution at 3.0T. For quantitative analysis, pixel-by-pixel signal-to-noise-ratio (SNR) maps were calculated using Matlab routines (Natick, USA). For qualitative analysis, images were evaluated by two independent readers using 5-point-Likert-scales. 1.5T and 3.0T were compared using t-tests.
Results: The quantitative analysis revealed significantly increased SNR for 3.0T compared to 1.5T (1.5T: mean±SD, 64.29±30.63; 3.0T: 102.45±43.63; $p<0.001$). For the qualitative analysis, inter-rater reliability ranged from "substantial" to "almost perfect" (Kappa, 0.84-0.97).The qualitative analysis showed significantly better image quality and visibility of clinically relevant anatomic structures (temporomandibular disc, posterior attachment, mandibular condyle) at 3.0T compared to 1.5T ($p<0.05$, corrected for multiple comparisons).
Conclusion: MR imaging of the temporomandibular joint at 3.0T using sequences optimized for high-resolution yields increased SNR, better image quality and visibility of clinically relevant anatomic structures compared to 1.5T.

SS149

MR findings: How to do and report MR of the TMJ

M. Pregarz[1], C. Bodin[2]; [1]Peschiera del Garda/IT, [2]Brescia/IT

Purpose: Modalities, protocols and report used for the patients with Temporo Mandibular Disorders (TMDs) are presented. Magnetic Resonance (MR) is an appropriate imaging modality for Temporo Mandibular Joint (TMJ) analysis because of soft tissues high contrast resolution and multiplanar data acquisitions. Multi Detector Computed Tomography (MDCT) or Cone Beam Computed Tomography (CBCT) are complementary when osseous analysis is required.
Methods and Materials: Since the image acquisition do not respond to the physiological posture, because of patient supine position durig data acquisition, all TMDs patients before MR exam, have a gnatologic evaluation and report.
Our image s are achieved through two 1.5 MR systems (Magnetom Aera, Erlangen, Germany and Signa Hdi, General Electric, Milwaukee, Winsconsin, USA).
Images are obtained with TMJ protocols using head or surface coils.
T1 and T2 images are obtained in closed and open mouth, without forcing the opening, sometimes with more cooperative patients, we complete the exam with a cine sequence. Individual patient device is prepared before data acquisition in the lateral jaw position.
Results: TMJ are evaluated in all three planes for better assessment of the morphological, for the intercondilar angle measurement and for the disc position and its changes with mouth closed and open.
Outline base are necessary in film reading.
Conclusion: TMDs exams require accuracy in preparation and execution; high relevance has the inter-professional communication.
Report must be thorough informative and easy understanding too.

SS201

Clinical utility of FDG-PET MRI for pre-operative breast cancer staging

A. Kalovidouri, C. Tabouret-Viaud, V. Garibotto, X. Montet, C. D. Becker, O. Ratib, D. Botsikas; Geneva/CH

Purpose: To evaluate the added value of FDG-PET/MRI for the purpose of pre-operative staging of patients with breast cancer.
Methods and Materials: The pre-operative FDG-PET/MRI exams of 58 consecutive women with known breast cancer were retrospectively reviewed. All breast lesions detected were classified according to the Birads® classification based on MRI by two radiologists in consensus. Pathologic lymph nodes and distant metastases were also recorded. The combined FDG-PET/MRI were then reviewed by two nuclear physicians in consensus. Maximal standard uptake values (SUV) were recorded for all lesions. ROC curves were created to choose the best cut-off values for lesion characterisation. A combined evaluation of MRI with FDG-PET based on the most appropriate uptake value was then performed.
Results: The 58 patients had a total of 101 breast lesions, 83 malignant and 18 benign, and 40 lymph nodes detected by imaging, 34 malignant and 6 benign. Three patients had distant metastases.
MRI sensitivity and specificity for breast lesions was 0.96 and 0.56 and for lymph nodes 0.82 and 0.50.
Combined FDG-PET/MRI sensitivity and specificity for breast lesions was 0.75 and 1.00 and for lymph-nodes 0.79 and 1.00.
Two patients with distal metastases were correctly identified on the basis of a focal PET uptake: all metastatic lesions could only be identified retrospectively on whole-body MRI images.
Conclusion: FDG-PET/MRI is a valuable tool for preoperative staging in breast cancer patients, combining the excellent sensitivity of MRI for local staging and specificity of PET for nodal and distant metastases.

SS202

Visibility of the nipple on mammography: Comparison of two-dimensional synthesized mammograms versus original digital mammograms

E. Tenisch[1], L. Alamo[1], C. Flick[2], C. Nakajo[1], J.-Y. Meuwly[1]; [1]Lausanne/CH, [2]Pontarlier/FR

Purpose: To compare the visibility of the nipple on generated 2D mammography (synthetic reconstructed mammography = SM) with standard full field digital 2D mammography (FFDM).
Methods and Materials: Four hundred seventy two diagnostic mammographic examinations were retrospectively reviewed by two radiologists. Bilateral views were obtained for 374 patients, unilateral in 98. Two views (CC and MLO) were evaluated for each side on standard FFDM and on SM. The size and the visibility of the nipple was assessed and compared in the two modes. T-Test and Wilcoxon sign rank test were used for statistical analysis.
Results: The nipple was visible on 61% of CC views and 63% of MLO view on FFDM. It was visible on 45%, respectively on 48% on SM ($p<0.05$). Comparison of the two modes revealed that the nipple was smaller and less visible on generated 2D than in FFDM ($p<0.05$).
Conclusion: The generated 2D mammograms hide or reduce the visibility of the nipple in almost all cases. This particularity has to be considered in the diagnostic process with mammograms.The nipples should systematically be clinically observed at the time of the mammogram, in order to recognize pathology potentially invisible on 2D generated mammograms.
Nipple diseases have the potential to be overlooked with the generated 2D mammography reconstructed by the SM software. In perspective of using SM in screening mammography, the radiographer should mandatory closely scrutinized the nipple during the performance of the examination and report any abnormality to the radiologist.

SS203

Preoperative Planning of DIEP Flaps: Comparison of native MRA with CTA and Duplex ultrasound as a reference

I. Zbinden, G. Bongartz, T. Haas, M. Haug, B. Ling, D. Babst; Basel/CH

Purpose: Accurate preoperative imaging of Deep Inferior Epigastric artery Perforators (DIEP) provides optimal surgical planning for autologous flap breast reconstruction. This study focusses on the ability of non-contrast MRA (native MRA) to delineate DIEP preoperatively. Native MRA and boodpool-CE-MRA were compared to standard Computed Tomography Angiography (CTA).
Methods and Materials: 15 patients were included with preoperative DIEP-CTA (gold standard). All patients underwent native 3D MRA and contrast-enhanced MRA with bloodpool agent (Gadofosveset Trisodium; Ablavar ® Lantheus Medical Imaging Inc.) in first pass and equilibrium phase.
Patients were investigated in prone position on a 3-Tesla scanner (PRISMA, Siemens, Erlangen). Following native acquisition of 3D T2w SPACE STIR (coronal or axial direction; 0x9 x 0.9 x 2mm3), by first-pass MRA and equilibrium MRA (isotrop 1.1mm). Post processing was applied on Aquarius iNtuition Workstation. All imaging results were compared and correlated with intraoperative findings.
Results: Bloodpool contrast enhanced MRA in steady state and native T2 SPACE STIR were able to demonstrate the main perforator vessels in all patients investigated. Comparison of the most important variables (intramuscular course, and position of the perforators with respect to the umbilicus) for both MRA-techniques demonstrated excellent concordance to CTA and intraoperative findings. In 3 cases, native MRA was superior to CTA in the delineation of small perforators. Patients' acceptance for the longer native MRI was inferior to the fast perfusion techniques.
Conclusion: Gadofosveset Trisodium-Enhanced 3.0-T MRA and native MRA may be used to accurately localize DIEP and to select the optimal perforator to be harvested for DIEP-flap reconstructive breast-surgery.

SS204

Advanced virtual monoenergetic images: Value for dual-energy CT pulmonary angiography

A. Meier[1], M. Wurnig[1], L. Desbiolles[2], S. Leschka[2], T. Frauenfelder[1], H. Alkadhi[1]; [1]Zurich/CH, [2]St. Gallen/CH

Purpose: To investigate the value of advanced virtual monoenergetic images from dual-energy (mono plus) for improving the contrast of CT pulmonary angiography.
Methods and Materials: Forty consecutive patients (25 women, median age 66 years, range 28-87 years) underwent 192-slice dual-source CT pulmonary angiography with dual-energy (90/150SnkVp) after the administration of 60ml contrast media. Conventional virtual monochromatic images at 60keV and 17 mono plus image datasets from 40-190keV (in 10keV steps) were reconstructed. Subjective image quality (artifacts, subjective noise) was rated. Attenuation was measured in the pulmonary trunk and right lower lobe pulmonary artery; noise was measured in periscapular musculature. Signal-to-noise (SNR) and contrast-to-noise ratio (CNR) were calculated for each patient and dataset. Comparisons between monochromatic images and mono plus images were performed by repeated measures ANOVA corrected for multiple comparisons (Bonferroni correction).
Results: Interreader agreement was good to excellent for subjective image quality (ICC:0.616-0.889). As compared to conventional 60keV, artifacts occurred significantly less in mono plus images at 40keV ($p=0.001$), and subjective noise was rated significantly lower in 40keV ($p<0.001$). Noise was significantly lower in mono plus at 40keV compared to conventional monoenergetic images at 60keV ($p<0.001$). SNR and CNR in the pulmonary trunk and right lower lobe pulmonary artery was significantly higher in mono plus images at 40keV as compared to conventional monoenergetic images at 60keV (all,$p<0.001$).
Conclusion: Compared to conventional virtual monoenergetic imaging, advanced mono plus images at 40keV improve the contrast of dual-energy CT pulmonary angiography, which indicates potential for further lowering of the contrast media volume.

SS205

CT arterial obstruction index predicts short-term mortality in pulmonary embolism in patients without cardiopulmonary comorbidities

C. Rotzinger, L. Veunac, S. Breault, A.-M. Jouannic, C. Beigelman, S. D. Qanadli; Lausanne/CH

Purpose: Our purpose was to evaluate the potential relationship between the pulmonary CT angiography (CTA) arterial obstruction index (CTOI) and 1-month mortality in pulmonary embolism (PE) patients.
Methods and Materials: Over a 5-year period, all suspected PE patients who underwent pulmonary CTA were prospectively included. In patients with PE, CTOI was calculated based on the Qanadli Index. The population was divided into three groups depending on the CTOI value: group A with CTOI <20%, group B with CTOI between 20 and 39% and group C with CTOI >40%. PE patients were further stratified into patients with (CPD+) or without (CPD-) preexisting cardiopulmonary disease. 1-month mortality rates were assessed for each CTOI category, in both CPD groups.
Results: We examined 2'588 consecutive patients (53.3% females, median age 66 years), of whom 691 (26.7%) were diagnosed with PE. In the CPD- patients (429 patients, 62.1%), 1-month mortality rates in groups A, B and C were 1.8%, 5.3% and 11.4%, respectively. In the CPD+ patients (262 patients, 37.9%), 1-month mortality rates in groups A, B and C were 8.5%, 20% and 7.4%, respectively. Significant differences in mortality rates depending on the CTOI were found in the CPD- (p=0.004), whereas no significant difference was found in the CPD+ (p=0.103).
Conclusion: Our results indicate that the CTOI (Qanadli Index) is an accurate predictor of 1-month mortality in PE patients with no preexisting CPD. In PE patients with CPD comorbidities, however, 1-month mortality rates have no significant correlation with the CTOI.

SS206

Pulmonary perfusion after endoscopic reduction of emphysema with Dual-Energy Computed Tomography

A.-L. Hachulla, F. Lador, O. Hoene, C. D. Becker, P. Soccal, X. Montet; Geneva/CH

Purpose: To assess pulmonary perfusion before and after endoscopic lung volume reduction (ELVR) by coils with dual-energy CT in order to better understand the consequences of this treatment on parenchymal lung perfusion.
Methods and Materials: 5 patients underwent DE-CT performed with Gemstone Spectral Imaging mode prior and after ELVR. For the lung perfusion study, iodine parenchymal concentration (Clung,ug.cm-3) was measured. 6 regions of interest (ROI) were selected in the anterior, lateral and posterior right and left lungs at 4 defined levels. The parenchymal ROIs were classified for each patient according to their pulmonary lobes and either determined in a treated or an untreated lobe. Clung was normalized by the left atrial iodine concentration (CLA) to take into account differences between successive DE-CT.
Results: 12 DE-CT were performed (dose-length-product:403±45mGy.cm; effective dose:5.65±0.64mSv) with 288 parenchymal ROIs measured. A significant increased perfusion in untreated lobes was observed (Clung/CLA from 37.8±8.9 to 45.0±11.4;p=0.016); this corresponded to a mean 36% Clung/CLA increase. A non-significant increased perfusion in treated lobes was observed (Clung/CLA from 41.6±9.5 to 56.7±11.5;p=0.32); this corresponded to a mean 19% Clung/CLA increase in the lung parenchyma adjacent to coils. In three cases, we observed a reduced perfusion in the treated lobes whereas perfusion remained stable or increased in all non-treated lobes.
Conclusion: ELVR by coil insertion increases perfusion in the non-treated lobes without significant perfusion changes in the coil-free adjacent parenchyma. This suggests a role of ELVR in the improvement of the ventilation/perfusion ratio.

SS207

Incidentally detected lymphangioleiomyomatosis like lesions in male patients on thoracic MDCT

S. Malekzadeh, M. Christodoulou, T. Christoforidis, V. Soubeyran, C. Constantin, M. E. Kamel; Sion/CH

Purpose: To describe the radiological pattern along with the potential causes of incidentally detected lymphangioleiomyomatosis (LAM) like lesions in male patients on MDCT of the thorax.
Methods and Materials: Thirteen male patients (38 to 89 y, mean 66 ±15) were identified with pericentimetric pulmonary cysts at high-resolution CT. For each patient, the distribution, form, and location of these cysts were noted. The radiological and clinical features along with the predisposing factors of pulmonary cystic diseases were all studied. Furthermore, potential causes or clues of hormonal imbalance were documented in the entire study group.
Results: In 10/13 patients (77%), cysts were located bilaterally. They presented as thin walled rounded structures diffusely distributed throughout the lung parenchyma. Strikingly, all patients had overt liver steatosis coupled with bilateral gynecomastia on CT, suggesting that the etiology of these lesions is likely hormonal related as previously established for women where LAM strikes during their childbearing age. Of note is that the majority of our patients (9/13, 69%) were non-smokers rendering the diagnosis of histiocytosis X or emphysema unlikely, and the same held true for tuberous sclerosis and lung firosis associated cysts since no clinical or radiological evidences of these two entities were identified.
Conclusion: In male patients with concomitant presentation of liver steatosis, gynecomastia, and pericentimetric pulmonary cysts, the diagnosis of LAM-like lesions should be considered besides other pulmonary cyst forming pathologies. Future prospective studies are required to further strengthen these preliminary observations.

SS208

Ultralow-Dose CT with tin-filtration for detection of solid and sub-solid pulmonary nodules: A phantom study

K. Martini, K. Higashigaito, B. Barth, S. Baumüller, H. Alkadhi, T. Frauenfelder; Zurich/CH

Purpose: To determine the lowest radiation dose level of CT with tin-filtration with maintained diagnostic image quality and high sensitivity for detection of solid and sub-solid pulmonary nodules.
Methods and Materials: Single-energy CT was performed using third-generation dual-source CT at 100kVp and tin-filtration with varying tube currents. An anthropomorphic chest phantom with solid and sub-solid pulmonary nodules (2-10mm, attenuation, 20HU to -800HU at 120 kVp) was used. The mean volume CT dose index $CTDI_{vol}$ of the standard chest protocol was of 2.2 mGy. The subsequent measurements resulted in $1/10^{th}$, $1/20^{th}$ and $1/70^{th}$ dose levels. Images were reconstructed with iterative reconstruction algorithms (ADMIRE). One blinded reader measured image noise, and two blinded readers determined overall image quality and nodule localization with confidence rates on a modified 5-point Likert scale.
Results: The overall image quality was diagnostic for all images scanned with $1/20^{th}$ of standard dose using iterative reconstruction techniques. Inter-observer agreement for image quality was excellent (k = 0.88). Objective noise has been significantly reduced using IR (ADMIRE5:70.41% for $1/20^{th}$; 71.6% for $1/10^{th}$, p=0.05) compared to FBP. Sensitivity of nodule detection was 97.14% (100% for solid, 93.75% for sub-solid nodules) at $1/20^{th}$ dose level and 100% for both nodule entities at $1/10^{th}$ dose level using ADMIRE5. Images obtained with $1/70^{th}$ dose level had moderate sensitivity (overall 85.71%; solid 94%; sub-solid 73.33%).
Conclusion: Our work suggests that with tin-filtration in combination with IR the effective radiation dose can be lowered to 0.042mSv while maintaining diagnostic image quality and high sensitivity for detection of solid and sub-solid nodules.

SS209

Dual-Energy subtraction radiography in cystic fibrosis

V. Obmann[1], L. Ebner[1], Z. Szucs-Farkas[2], A. Christe[1], S. Ott[1], E. Stranzinger[1]; [1]Bern/CH, [2]Biel/CH

Purpose: To correlate Dual Energy (DE) subtracted lung images compared to conventional radiographs (CR) with lung function tests and confidence of cystic fibrosis (CF)-score.
Methods and Materials: 49 DE-radiographs of 24 patients (16 males, 8 females) with CF (mean 32y, range 18-71y) were included. Lung function tests (FEV1%/predicted and FVC%/predicted) were performed within 10 days of the radiography. Two blinded radiologists evaluated all CR and DE in a randomized order. The modified Chrispin Norman score (CNS), including the extend of overinflation, bronchial line, ring, mottled and large shadows, was used to assess changes in the lung parenchyma. Wilcoxon statistics and Spearman's rank-test were used to compare the CNS and confidence of CNS on CR and DE and to correlate those with lung function tests.
Results: There was no significant difference of CNS between CR and DE. CNS of both the CR images and DE-radiographs correlated significantly with FEV1% (R=-0.729 and 0.659; P<0.001) and FVC% (R=-0.709 and -0.628; P<0.001). Higher confidence was achieved with DE-radiographs compared to radiographs alone (median, 3.6 vs 3.4; P=0.01).
Conclusion: CR and DE-radiographs are equally suited for the evaluation of patients with CF. A good correlation with the clinical parameters was observed. The confidence of the readers to interpret pulmonary changes in CF is significantly higher with DE radiographs.

SS210

Ultra-fast 3D balanced steady-state free precession MRI of the lung: Assessment of anatomic details in comparison to low-dose CT

T. Heye, G. Sommer, N. Hainc, J. Bremerich, O. Bieri; Basel/CH

Purpose: To evaluate the anatomical details offered by a new single breath-hold ultra-fast 3D balanced steady-state free precession (uf-bSSFP) sequence in comparison to low-dose chest CT.
Methods and Materials: This is an IRB approved, HIPAA compliant prospective study. A total of 20 consecutive patients enrolled in a lung cancer screening trial underwent same day low-dose chest CT and 1.5 Tesla MRI. The presence of pulmonary nodules and anatomical details on 1.9mm isotropic uf-bSSFP images was compared to 2mm lung window reconstructions by two readers. The number of branching points on 6 pre-defined pulmonary arteries and the distance between the most peripheral visible vessel segment to the pleural surface on thin slices and 50mm maximum intensity projections (MIP) were assessed. Image quality and sharpness of the pulmonary vasculature were rated on a 5-point scale.
Results: The uf-bSSFP detection rate of pulmonary nodules (32 nodules visible on CT and MRI, median diameter 3.9 mm) was 45.5% with 21 false positive findings (pooled data of both readers). Uf-bSSFP detected 71.2% of branching points visible on CT data. The mean distance between peripheral vasculature and pleural surface was 13.0±4.2mm (MRI) versus 8.5±3.3mm (CT) on thin slices and 8.6±3.9mm (MRI) versus 4.6±2.5mm (CT) on MIPs. Median image quality and sharpness were rated 4 each.
Conclusion: Although CT is superior to MRI, uf-bSSFP imaging provides good anatomical details with sufficient image quality and sharpness obtainable in a single breath-hold covering the entire chest.

SS211

Clinical feasibility of 3D ultra-fast balanced steady-state free precession MRI of the lung in patients with severely limited breath-holding capability

G. Sommer, M. Wiese, N. Hainc, D. Lardinois, J. Bremerich, O. Bieri, G. Bauman; Basel/CH

Purpose: In this work, the clinical feasibility of a new 3D ultra-fast balanced steady-state free precession (ufSSFP) MRI technique [Bieri O, MRM 2014] was tested in five patients with advanced pulmonary disease and severely limited breath-holding capability.
Methods and Materials: Five patients (2 female, 3 male, age 28-69y) with known pulmonary disease were enrolled in this study. All patients had severely reduced pulmonary function (FEV1=14-68% of normal) secondary to their pulmonary disease. Examinations were performed on a clinical 1.5T whole body MRI system with TR=1.31ms, TE=0.54ms, FA=15°, resolution=2.5mm^3, and parallel imaging factor 2. Total acquisition time in inspiratory breath-hold was 9.8s. CT images of the chest acquired within a narrow time frame to MRI (0-7 days) were available for comparison in all cases. Image interpretation including assessment of image quality and a comparison of findings in MRI and CT was performed by a radiologist with seven years experience in clinical MRI.
Results: The ufSSFP sequence provided good image quality in all patients. Slight breathing artifacts not impairing diagnosis were visible in two out of five patients. No banding artifacts were seen. The salient pathology as appreciated on CT was also visible on the ufSSFP MRI exam in all cases.
Conclusion: 3D ultra-fast bSSFP imaging of the lung is clinically feasible at 1.5T even in patients with severely limited breath-holding capability. In our small case series, ufSSFP MRI was able to depict all relevant pathology in comparable manner to CT. The sensitivity of this method to depict morphologic changes in particular pulmonary diseases remains to be investigated.

SS212

Bedside versus fluoroscopically guided insertion of peripherally inserted central catheters in term of tip malposition: A prospective randomized controlled Trial

F. Glauser, S. Breault, A.-M. Jouannic, F. Doenz, S. D. Qanadli; Geneva/CH

Purpose: Peripherally inserted central catheter (PICC) is increasingly used to provide access to central veins. It has led to the development of a bedside placement of PICC, which could result in tip malposition. The aim of our study was to compare a bedside blind PICC placement to a fluoroscopically guided procedure with a specific regards to tip position.
Methods and Materials: One hundred eighty patients were randomized to either bedside placement (Group 1) or fluoroscopically guided PICC insertion (Group 2). All procedures were done by the same interventional team and included post-procedural chest radiography to assess catheter tip position. Depending on the International Guidelines for optimal tip position, patients were classified in three types: optimal, suboptimal not needing repositioning, non-optimal requiring additional repositioning procedures.
Results: One hundred seventy four inserted PICCs were technically successful. In the group 1, 26% of patients had suboptimal tip position and 31% needed repositioning. In the group 2, 6% had had suboptimal tip position and 0% needed repositioning. Using the Fisher's test, we found that suboptimal and non-optimal tip position were highly statistically significantly lower in the group 2 (P< 0.001) .
Conclusion: Tip malposition rates are high using blind bedside PICC placement exposing the patient to an increased risk of deep venous thrombosis and catheter malfunction rates. Emerging technologies such as ECG placement techniques should be used to diminish the risk of malposition.

SS213

Normative values of the superior vena cava system using CT: Rationale for defining the optimal tip position of peripherally inserted central catheters

F. Gay, J. M. Grimm, S. Hajdu, A.-M. Jouannic, F. Doenz, S. D. Qanadli; Lausanne/CH

Purpose: Peripherally inserted central catheter(PICC) is increasingly used which has lead to blind insertions at bedside. Optimal distal positioning of the PICCs is mandatory to prevent complications. The study objective is to establish normative values of the venous segments of the superior vena cava(SVC) system using computed tomography(CT) and subsequently, to compare these values with estimations based on anatomical landmarks as previously reported in PICC insertions.
Methods and Materials: We evaluated 100 consecutive patients who underwent thoracic CT. Vessel lengths between the peripheral vein and the cavoatrial junction was segmented and measured based on center-line reconstruction technique and MIP reconstructions. Estimations for the length of a potential PICC were calculated using the MIP reconstructions and CT tomograms for both sides. A multivariate statistical analysis of segmental lengths was used to compare values and evaluate the influence of age, sex, height, weight.
Results: Large inter-individual variations were observed in the different segments (maximum of 22 mm, coefficient of variations of 63%). Significant differences were observed between measured distances and estimations obtained from anatomical landmarks to estimate the PICC length. Differences were higher for the left side than for the right side. There was no significant correlation between these measurements and age, sex, height, weight.
Conclusion: Large interindividual variations and significant differences between the measured values and the estimated values were observed. Given these observations, optimal tip position of the PICC using a bedside technique remains a challenging and difficult to standardize. However, with this technique, the right side is less prone to variations than the left side.

SS214

Endovascular embolization is a successful and save treatment for arterial complications after total hip arthroplasty and revision surgery

J. Den Hollander, M. Erschbamer, D. Sauter, L. Hechelhammer, F. Külling; St. Gallen/CH

Purpose: Arterial complications are rare but clinically critical complications in total hip arthroplasty (THA) surgery and usually require secondary interventions, either through open or endovascular approaches. We retrospectively analysed the indication, success and safety of an endovascular embolization after arterial complications after THA.
Methods and Materials: We analysed all arterial complications that occurred after THA that were routinely treated by endovascular embolization. We analysed angiographic findings, endovascular treatment, location in relation to the surgical approach and success of the intervention.
Results: Between 1997 and 2007 we performed 3891 THA at our institution. We identified 14 Patients with acute arterial complications which were treated by minimal invasive endovascular embolization. Clinical findings included swelling of the ipsilateral leg, pain, prolonged wound bleeding, decreases haemoglobin, and/or haemodynamical instability. Angiography showed in 11 patients a pseudoaneurysm, in two an arteriovenous fistula, in one a extravasation. In two patients no signs of acute bleeding could be detected. Twelve patients could be managed with a single session of endovascular embolization; in two an additional evacuation of the haematoma was performed. No complications could be observed in this series.
Conclusion: Endovascular embolization is a save and successful minimal invasive method for the treatment of arterial injury occurring after THA. Therefore this technique should be considered as first line option for the treatment of vascular injuries after THA.

SS215

Influence of needle diameter and depth of penetration on biopsy path adjustments – When can we still correct our path without withdrawing the needle?

G. M. Karwacki, C. J. Zech; Basel/CH

Purpose: Minimal invasive medical techniques which require an insertion of needles into soft tissues are still a growing field in medicine. Planned needle trajectories have to be frequently adjusted during the procedure by angulation of the extracorporal part of the needle, when the needle tip is already at a certain depth. To the best of our knowledge there are no documented fluoroscopic observations on the corresponding behaviour of the intracorporal part of the needle on angulation of its external part.
Methods and Materials: Needles of different diameters (22G, 20G, 19G and 17G) and tip shapes (asymmetric and symmetric) were inserted into phantoms of porcine origin. Three phantoms were used: 1 - consisting of skin and fat tissue; 2 - skin, prominent fat layer and muscle tissue underneath; 3 – skin, thin fat layer and mostly muscle tissue. Phantoms were firmly fixed to a fluoroscopy table. A force vector was applied to hub of needles inserted at different depths (2, 4, 6 and 8 cm) into phantoms. Under fluoroscopy the angulation, travelled distance (in relation to initial trajectory) of needle tips as well as the deformation of the intracorporal part of needle was investigated.
Results: The maximal achievable deviation of the needle tip from the initial trajectory is dependent on the diameter of the needle and depth of penetration as well as on characteristics of punctured tissue.
Conclusion: Our observations illustrate the potentially achievable corrections of needle trajectory being a valuable source of information for physicians performing image-guided needle-based procedures.

SS216

Phase-contrast imaging for the characterization of human coronary atherosclerotic plaques

S. Winklhofer[1], F. Morsbach[1], S. Peter[2], V. Tischler[1], M. von Werdt[1], S. Berens[1], P. Modregger[2], L. Buser[1], H. Moch[1], M. Stampanoni[1], M. Thali[1], H. Alkadhi[1], P. Stolzmann[1]; [1]Zurich/CH, [2]Villigen/CH

Purpose: Purpose of this study was to investigate into X-ray grating interferometry phase-contrast (PC) imaging for the characterization of human coronary artery plaque.

Methods and Materials: PC X-ray and absorption computed tomography (CT) imaging was performed ex vivo in forty human coronary artery segments using a synchrotron radiation source (Swiss Light Source; Paul Scherrer Institute, Switzerland). Two independent readers performed qualitative analyses of image quality, plaque components, and plaque classification according to the modified American Heart Association (AHA) criteria in 38 plaques detected by histopathology, the latter serving as the reference standard. Quantitative measurements of plaque components (i.e., collagen, lipid, smooth muscle, and calcification) were performed and compared among PC and absorption images using analysis of variances (ANOVA) for repeated-measures with a post hoc Bonferroni correction.

Results: Image quality was superior in PC images as compared with absorption imaging (P<0.001). Plaque components were detected by PC imaging without significant differences to histopathology, whereas absorption imaging detected calcifications without statistical differences only. Of the 38 detected coronary artery plaques, characterization was accurate in 33 plaques (87%) with PC; absorption imaging allowed for correct characterization of 7 plaques (13%, P<0.001). Hounsfield units (HU) of PC images were significantly different for all plaque components (pairwise P<0.05). Absorption images demonstrated significant differences (κ=0.81, P<0.001) between calcification and other plaque components, but were similar for collagen, lipid, and smooth muscle (P=1.00).

Conclusion: PC imaging allows for accurate characterization of human coronary artery plaque and quantitative assessment of plaque components, thereby outperforming absorption imaging.

SS217

Comparison of three iodine concentrations in the visualization of coronary arteries by CT angiography: A randomized European multicenter trial.

S. D. Qanadli; Lausanne/CH

Purpose: To assess the diagnostic efficacy of iobitridol (Xenetix® 350) compared to iopromide (Ultravist® 370) and iomeprol (Iomeron® 400) in the visualization of coronary arteries by CT.

Methods and Materials: Prospective, randomized, multi-center, double blind, non-inferiority phase IV trial including 468 patients with suspected coronary artery disease (CAD) and scheduled for clinically indicated coronary CT angiography. The primary endpoint was the CT scan evaluability for CAD diagnosis in terms of quality and interpretability of images. It was based on the full evaluation of 18 coronary segments for each patient assessed by 2 off-site independent readers. Secondary endpoints were related to the safety and efficacy of the 3 contrast media (mainly image quality, stenosis assessment, and signal quantification).

Results: Out of the 452 patients completed for the primary analysis, 92.1% had their 18 segments fully evaluable in the iobitridol group, vs. 94.6 and 95.4% in the iomeprol and iopromide groups respectively. Non-inferiority for the primary outcome was statistically demonstrated (p<0.05). Mean image quality was good to excellent for all contrast media, and no relevant differences were observed for the other secondary endpoints between the 3 groups. The mass of iodine (in g) injected was significantly different between the 3 groups: 27.8±3.4 (iobitridol), 29.3±3.8 (iopromide) and 31.7±3.8 (iomeprol), p<0.001. The good general safety profile of products was confirmed.

Conclusion: Coronary CT angiography using Xenetix® 350 is non-inferior to higher concentration contrast agents regarding image quality and evaluability while the amount of iodine required can be significantly reduced.

SS218

ECG-gated CT of the aorta with a 50% reduced iodine injection before trans-catheter aortic valve implantation: Image quality of the aorta and coronary arteries

A.-L. Hachulla, J. Gariani, S. Noble, X. Montet, J.-P. Vallee; Geneva/CH

Purpose: To evaluate a 50% reduction of iodine injection on the image quality of a thoracic and abdominal aortic and coronary CT, obtained with a high-pitch ECG-gated CT imaging.

Methods and Materials: Thirty-six patients underwent gated-aortic CT without λblockers on a Somatom Definition Flash CT scanner before trans-catheter aortic valve implantation using a high pitch of 3.2 with sinogram-affirmed iterative reconstruction(SAFIRE®).

18 underwent a standard iodine injection protocol(120mL-350 mg/mL)(P1); 18 with a 50% reduced iodine injection protocol(60mL-350 mg/mL)(P2).

Mean attenuation and contrast-noise ratio (CNR) were calculated of the ascending thoracic and abdominal aorta. Subjective image quality of the ascending aorta, abdominal aorta and the coronary arteries were rated on a 3-point scale.

Results: Mean effective dose, median kV and mean heartbeat were not significantly different (3.6mSv±0.9 vs. 4±1.9; 100kV[100-120] vs. 100[100-120] and 71bpm±15 vs. 68±9 for P1 and P2 respectively).

A significant difference of mean attenuation was noted in the ascending aorta (581±156HU vs 409±117HU;p=0.001;) and in the abdominal aorta (585±152HU vs 419±103;p=0.001), corresponding to a difference of mean CNR (p=0.02).

No significant difference was observed in image quality of the aortic valve (p=1), of the ascending aorta (p=0.23), and the abdominal aorta (p=1).

The diagnostic quality of the proximal and mid-segments of coronary arteries was graded as excellent in 14/18 and 13/18 patients for P1 and P2 respectively.

Conclusion: Despite of a difference in aortic mean attenuation and CNR, a relative high aortic mean attenuation with a 50% reduced iodine injection protocol had no consequences on the image quality of the aorta and coronary arteries.

SS219

Non-contrast enhanced scar imaging with MRI. A potential alternative to LGE

X. Deligianni[1], J. Bremerich[1], M. Zellweger[2], N. Kawel-Böhm[3], P. Haaf[1], T. Dellas Buser[4], O. Bieri[1], F. Santini[1]; [1]Basel/CH, [2]Onex/CH, [3]Chur/CH, [4]St. Gallen/CH

Purpose: The gold standard for the detection of focal myocardial scar with cardiovascular magnetic resonance is late gadolinium enhancement (LGE), which requires administration of contrast agent. Cardiac scar is characterized by the presence of collagen, which is not detectable with conventional non-enhanced MRI. A collagen-sensitive positive contrast technique based on a single-breath hold submillisecond-echo-time spoiled gradient echo (SPGR) sequence is presented here as a potential alternative to LGE for non-contrast enhanced cardiac MRI.

Methods and Materials: Three patients that showed late-enhancement in standard LGE were scanned at a 1.5T (two) and 3T (one) clinical MR scanner. The 2D submillisecond vTE SPGR sequence was applied in a breath hold at diastolic phase with TE_1/TE_2 0.6-0.8/3.0-3.5 ms (voxel=1.9x1.9x5.5mm^3, acquisition time 7-12 sec). A standard clinical protocol of an LGE inversion recovery SPGR axial image was acquired (3D at 1.5T and 2D at 3T) after administration of Gd-BOPTA.

Results: Submillisecond vTE SPGR showed suppressed signal on the difference of the two echoes (TE_1-TE_2) in normal myocardium. Infarcted myocardium was readily identified with positive contrast on the difference image at locations that showed high signal with standard LGE MRI.

Conclusion: This study shows feasibility of submillisecond vTE MRI for collagen sensitive scar imaging of the heart without contrast administration. This technique might be an attractive alternative to LGE, particularly in patients with contraindications to contrast material.

SS220

Simultaneous T1 and T2 quantification of the myocardium using cardiac balanced-SSFP inversion recovery with interleaved sampling acquisition (CABIRIA)

F. Santini[1], N. Kawel-Böhm[2], J. Bremerich[1], O. Bieri[1]; [1]Basel/CH, [2]Chur/CH

Purpose: This study aims to develop, optimize and validate a new MR method using inversion recovery balanced steady-state free precession (IR-bSSFP) named "Cardiac Balanced-SSFP Inversion Recovery with Interleaved Sampling Acquisition (CABIRIA)" for relaxometry of the cardiac muscle. Quantitative imaging of the heart has become a major focus of interest in the recent years and its applicability to both chronic (in the form of T1 quantification for the detection of fibrosis) and acute (in the form of T2 quantification for the detection of edema) conditions.
Methods and Materials: For data acquisition, a custom two-dimensional, real-time IR-bSSFP sequence was used. The sequence was triggered on the ECG signal and at the beginning of the heart diastolic phase; a 180° inversion pulse preceded a train of real-time bSSFP acquisitions (130ms/image). A pixelwise fit of the acquired images was performed to calculate T1 and T2 relaxation times. The method was validated on 5 healthy volunteers at 3T and the resulting T1 values were compared with commercial T1 (MOLLI) and T2 (T2-prepared bSSFP) mapping implementations.
Results: The average T1 over all volunteers calculated by CABIRIA was 1227±39 ms (1225±41 ms by MOLLI). For the T2 measurements, the average over the volunteers was 37.9±2.4 ms (38.6±3.3 by T2-prepared bSSFP).
Conclusion: The proposed implementation of simultaneous T1 and T2 mapping of the myocardium by means of the CABIRIA method shows good potential for an integrated quantitative cardiac MRI protocol.

SS221

Aortic strain measurement with MRI – Does intraobserver variability improve with training?

M. Hrabak Paar[1], J. Bremerich[1], A. Redheuil[2], T. Heye[1]; [1]Basel/CH, [2]Paris/FR

Purpose: Aortic strain is a widely used marker of aortic stiffness. Low variability of measurements is required for clinical and research purposes. In this study we evaluated the influence of self-paced training in ArtFun software on the intraobserver variability of aortic strain measurement using magnetic resonance imaging (MRI).
Methods and Materials: Fifteen patients (11 males, age 39-78 years) with arterial hypertension underwent cardiovascular MRI using a 3.0 Tesla MRI scanner. One axial gradient-echo cine image (TR/TE 50.8/4.2, slice thickness 6mm, 50 cardiac phases) of the chest at the level of the right pulmonary artery was acquired three times within an examination. To calculate aortic strain, largest and smallest cross-sectional area of the aorta was measured using ArtFun software three times in the ascending aorta by the same reader with 5 years of experience in cardiovascular imaging, before and after 3 weeks of self-paced training in abovementioned software. The paired-sampled sign test was used to compare the differences in the coefficient of variation (CV) of aortic strain measurement before and after training.
Results: The mean intraobserver CV before training was 11% (median 3.4%, range 0-55%), which was significantly higher than mean CV of 5% after training (median 1.7%, range 0-26%; p=0.01). The precision of the measurement also improved (SD 15% before training vs. 5% after training).
Conclusion: Even though reader was experienced, results show that with short training period results for reproducibility and precision improved significantly. The reader should familiarize with new software in order to achieve lowest possible intraobserver variability.

SS222

Exposure of the Swiss population by medical x-rays: 2013 update

R. Le Coultre[1], M. Champendal[1], D. Wittwer[2], P. Trueb[2], B. Ott[2], F. R. Verdun[1]; [1]Lausanne/CH, [2]Bern/CH

Purpose: Nationwide surveys on radiation dose to the population from X-ray image are mandatory to follow the trends in population exposure to strengthen radiation protection actions when required. The last survey in Switzerland was conducted in 2008 and the annual effective dose from medical radiology was estimated to 1.2 mSv per year and per inhabitant. The purpose of this work is to update the 2008's data by investigating the practice in 2013.

Methods and Materials: All university hospitals and radiological practices were contacted to either send their Tarmed data or answer to the Raddose website specifically developed for this survey. A representative sample of other practices is also including in the survey.

Results: All university hospital and about 30% of the contacted centers participated. Concerning the frequency of examinations the preliminary analysis of the results showed the following trends: radiography: no evolution; CT: increase by 15 to 20%; conventional fluoroscopy: reduction by 15%; cardiology: increase by 8%. CBCT represents 5% of the dental examination, 9% being OPG.

Conclusion: The major plus value of this survey is that the access to Tarmed data allowed to properly count the CT examinations (major weakness of our previous survey), get data concerning the gender repartition and provide annual trends from 2008 to 2013. From these results a slight increase in annual dose per inhabitant is expected. The final results of the survey will include the use of a generic dose vector (as previous surveys) and the use of actual delivered dose using DoseWatch and Radimetrics data.

SS223

CT in trauma patients: Automatic dose monitoring for demonstrating the effect of iterative reconstructions

K. Higashigaito, A. Becker, K. Sprengel, G. Wanner, H. Alkadhi; Zurich/CH

Purpose: To illustrate how automatic dose-monitoring software can be used in a clinical setting to control and reduce radiation dose of CT in polytrauma patients using advanced iterative reconstruction (IR).

Methods and Materials: 378 consecutive thoraco-abdominal CT examinations in polytrauma patients were identified using automatic dose-monitoring software (DoseWatch,GE). Patients were split into three cohorts depending on the scanner, protocol, and reconstruction algorithm: *cohort 1*: 64-slice dual-source CT without IR, tube current-time product 200mAs; *cohort 2*: 128-slice dual-source CT with IR and identical scan protocol; *cohort 3*: 128-slice dual-source CT with advanced modeled IR, tube current-time product 150mAs. Radiation dose parameters ($CTDI_{vol}$, DLP, and effective dose (ED)) were extracted using the dose-monitoring software; noise and image quality were determined and compared among cohorts.

Results: All CT examinations were of diagnostic quality. There were no significant differences between cohort 1 and 2 regarding $CTDI_{vol}$ (p=0.62), DLP, and ED (both p=0.95), while noise was significantly lower (chest and abdomen, both -38%, p<0.017). Compared to cohort 1, $CTDI_{vol}$, DLP, and ED in cohort 3 were significantly lower (all -25%, p<0.017), similar to the noise in the chest (-32%) and abdomen (-27%, both p<0.017). Compared to cohort 2, $CTDI_{vol}$ (-28%), DLP, and ED (both -26%) in cohort 3 was significantly lower (all p<0.017), while noise in the chest (+9%) and abdomen (+18%) was significantly higher (all p<0.017).

Conclusion: Automatic-dose monitoring software can be used in a clinical setting including a large cohort of patients for demonstrating and evaluating the effect of radiation dose lowering techniques.

SS224

Implementation of a dose monitoring software in clinical routine: First experiences with computed tomography scanners

C. Heilmaier, N. Zuber, D. Weishaupt; Zurich/CH

Purpose: Radiation exposure due to medical imaging considerably increased during the last decades, now making up almost 50% of the yearly background radiation exposure of the public. Especially, computed tomography (CT) contributes to irradiation. We therefore first implemented a dose monitoring software at our institute's 2 CT scanners.

Methods and Materials: We retrospectively analyzed dose data from June to September 2014 using GE's dose monitoring software DoseWatch® with reference levels set as 75th percentile. Analysis focused on number of alerts and reasons for alerts. Moreover, we compared data gained from our emergency CT (LightSpeed® VCT, GE) with that from our "clinical routine" CT (Discovery CT750 HD, GE, Milwaukee, WI).

Results: A total of 4,263 CTs were included in analysis. Of these 221 caused an alert: 66 (June), 61 (July), 43 (August), and 51 (September), respectively. Reasons were wrong protocol name (e.g. abdomen portal-venous chosen, but additional delayed phase scanned; 99/221), patient centering (not perfectly in isocenter of scanner; 26/221), scan repeat (e.g. due to severe motion artifacts; 13/221), osteosynthesis in situ (10/221), high body weight (68/221), and scan of the paranasal sinuses (5/221). Alert quota was relatively stable, fluctuating between 4.1-6.2%. When comparing both CT scanners we detected the following differences: more often scan repeat and wrong protocol name at emergency CT (possibly due to stress), while high body weight or osteosynthesis in situ were less frequently; no significant difference between scanners in patient centering and scan of sinuses.

Conclusion: Dose monitoring software provides important information useful to improve patients' safety.

SS225

Optimizing radiation dose by using advanced iterative reconstruction in high-pitch coronary CT angiography

S. Gordic[1], D. B. Husarik[1], S. Wildermuth[2], H. Alkadhi[1], S. Leschka[2]; [1]Zurich/CH, [2]St. Gallen/CH

Purpose: To evaluate the potential of advanced iterative reconstruction (IR) for optimizing radiation dose of 3rd generation 192-slice dual-source CCTA with prospective ECG-gating in the high-pitch mode.

Methods and Materials: CCTA at a pitch of 3.2 was performed in 50 consecutive patients (heart rate 49-74bpm). In the first 25 patients *(group 1)*, high-pitch CCTA was performed according to standard settings (reference tube voltage 100kVp, reference tube current-time product 270mAs/rot). Images were reconstructed with FBP and advanced modeled IR (ADMIRE, levels 1-5). In the latter 25 patients *(group 2)*, CT protocol parameters were adapted according to results from *group 1* (reference tube current-time product 156mAs/rot); images were reconstructed with ADMIRE level 4. In ten patients of *group 1*, image sharpness using signal intensity profiles across vessel borders were analyzed and the full-width-at-half-maximum (FWHM) was calculated. Image quality was assessed; radiation dose parameters were noted.

Results: None of the studies was of non-diagnostic quality. In *group 1*, the least IR-related image appearance was encountered with ADMIRE level 1. Images with ADMIRE level 4 were most often selected by both readers as preferred dataset, with an average noise reduction of 40% compared to FBP. Signal intensity profiles showed an increasing sharpness of vessel borders with increasing levels of ADMIRE (p<.05). Radiation dose in *group 2* (0.3±0.1mSv) was significantly lower than in *group 1* (0.5±0.3mSv;p<.05).

Conclusion: Advanced IR can be used for optimization of radiation dose in 192-slice dual-source CCTA in the high-pitch mode, resulting in an effective dose of 0.3mSv.

SS226

Real-time dosimetry as an optimization tool for radiation protection in interventional radiology

J. Binder, N. Icken, T. V. M. Lima, I. Özden, G. Lutters; Aarau/CH

Purpose: Medical staff performing x-ray supported interventions is among the professionals most highly exposed to ionizing radiation. To avoid the limitations of long term averaging inherent in the legally required TLD personal dosimeters and gain better insight into the circumstances of high exposure rates studies using a real-time dose reporting and recording system were performed.
Methods and Materials: The dosimetry system consisted of solid-state detectors connected wirelessly to a real-time display also offering the opportunity of reviewing the received dose rate curves. Each participant carried a dosimeter at chest level over the apron and simultaneously all interventions were recorded in a time-synchronized video to facilitate explaining significant exposure situations. The records were retrospectively analyzed to identify these situations and find reasons. Based on this learning sessions on radiation protection were prepared for the IR team presenting the results and most important findings.
Results: Observations in more than 50 interventions in 5 interventional radiology and angiology, 2 neuroradiology, 5 cardiology, 2 gastroenterology and 2 urology suites are reported showing very widespread distributions with standard deviations not rarely of 100% in cumulative dose, fluoroscopy time and dose area product even in equal procedure types.
Conclusion: Obviously poor or inadequate radiation protection equipment on site impeded low exposure and imprudent handling gave raise to unnecessary organ doses with special emphasis to eyes.
Conversely a concerned and well trained use of the equipment, careful selection of imaging protocols, predominant use of fluoroscopy modes and retrospective appraisal can significantly reduce the dose to patient and staff.

SS227

The more the merrier? About the definition of temporal resolution for blood velocity measurements: A multimodal study

T. Schubert, M. Pansini, O. Bieri, F. Santini; Basel/CH

Purpose: To analyze the spectral frequency content of the velocity signal of the arterial waveform in healthy volunteers in various anatomical locations with PC-MRI and Doppler ultrasound. The possibility of optimizing the temporal resolution to adapt it to the frequency content of the signal is also investigated.
Methods and Materials: Five healthy volunteers were scanned on a 3T whole-body scanner at 4 different anatomical locations: Common Carotid Artery, Aorta (ascending, descending), Femoral Artery. A retrospectively gated 2D PC-MRI sequence was applied. In addition, all volunteers underwent Doppler ultrasound measurements of the CCA and FA. The corresponding power spectrum of the velocity waveform was calculated. A cutoff frequency fmax was defined, containing 99% of the energy, and assumed to reflect the maximum frequency content of the signal.
Results: In the CCA, MRI gave a cutoff frequency fmax of 11.4±2.2 Hz, whereas Doppler revealed 13.2±2.8 Hz ($p>0.1$). For the FA, a fmax of 14.6±4.8 Hz was observed with MRI and 10.8±2.7 with Doppler ($p>0.1$). In the AAo and DAo fmax was 7.7±1.2 Hz and 9.2±0.9 Hz, respectively ($p=0.03$). The temporal signal retained its important characteristics up to a sampling rate of 25Hz in accordance with theoretical expectations.
Conclusion: Our analysis of the frequency content of the velocity waveform indicates that a true temporal resolution of 30 to 40ms is necessary to correctly retain the signal characteristics of the peripheral vessels. In the Aorta, this can probably be reduced to 50ms.

SS228

Accuracy of velocity measurements in small vessels by spectral and color Doppler ultrasound: Comparison of the built-in spectral analysis software against an automated color doppler analysis software.

A. Becker[1], M. Pinto[1], T. Frauenfelder[1], V. Klingmüller[2], M. Rominger[1]; [1]Zurich/CH, [2]Marburg/DE

Purpose: To assess the accuracy of spectral and color Doppler ultrasound for flow quantification in small vessels using a special flow phantom.
Methods and Materials: Constant, adjustable flow with a syringe-pump was our reference. Pulsatile flow was achieved by interposed reservoir compression using a motor driven lever arm. Flow within a silicone tube (0.5 mm) was measured with a linear-9-MHz-ultrasound-probe (GE Logiq E9). Mean velocity was measured with the built-in software in the whole pulsatile cycle and independently the antero- and retrograde flow components. Short color Doppler videoclips were assessed for mean velocity with a commercially available software (PixelFlux, www.chameleon-software.de). We used Bland-Altman Plots (systematic and random errors shown as mean deviation and two standard deviations) for differences in measurement techniques, as well as percentage calculation of flow deviation.
Results: In spectral Doppler constant flow assessment was more accurate than pulsatile flow. Smaller flow volumes were less accurate than larger volumes. Flow calculation based on independent assessment of flow components compared to whole automatic cycle assessment showed less systematic (0.07 vs -0.23 ml/min) and random errors (0.26 vs 0.37 ml/min).
PixelFlux allowed reliable, easy and fast flow measurements, though it systematically underestimated in our setting flow with -0.39 ml/min and showed greatest random errors with up to 0.86 ml/min.
Conclusion: Spectral Doppler analysis achieved exact mean velocity quantification in small vessels. Mean velocities based on color Doppler can be assessed with PixelFlux, though in our setting true mean velocity was systematically underestimated and random errors were larger.

SS229

Simple pulsatile flow phantom for validation and teaching of flow measurements in ultrasound

A. Becker[1], M. Pinto[1], T. Frauenfelder[1], E.-M. Müller-Stüler[2], M. Rominger[1], V. Klingmüller[1]; [1]Zurich/CH, [2]Marburg/DE

Purpose: To construct a simple phantom model to validate and teach and validate pulsatile flow and perfusion measurements in ultrasound.
Methods and Materials: Constant flow (0,3 - 4 ml/min) was obtained from a medical syringe pump (20 ml) for an out-bound silicone tube (inner lumen 0,5 mm). Pulsatile flow was achieved by compression of an interposed reservoir using a motor driven lever arm. Different flow patterns were pre-programmed into an integrated microchip controlling the electrical engine. Commercially available microbubble contrast media diluted in physiological saline solution served for ultrasound visibility. For imaging and flow analysis the tube was guided obliquely through a water bin. An ultrasound probe attached to a fixed rack was inserted into the bin parallel to the water surface.
Results: Exact flow of the syringe pump served for flow validation. The modulator was able to simulate different vascular and cardiac flow profiles including some flow disorders. Spectral flow analysis, color Doppler based flow measurements, as well as time intensity curves for perfusion imaging were derived. Peak velocities of 135 cm/s for 3 ml/min were achieved.
Conclusion: The phantom allows non-pulsatile and pulsatile flow and perfusion measurements. The small size and low cost make this model excellently suited for validation of flow quantification experiments or software, as well as skills lab teaching or standardized examinations.

SS230

Accelerated magnetic resonance diffusion tensor imaging of the median nerve using simultaneous multi-slice echo planar imaging with blipped CAIPIRINHA

L. Filli, M. Piccirelli, D. Kenkel, A. Boss, J. Richter, G. Andreisek, V. M. Runge, R. Guggenberger; Zurich/CH

Purpose: To investigate the feasibility of magnetic resonance diffusion tensor imaging (DTI) of the median nerve using simultaneous multi-slice echo planar imaging (EPI) with blipped CAIPIRINHA.

Methods and Materials: After institutional review board approval, MRI of the median nerves of eight healthy volunteers (mean age, 29.4 years; range, 25-32 years) was performed at 3.0T (Skyra, Siemens) using a 16-channel hand/wrist coil. An EPI sequence (b-value, 1000 s/mm^2) was acquired without acceleration as well as with 2-fold and 3-fold slice acceleration. Fractional anisotropy (FA), mean diffusivity (MD) and quality of nerve tractography (number of tracks, average track length, track homogeneity, anatomical accuracy) were compared between the acquisitions using multivariate ANOVA and Kruskal-Wallis test.

Results: Acquisition time was 6:08min for standard DTI, 3:38min for 2-fold and 2:31min for 3-fold acceleration. No differences were found regarding FA (standard DTI: 0.620±0.058; 2-fold acceleration: 0.642±0.058; 3-fold acceleration: 0.644±0.061; p≥0.217) and MD (standard DTI: 1.076±0.080 mm2/s; 2-fold acceleration: 1.016±0.123 mm2/s; 3-fold acceleration: 0.979±0.153 mm2/s; p≥0.074). 2-fold acceleration yielded similar tractography quality compared to standard DTI (p>0.05). With 3-fold acceleration, however, average track length and track homogeneity decreased (p=0.004-0.021).

Conclusion: Accelerated DTI of the median nerve is feasible. 2-fold acceleration yields similar results to standard DTI.

SS231

Sequence design optimization for acoustic noise reduction in MRI of the knee

C. Reisinger[1], F. Schwartz[1], M. Klarhöfer[1], D. Grodzki[2], A. Hirschmann[1]; [1]Basel/CH, [2]Erlangen/DE

Purpose: Prospectively assess acoustic noise levels and image quality while using a noise reduction algorithm on TSE sequences in knee MR imaging.

Methods and Materials: MRI examinations of the knee were obtained of 60 patients using a 3 Tesla whole body system with a standard knee protocol. Out of this protocol a standard TSE sequence (A) was adapted using a prototype noise reduction algorithm that smooths gradient pulses wherever possible while keeping imaging parameters constant (B). In total 3 different TSE sequences were evaluated (comparing A1-3 to B1-3). Acoustic noise was assessed quantitatively with a sound level meter and qualitatively on a 10-point scale (0=silence, 10= painful noise). Image quality was evaluated quantitatively by SNR and qualitatively by image impression. Significant differences between acoustic noise levels and SNR were sought using Wilcoxon signed-rank test.

Results: Acquisition time was identical for sequences A1-3 and B1-3 (2.53 min, 4.30min, 4.33min). Noise levels for the correlating sequences were 87.8 dB (A1), and 82.2 dB (B1), 93.9 dB (A2) and 83.0 dB (B2), 90.7 dB (A3) and 80.2 dB (B3), respectively. Noise levels as perceived by the patients were significantly lower when comparing sequences B (mean 4.5) and A (mean 6.4). SNR showed no significant differences when comparing sequences A (mean 73) and B (mean 71).

Conclusion: Noise reduction can easily be achieved by applying a noise reduction algorithm without changing imaging parameters and without relevant decrease of image quality.

SS232

Medical quality improvement of radiological reports using autodidactic teaching

A. Schiffmann[1], C. Westerhoff[2], A. H. Kaim[1]; [1]Aarau/CH, [2]Zurich/CH

Purpose: Quality management in medicine includes assessment and improvement of infrastructure, processes and quality of results in diagnosis and therapy. Topic of the underlying study is to measure the improvement of medical quality (MQ) in radiological reports (RR) after establishing a standardized feed-back process. The study examplarily considers MRI scans of knee and investigates the integrity, excellence and overall quality.

Methods and Materials: The integrity (12 anatomical structures) and excellence (sensitivity and specificity of pathologies) of 103 RR (written by 5 general radiologists, knee MR, standardized protocol) were retrospectively evaluated. Arthroscopy reports were used for gold standard. Subsequently, an autodidactic teaching period of 6 months followed by providing all radiologists with arthroscopy reports of patients who had undergone a knee MR scan. A second retrospective analysis of radiological reports (made after the self-responsible teaching interval)was initiated, using the same criteria and MRI.

Results of integrity were expressed by absolute values and 95% confidence interval, excellence by sensitivity and specificity, and overall quality by combined expression of interity and excellence. Statistical analysis (binominal test, p<0,01) was performed to compare quality before and after teaching.

Results: Integrity of RR definitively improved after teaching intervall. Sensitivity increased in many anatomical locations wheras specificity widely improved. Overall integrity significantly improved in all locations (p=0,0009-0,0098). The integrity was directly related to the excellence.

Conclusion: MQ in MR knee scans can be measured by determining integrity, excellence and overall quality of reports and improves by direct autodidactic training as it is possible with modern clinical information systems. However, oversensitizing may occur.

SS233

4D aortic haemodynamics in patients with Turner syndrome

J. Geiger[1], M. Neu[2], D. Hirtler[3], C. Gimpel[3], M. Markl[4], R. Arnold[5]; [1]Zurich/CH, [2]Mainz/DE, [3]Freiburg/DE, [4]Chicago/US, [5]Heidelberg/DE

Purpose: To apply flow-sensitive 4D MRI for the characterisation of aortic flow alterations in patients with Turner syndrome compared with aged-matched controls.
Methods and Materials: Flow-sensitive 4D MRI (venc=150cm/s, spatial/temporal resolution ~ 2.5mm³/38ms) was performed in 25 Turner patients and 16 age-matched female healthy controls (age=16±5 vs. 17±4 years). Blood flow was visualised by time-resolved 3D particle traces. Visual grading (ranking 0-2) of aortic flow disturbances (vortices, helices) was performed by two independent observers. Quantitative analysis included measurement of aortic diameters (normalised to BSA) and evaluation of peak systolic wall shear stress (WSS), pulsatility index (PI) and oscillatory shear index (OSI) at eight sites. For statistics Fisher exact-Test, unpaired t-tests and linear regression were applied.
Results: Patients had significantly more helices in the ascending (AAo) and descending aorta (DAo) compared to controls ($p<0.03$). Patients' vorticity was also increased in the AAo ($p=0.03$). The interobserver correlation for the helices and vortices in the AAo and DAo was excellent ($\kappa=0.71$-0.85). Patients with helices more than 1° and vortices over 0.5° in the AAo had significantly larger aortic diameters ($p=0.02$). WSS, PI and OSI were significantly decreased in Turner patients compared to controls ($p=0.02$, <0.003, <0.02).
Conclusion: 4D flow MRI gives an overview of aortic geometry and haemodynamics in Turner patients: They show increased helical and vortical flow patterns, decreased WSS and larger aortic diameters in AAo and DAo compared to healthy age-matched volunteers.

SS234

The pediatric dose-landscape in Switzerland - How homogeneous are the X-ray units used in pediatric radiology?

L. Hari, M. Ith, R. Wolf; Bern/CH

Purpose: The objective of the study was to determine the range of dose-variations of different X-ray units used in pediatric radiology by means of simulated patient doses for standard X-ray examinations, and the comparison of examination parameters.
Methods and Materials: The X-ray units of all pediatric radiology departments in Switzerland (11 sites) were characterised by a Barracuda dose measuring system for the determination of the entrance skin dose (ESD) and by a Diamentor CX for the measurement of the dose area product (DAP) for all pediatric age and weight categories. Chest, abdominal, pelvis, skull and spine radiographs were included.
Results: The study shows a considerable heterogeneity of patient doses. This can be explained by three factors: 1. heterogeneous exposure parameters of the applied examination protocols, 2. variable grouping and stratification of the patients (e.g. age categories), 3. device-specific differences (e.g. filter configuration).
Conclusion: The characterisation of the X-ray units demonstrates a distinct inhomogeneity of patient doses and therefore a major optimisation potential.
The establishment of national diagnostic reference levels (DRLs) could be a reasonable and effective incentive to achieve a harmonisation of pediatric patient doses.

SS235

Relevance of emergency brain CT for minor to moderate cranial traumas in children

F. Struebin, K. Wiskott, S. Hanquinet; Geneva/CH

Purpose: CT imaging is required in emergencies associated with minor to moderate traumas to the skull (MMTS) in children is often based on recommendations set by local institution but also on guidelines set by multicentric studies. The object of our study is to assess the relevance of brain CT in MMTS by analyzing our data in comparison to the literature and to re-affirm or amend our clinical guidelines.
Methods and Materials: 202 patients (1mo to 17yrs) who had undergone CT in the context of MMTS were included. Patients presenting Glasgow coma scales (GCS) < 10, multiple traumas and suspected child abuse were excluded. Data collection consisted: patients' history, clinical findings on admission, CT results and treatment.
Results: Lesions of brain and/or fractures were found in 25 % of CT (GSC 15: 23%; CGS 14: 22%; GCS 13: 50%) while the literature reports only 10%. The main predictors for pathological findings were: GCS < 13; age < 2 years; lesions of the scalp. No differences were found between patients with GCS 14 and 15. Surgical treatment was required in 18% of which category of the patients.
Conclusion: When faced with MMTS in children, clinicians do not seem to request an excessive number of CT investigations at our hospital. Still, we suggest further adaptation of the clinical guidelines for CT imaging to prevent needless x-ray exposure by considering the age of the patient first. A CT is mandatory for GCSs ≤ 13. A balanced judgment based on clinical findings is indicated for GCS 14 and 15.

SS236

Tibial bowing in children: A new measurement system and development of normal values

I. Zbinden[1], J. A. Jacobson[2], E. Rutz[1], O. Magerkurth[3]; [1]Basel/CH, [2]Ann Arbor/US, [3]Baden/CH

Purpose: To characterize normal values describing physiological tibial bowing with easy to define landmarks in all age groups on plain film of the lower leg.
Methods and Materials: IRB approval was obtained. Patients with normal plain films of the lower leg in anteroposterior (ap) and lateral (lat) views were included. Distance from the proximal to the distal corner of the metaphysis of the tibia (A), two lines proximal (prox) and distal (dist), each connecting the corners of the metaphysis (B, C) and a tangent (D) to the apex of the curved tibia were defined. Following measurements were obtained: Angle between A-B, angle between A-C, distance between line A-D(depth of curve). Normal values with 95% confident intervals were calculated by linear regression. Intra-/Interreader agreement were tested by using the paired-t-test and a Pearson-correlation.
Results: Over a 6years period 526 out of 4227 patients were included (292 males, 234 females, mean 6 years, range:0.1-16.8). Tibial angle ap was proximal 80°-100° (mean 87) and distal 82°-107° (mean 95). Tibial angle lat was prox 81-107° (mean 95) and dist 76°-102° (mean 88). Percentage of depth of curve was ap 0-11% (mean 7) and lat 2-13% (mean 7). Interreader-agreement showed no statistical significant difference and a high correlation ($p=0.3180$, $r=0.9997$). Intrareader-agreement was similar for Reader 1 ($p=0.2404$,$r=0.9990$), and Reader 2 ($p=0.1021$,$r=0.9720$).
Conclusion: Presented measurements assessing tibial shape allow reproducible results with high intra-- and interreader reliability. Normal values calculated in this study may allow to define abnormal tibial bowing in patients.

SS237

Value of plain skull x-ray imaging in long term follow up after cranioplasty for synostosis – A prospective study

R. Wolf, G. L. Kaiser; Bern/CH

Purpose: 1. Significance of plain x-ray in sagittal synostosis (SS) and deformational brachycephaly (DB) for work-up and follow-ups
2. Visualization of reossification by mosaic-like cranioplasty
3. Confirmation of results of clinical evaluation

Methods and Materials: Clinical and radiological work-up and follow-ups including anthropometry and craniometry (Haas). Comparison of results with those of earlier cohort without regular, mosaic-like cranioplasty. 17 infants with SS and 24 with severe DB were operated at median age 4.0 and 6.5 months from 2001-2003 by vertex and transposition craniectomy combined with mosaic-like cranioplasty. Prospective clinical and radiological follow-ups till 2013 with means of 7.8 and 7.3 years. 24 infants with earlier operated SS with mean follow-time of 9.7 years.

Results: Radiological follow-ups display visible remodelling of skull shape, significant change of cephalic index (CI): 67±3.9 vs. 77.6±3.7 in SS and 98±2 vs. 87.5±3.9 in DB at 1.5 years postoperatively and no significant change thereafter. Pieces of mosaic-like cranioplasty survive and lead to complete reossification. Remodelling of skull is superior to that of earlier cohort without need for secondary cranioplasty. Extent of correlation of radiological with clinical data are discussed.

Conclusion: X-ray and clinical examinations are complementary tools. At work-up SS without overt scaphocephaly and lambdoid synostosis cannot be recognized without x-ray. It is indispensable for comparison with follow-up x-rays by which objective quality control of surgery is more reliable, (re-)synostosis of sutures and residual skull defects is recognizable. Because of regular reossification in known period of time, x-rays can be reduced by >40%.

SS238

Post-operative brain imaging in children with congenital heart disease: Brain MRI protocol optimization

E. Hervier, A. Wanders, L. Merlini; Geneva/CH

Purpose: Post-operative neurological complications in children with congenital heart disease are common, however little is known about the physiopathology. The aim of our study was first to define what are the risk factors for developing neurological complications and second to retrospectively evaluate the most appropriate brain MRI protocol in order to understand the type and the timing of lesions.

Methods and Materials: We included every children operated for congenital heart disease in our hospital during the last 4 years. The analysis of the risk factors (age, type of pathology, surgery procedure...) was performed by uni- and multivariate statistics considering two groups of patients (with vs. without post-operative neurological complications). We reviewed the post- surgery brain MRIs from children who had neurological complications. Type of brain lesions and timing of appearance on the different MRI sequences were recorded.

Results: Among the 71 children, 20 had post-operative neurological complications. Older age at the time of surgery, cyanogen congenital cardiopathy and palliative surgery were identified as risk factors for neurological complications. Each MRI systematically included conventional sequences and Diffusion Weighted Imaging (DWI). Susceptibility Weighted Imaging (SWI) and Arterial Spin Labeled (ASL) were significantly less employed. SWI and ASL detected 100% of early lesions (< 3 days) in comparison to conventional sequences. Finally, SWI demonstrated a high sensibility for the early detection of microbleds.

Conclusion: An early corrective surgery can minimize the risk of neurological complications in patients suffering from congenital heart disease. ASL and SWI sequences provide valuable information for the early diagnosis of neurological complications and must be incorporated in the imaging protocol.

SS239

Osteochondritis dissecans in the adolescent elbow: Role of MRI in presurgical evaluation

N. Meunier Carus Vincent, S. Toso, L. Merlini, A. Dhouib-Chargui, D. Ceroni, S. Hanquinet; Geneva/CH

Purpose: MRI criteria for osteochondritis deissecans have recently been modified in the literature to avoid unnecessary suger. The aim of this study is to apply these diagnostic criteria restrospectively to our pediatric series of patients.

Methods and Materials: A retrospective case series of eleven children (10-16yrs) with osteochondritis dissecans of the elbow were identified betwenn June 2012 and october 201. Our standard MRI sequences included : 3D TRUFISP, T1 Sagittal, STIR coronal, and T2 axial images.MRI findings of high T2 ri, surrounding cysts, subchondral high signal T2 fracture line, and fluid-filled osteochondral defects were identified. MRI results were correlated with clinical evolution or arthroscopy (performed within 15 days of injury).

Results: In five children with none or only one criteria, arthroscopy demonstrated stable lesions. Tow of them had a favorabe clinical evolution and were treated conservatively. Three had persitent pain three month after the initial MRI, despite sport stoppage, and therefore underwent preventive surgical technique (drilling). In six patient with tow or more positive MR criteria, arthroscopy showed potential signs of instability, with susequent surgery for mbile fragment ablaion and chonral surface reconstruction.

Conclusion: MRI criteria seem to correlate well with arthroscopic findings, allowing prompt and adequate treatment, either conservative or by surgery (preventive or curative).

SS240

Imaging findings of torticollis in children

N. Stahr, I. Scheer, C. J. Kellenberger; Zurich/CH

Purpose: Torticollis can be secondary to an underlying congenital or acquired disease process. As torticollis is a non-specific clinical sign the spectrum of differential diagnoses is wide. The diagnostic imaging approach may be different depending on patient's age and clinical setting. The aim of this study is to describe the spectrum of typical imaging findings in children with torticollis.

Methods and Materials: All patients referred to our radiology department for evaluation of torticollis over a period of 7 years were reviewed. All imaging performed was assessed for pathologic findings. Radiology reports and medical charts were assessed for diagnosis and clinical setting.

Results: 174 patients (age range: 5weeks–16years) were referred with the clinical diagnosis of torticollis. Ultrasound was performed in 9%, radiographs in 63%, computed tomography in 30% and magnetic resonance imaging in 17%of cases.
In 64% of the patients diagnostic imaging did not reveal any pathology; in the remaining 36% (63 patients) underlying causes of torticollis could be diagnosed. Inflammatory causes were 25 cases of peripharyngeal infection, 8 cases of cervical lymphadenitis, 4 cases of otitis and 3 cases of cervical spine arthritis. 14 cases were of congenital origin including 6 cases of fibromatosis colli and 8 cases with vertebral anomalies. In 5 cases there were pathologic findings in the neuroaxis, 2 cases showed trauma related changes and another 2 were due to Langerhans cell histiocytosis.

Conclusion: Most common causes for Torticollis evident on imaging studies are inflammation and congenital anomalies. Mass lesions of the neuroaxis or destructive bone lesions are less common causes

NSS110

1,2,3-Triazole stabilized radiopeptidomimetics for improved tumour targeting

T. L. Mindt, I. E. Valverde, A. Macscarin, S. Vomstein; Basel/CH

Purpose: Radiolabelled regulatory peptides represent a key class of compounds for the development of tumor-targeting radiopharmaceuticals. A drawback of these peptides as vectors is represented by their inherent instability *in vivo* due to rapid degradation by proteases. It is known that metabolic stabilization of the peptide vector can result in an improved accumulation of the radiotracer in tumors. Not surprisingly, substantial research of the communities involved in the development of tumor-targeting peptides focuses on this aspect, however, with varying success.
Methods and Materials: We are exploring a novel approach for the stabilization of peptidic vectors by systematically replacing labile amide bonds with metabolically stable 1,2,3-triazole heterocycles as trans amide bond bioisosters. The introduction of 1,2,3-triazoles into the backbone of peptides by the Cu(I)-catalyzed azide-alkyne cycloaddition (CuAAC, click chemistry) is fully compatible with established solid phase peptide synthesis. The strategy was exemplified with the tumour-targeting peptides bombesin [Valverde et al. Angew. Chem. Int. Ed. 2013, 52, 8957] and neurotensin to which DOTA was conjugated to N-terminally for labelling with Lu-177.
Results: A series of novel peptidomimetics containing single or multiple triazole units were evaluated *in vitro* and *in vivo*. Some derivatives exhibit a significantly increased stability in blood serum while a nanomolar affinity towards the corresponding receptors is maintained. *In vivo* experiments with xenografted nude mice revealed an improved tumor uptake of the peptidomimetics in comparison to reference compounds.
Conclusion: The novel amide-to-triazole exchange strategy is a promising and universal methodology for the development of stabilized radiolabeled peptidomimetics with promising tumor-targeting properties.

NSS111

Comparison of alpha and gamma-conjugated folate derivatives for tumour imaging with PET

S. Boss[1], T. Betzel[1], C. Müller[2], S. Haller[2], V. Groehn[3], C. Fischer[1], R. Schibli[2], S. M. Ametamey[1]; [1]Zurich/CH, [2]Villigen/CH, [3]Schaffhausen/CH

Purpose: The folate receptor (FR) has emerged as an interesting target for imaging FR-positive tumors due to the overexpression of FR on a variety of epithelial cancer types. The two carboxylic functionalities at the alpha (α) and gamma (γ) positions of folic acid are accessible for chemical modification. We present the syntheses, biological evaluation and comparison of three pairs of fluorine-18 labeled α- and γ-conjugated folate isomers.
Methods and Materials: Click chemistry was used for the syntheses of the three different pairs of folate regioisomers (α/γ-FDG-, α/γ-fluoroethyl- and α/γ-fluorobutyl-folates). Binding affinities of the non-radioactive reference compounds to the FR were determined using FR-expressing KB tumor cells. The radiosyntheses of the fluorine-18 labeled analogues were established via nucleophilic substitution and subsequent coupling. The ^{18}F-radiotracers were evaluated *in vivo* using tumor-bearing mice.
Results: All synthesized folate regioisomers exhibited nanomolar binding affinities (IC_{50} values in the range of 1 to 18.0 nM). Biodistribution studies revealed slight differences in uptake favoring the α-regioisomers (FDG-folates, α:10.90±0.52%ID/g, γ:9.05±2.12%ID/g; fluoroethyl-folates, α:12.49±1.25%ID/g, γ:7.24±1.36%ID/g; fluorobutyl-folates, α:4.25±0.85%ID/g, γ:2.77±0.69%ID/g). However, liver uptake was up to two times higher for the γ-regioisomers in comparison to the α-regioisomers, whereas the kidney uptake was up to 50% lower for the γ-compounds. These results were also confirmed by *in vivo* PET imaging.
Conclusion: We concluded that the site of conjugation on the glutamyl moiety of folic acid has a significant impact on the *in vivo* behavior of radiofolates but not on their *in vitro* FR-binding affinity.

NSS112

152Tb and 68Ga-labeled DOTA-neurotensin analogues for targeting human ductal pancreatic cancers

D. Viertl[1], F. Buchegger[1], D. Tourwe[2], T. Stora[3], L. Bühler[3], J. Prior[1]; [1]Lausanne/CH, [2]Brussels/BE, [3]Geneva/CH

Purpose: Neurotensin (NT) receptors are overexpressed in several human tumours, such as pancreatic adenocarcinoma. We studied NT-analogues radiolabeled with 68Ga and 152Tb targeting human pancreatic tumours in mouse models.
Methods and Materials: MiaCaPa2 and Capan-2 human ductal pancreatic cancer cells both NT-receptor positive were grafted in SCID mice for biodistributions and microPET/CT imaging (Albira II, Bruker Biospin AG). Two NT-analogues were used: DOTA-NT20.3 (Ac-Lys(DOTA)-Pro-(NMe)-Arg-Arg-Pro-Tyr-Tle-Leu) and DOTA-NT20.3-Ile (Ac-Lys(DOTA)-Pro-(NMe)-Arg-Arg-Pro-Tyr-Ile-Leu) Ile replacing Tle like natural form of NT (Glu-Leu-Tyr-Glu-Asn-Lys-Pro-Arg-Arg-Pro-Tyr-Ile-Leu). The NT-analogues were radiolabelled either with generator-eluted ^{68}Ga or with ^{152}Tb produced at CERN using a high-energy proton beam and separated by online isotope mass-separation at ISOLD facility. Mice were injected with 0.1-0.2µg of ^{68}Ga or ^{152}Tb-DOTA-NT-analogues corresponding to 0.3-1MBq for biodistributions and with 1µg corresponding to 12.6MBq of ^{68}Ga-DOTA-NT20.3-Ile for microPET/CT. Biodistribution and microPET/CT imaging were done 90 minutes after injection.
Results: Labelling of ^{68}Ga and ^{152}Tb-DOTA-NT-analogues yielded radiotracers of high radiochemical purity. ^{68}Ga-DOTA-NT20.3 and ^{68}Ga-DOTA-NT20.3-Ile specifically localized in MiaPaCa2 and Capan-2 tumours. MiaPaCa2 tumours uptake was 3.3±1.6%ID for ^{68}Ga-DOTA-NT20.3 and 4.2±1.2%ID for ^{68}Ga-DOTA-NT20.3-Ile. Capan-2 tumour uptake for ^{68}Ga-DOTA-NT20.3-Ile was 5.2±0.8%ID. Kidney uptake was ranging from 4-6%ID and from 1.5-2.5%ID in small intestine. MicroPET/CT supported biodistribution results with a high tumour and kidney uptake and very low unspecific binding 90 minutes after injection.
Conclusion: ^{68}Ga and ^{152}Tb-DOTA-NT-analogues were specific for human pancreatic tumour with an excellent tumour-to-normal-tissue-ratio and may be valuable for clinical evaluation of NT receptor expressing tumours.

NSS113

Diagnostic value of 68Ga-NODAGA-MJ9 (bombesin) for the diagnosis of recurrent prostate cancer: A direct comparison study to 18F-FCH

P. Mitsakis[1], T. Zilli[2], M. Kosinski[1], H. Maecke[3], R. Mansi[3], F. Buchegger[1], R. Miralbell[2], J. Prior[1]; [1]Lausanne/CH, [2]Geneva/CH, [3]Freiburg/DE

Purpose: We wanted to compare the diagnostic accuracy of ^{68}Ga-NODAGA-MJ9 (targeting the gastrin releasing peptide receptors) PET/CT in recurrent prostate cancer (PC) in comparison to ^{18}F-FCH PET/CT.
Methods and Materials: NODAGA-MJ9 was radiolabelled with the eluate of a ^{68}Ge/^{68}Ga generator using an automatic processor unit (PharmTracer). ^{18}F-FCH PET/CT was performed with ^{18}F-labelled fluoromethycholine. We included 22 PC patients (average age 68±7y) treated by prostatectomy (18/22=82%) or radiation therapy without prostatectomy (4/22=18%) with biochemical PC relapse (PSA 5.0±4.0ng/mL [range 0.3-18.1]) and mean Gleason score 7.2±1.0 [5-9]. They underwent within a 10-day period ^{68}Ga-NODAGA-MJ9 (median=191MBq) and ^{18}F-FCH (median=201 MBq) PET/CT imaging 70 min p.i
Results: Thirty-seven lesions (7 local, 25 lymph nodes [LN], 5 bone) were detected in 15 patients using ^{68}Ga-NODAGA-MJ9, while 54 (7 local, 26 LN, 21 bone) were detected in 19 patients using ^{18}F-FCH. In 2 patients no lesion was found with both methods. Thirty-three lesions were detected on both modalities, 21 (1 local, 4 LN, 16 bone) only with ^{18}F-FCH and 4 (1 local, 3 LN) only with ^{68}Ga-NODAGA-MJ9. Of all 33 lesions detected in both methods, 25 presented higher uptake with ^{68}Ga-NODAGA-MJ9 and 8 were more intense with ^{18}F-FCH.
Conclusion: ^{18}F-FCH PET/CT detected more lesions, mainly in the bone, while for lesions seen with both modalities, ^{68}Ga-NODAGA-MJ9 uptake was more intense.

NSS114

Prognostic value of pretreatment 18F-FDG PET/CT volumetric parameters in patients with locally advanced larynx carcinoma treated with concurrent chemo-radiotherapy

G. Paone, G. Treglia, T. Ruberto, L. Ceriani, L. Giovanella; Bellinzona/CH

Purpose: The aim of this study was to assess the prognostic value of volumetric parameters measured on ^{18}F-FDG PET/CT determining event free survival (EFS) and overall survival (OS) in patients with locally advanced larynx carcinoma treated with concurrent chemo-radiotherapy.
Methods and Materials: We retrospectively analyzed 31 patients who performed a staging PET/CT for larynx carcinoma between 2008 and 2011. All patients had stage III-IV squamous cell carcinoma of the larynx treated with IMRT and concurrent chemotherapy. MTV, SUV max/mean and TLG were recorded. Univariate and multivariate analyses in association with Kaplan-Meier method were used to evaluate the prognostic value of these parameters considering EFS and OS.
Results: In the univariate analysis, MTV (>20cm^3) using a 2,5 SUV threshold had the best prognostic value than the other PET/CT parameters. We found a significant difference for predicting EFS (p<0,0001) and OS (p>0,0001) between the high MTV 2.5 (>20 cm^3) and low MTV 2.5 (≤ 20cm^3). In multivariate analysis, MTV and visual interpretation of local invasion remained significantly associated with EFS and OS (p= 0.012) while SUV max and TLG became non-significant (p=0.4 for EFS and p=0.7 for OS). At median follow up of 40 months the relapse rate was 42% (13/31 pts)
Conclusion: Our data suggest that the pre-treatment ^{18}F-FDG PET/CT MTV (>20cm^3) provide better prognostic information in patients with locally advanced larynx cancer than other PET/CT parameters. A 58% cure rate in this high risk population is encouraging and confirm that chemoradiation may be a therapeutic option.

NSS115

Primary mediastinal large B-cell lymphoma: Can we adopt Deauville score to assess end-treatment 18FDG-PET/CT? Results of the IELSG-26 study

L. Ceriani[1], E. Zucca[1], M. Martelli[2], P. L. Zinzani[3], A. J. M. Ferreri[4], U. Vitolo[5], P. Johnson[6], L. Giovanella[1]; [1]Bellinzona/CH, [2]Rome/IT, [3]Bologna/IT, [4]Milan/IT, [5]Turin/IT, [6]Southampton/UK

Purpose: To assess the accuracy of 18FDG positron emission tomography/computed tomography (PET/CT) after chemoimmunotherapy and involved field radiotherapy (IFRT), reported visually using the Deauville 5-points scale (DS), to predict outcome in patients with primary mediastinal large B-cell lymphoma (PMLBCL).
Methods and Materials: Among 125 patients prospectively enrolled, 88 were eligible for central review of PET/CT scans at the completion of treatment. According to the Lugano Classification a complete metabolic response (CMR) was defined by a DS ≤3.
Results: 78 patients (89%) achieved a CMR (DS 1,2,3). In the remaining 10 cases (11%), the residual uptake was slightly higher than the liver uptake in 6 (DS 4; 7%), and markedly higher in 4 (DS 5; 4%). Patients with a CMR after IFRT did not show relapse of disease at a median follow-up of 36 months, with a negative predictive value of 100%. In the PET-CT positive group only 3 patients had progression of disease after IFRT and died with a positive predictive value of 30%. All of these 3 cases were classified as DS 5, while patients with DS 4 had good outcomes without any recurrence. The DS ≤3 discriminated most effectively between high or low risk of failure, with 5-year PFS and OS of 100% versus 70% (P< .001 for both).
Conclusion: A CMR defined by a DS ≤3 identifies more than 90% of patients projected to be alive and progression-free at 5 years confirming the accuracy of the Lugano classification to predict the outcome also in PMLBCL patients.

NSS116

Comparison of detection rates for pulmonary nodules in tumour patients with PET alone, PET/low dose CT, PET/diagnostic thin slice CT and CAD

U. Bhure[1], A. Zander[2], L. Michel[2], H. S. Grünig[2], M. Pérez Lago[2], K. Strobel[2]; [1]Mumbai/IN, [2]Lucerne/CH

Purpose: To evaluate the detection rates of PET alone (PET), PET/low dose CT (PET/lCT), PET/diagnostic thin slice CT (PET/dCT) and CAD (computer aided detection – PET/CT/CAD) for pulmonary nodules (PN) in tumor patients.
Methods and Materials: The study encompassed 212 PET/CT investigation in 106 tumor patients (58 male; 48 female; age range: 22 to 93 years, mean age: 59.68 years). In all patients FDG PET images, low dose CT (5mm slice thickness) and diagnostic thin slice CT (1mm) were available and retrospectively evaluated for the presence of pulmonary nodules. Additionally images were retrospectively analyzed with a commercially available CAD software program (Lung VCAR, GE Healthcare). PN were defined as round nodules without calcifications or fat component.
Results: 74 PN were detected in 22 of 212 scans (9%) with PET, 112 PN in 56 scans (26%) with PET/lCT, 240 PN in 96 scans (45%) with PET/dCT and 410 PN in 124 scans (58%) with PET/CT/CAD. Tanking PET/CT/CAD as reference detection rates for PN of PET were 18%, 27% for PET/lCT, and 59% for PET/dCT.
Conclusion: Implementation of CAD for the detection of pulmonary nodules in PET/CT image postprocessing and reporting is feasible. The combination of diagnostic thin slice CT and CAD increases significantly the detection rate of pulonary nodules in tumor patients. The clinical relevance of the higher detection rates has to be evaluated in further studies.

NSS201

Treatment of Rip1Tag2 mice with PRRT using Lu-177-Exendin-4 and/or with the mTOR inhibitor Everolimus: Long-term survival analysis

O. C. Maas, V. Pretre, M. Fani, R. Mansi, R. von Wartburg, S. Vomstein, A. Wicki, D. Wild; Basel/CH

Purpose: Aim of this study is to evaluate the combined treatment of neuroendocrine tumours with PRRT and mTOR inhibitor Everolimus in a preclinical setting. Rip1Tag2 mice develop insulin producing tumours in the pancreas that are known to express GLP-1-receptor and being dependent on mTOR. This makes Rip1Tag2 mice ideal to study PRRT with Lu-177-Exendin-4 and Everolimus. We present results of long-term experiments tumour histology.

Methods and Materials: Rip1Tag2 mice were treated with Lu-177-Exendin-4 (2MBq day1, 1MBq day36), Everolimus 5mg/kg daily or every third day and combination of both. n=10 planned.

One series is carried out over 20days, a second series over a maximum of 9month. Besides tumour size and "survival", AKT/mTOR-pathway activity was immunohistochemically analysed.

Results: Preliminary long-term results (5-7 mice/group) showed minor prolonged survival for PRRT alone (37.8+/-11.9days) over control (27.3+/-5.9 days). Everolimus (73.1+/-14.1 days) as well as the combined treatment (>50days) clearly extended survival.

While treatment over 20 days with Everolimus daily lead to reduced tumour weight (41.8+/-40mg; control 73.4+/-26mg), Everolimus given every third day didn't alter tumour weight (81.5+/-44mg). Combination of Everolimus daily and PRRT showed high synergistic potential (7.8+/-10mg).

Histology showed no alteration in mTOR/AKT-pathway activity through PRRT but reduced activity in combination with Everolimus daily. Everolimus administered every third day showed paradox effects with a tendency to activate mTOR/AKT-pathway.

Conclusion: These results demonstrate efficacy of both treatments alone and the potential of combined treatment. Everolimus is only effective when given daily. Intermittent administration of Everolimus isn't effective, which explains previous contrary results published by Pool et al., CancerRes2013.

NSS202

Improved image contrast and therapeutic index of the antagonists 68Ga-OPS202/177Lu-OPS201 over the agonists DOTA-TATE/TOC: Preclinical results and translation in a phase I/II clinical study

G. Nicolas[1], R. Mansi[1], F. Kaul[1], S. Vomstein[1], J. Kaufmann[2], H. Bouterfa[2], H. Maecke[3], D. Wild[1], M. Fani[1]; [1]Basel/CH, [2]Berlin/DE, [3]Freiburg/DE

Purpose: We aim at evaluating a novel theranostic pair of the somatostatin receptor (sst)-antagonist Cpa-c(DCys-Aph(Hor)-DAph(Cbm)-Lys-Thr-Cys)-DTyr-NH_2 (JR11) for PET imaging and targeted radionuclide therapy of neuroendocrine tumours (NETs) and compared it with the clinically used compounds, DOTA-TATE and DOTA-TOC (sst-agonists).

Methods and Materials: Comprehensive biodistribution and pharmacokinetics studies of ^{177}Lu- and ^{90}Y-OPS201 (DOTA-JR11) and of ^{68}Ga-OPS202 (NODAGA-JR11) were performed in HEK-hsst2 xenografts and compared head-to-head to ^{177}Lu-DOTA-TATE/^{68}Ga-DOTA-TATE. A phase I/II clinical trial comparing 2 microdoses of ^{68}Ga-OPS202 PET/CT with ^{68}Ga-DOTA-TOC in the same patients with NETs is currently open for recruitment.

Results: ^{177}Lu-OPS201 vs. ^{177}Lu-DOTA-TATE showed a 2.6-times higher tumour dose but also 1.8-fold higher kidney dose. The therapeutic index, defined as tumour-to-kidney dose ratio, was increased by 34% in favour of ^{177}Lu-OPS201. For example tumour-to-kidney uptake ratio at 4h was 3.5±0.7, 3.9±0.5 and 4.2±0.6 for ^{177}Lu-DOTA-TATE, ^{177}Lu-OPS201 and ^{90}Y-OPS201, respectively. Importantly, increased amounts of ^{177}Lu-OPS201 (10-2000 pmol) significantly increased tumour-to-background ratios, i.e. tumour-to-liver from 16 to 84 and tumour-to-bone-marrow from 25 to 159.. Similarly, in the PET tracers, ^{68}Ga-OPS202 vs. ^{68}Ga-DOTA-TATE showed 1.7-fold higher tumour uptake, at 1h p.i. and higher tumour-to-liver and tumour-to-pancreas ratios. Results of the clinical trial will be presented.

Conclusion: Improved tumour-to-background ratios of ^{68}Ga-OPS202 in NET patients' holds promise for increased sensitivity in tumour staging. The increased tumour uptake and prolonged residence time of ^{177}Lu-OPS201 compared to ^{177}Lu-DOTA-TATE may improve the safety window of PRRT. The preclinical mass-dependent study provides important information that an optimized antagonist-mass is likely to reduce liver and bone marrow toxicity.

NSS203

New radiolabelled minigastrin derivitives for therapeutic application in medullary thyroid cancers

M. Behe, U. Reigl, A. Moscaroli, A. Blanc, R. Schibli; Villigen-PSI/CH

Purpose: The CCK-2 receptor is expressed in tumors like medullary thyroid carcinoma (MTC; >90%) and small cell lung cancer (>50%). Therfore different research project started in the late ninetie's to develop a suitable radiolabelled ligand for the CCK-2 receptor. The most promising compounds were developped based on minigastrin. But they suffer from a high kidney uptake and/or low in vivo stability.

We developped two new Lu-177 labelled minigastrin derivative (PSIG-1 and PSIG-3) with a low kidney uptake and evaluated them with respect to stability, internalisation, bindinging affinity and in vivo behaviour.

Methods and Materials: We radiolabelled DOTA-DGlu6-Ala-Tyr-Gly-Trp-Met-Asp-Phe-NH_2 (PP-F11; lead compound), DOTA-DGlu6-Ala-Tyr-Gly-Trp-Nle-Asp-Phe-NH_2 (PSIG-1) and DOTA-DGlu6-Ala-Tyr-Gly-Trp-Nle-Asp-Phe-NH_2 (PSIG-3) with Lu-177 and evaluated the compound for binding affinity to the CCK-2 receptor as well as the internalisation on a human MTC cell line. The biodistribution was performed in a s.c. model of this cell line at 1 h, 4 h and 24 h. The blocking experiments were performed at 4 h.

Results: All the compounds could be labelled with a high specific activity (~70 GBq/µmol) and high radiochemical purity (>95 %). IC_{50}-values for all compounds range from 20 to 50 nM. The highest internalisation rat was shown by PSIG-3. The biodistribution show high tumor uptake for all compounds (9-15 % i.A./g) and low kidney uptake (<5% i.A./g).

Conclusion: All three compounds show very promising properties with some advantages for PSIG-1/3. Remarkable is that the kidney uptake for all compounds is in the same low range indicating the high specific mechanism.

NSS204

Localisation of insulinoma: Comparison of Glucagon-like Peptide-1 Receptor (GLP1-R) SPECT/CT, PET/CT and MRI. Preliminary results of a prospective clinical study

K. Antwi[1], M. Fani[1], T. Heye[1], G. Nicolas[1], E. M. Merkle[1], J. C. Reubi[2], M. P. D. B. Gloor[2], E. Christ[2], D. Wild[1]; [1]Basel/CH, [2]Bern/CH

Purpose: We aimed at prospectively comparing the detection rate of GLP1-R PET/CT vs GLP1-R SPECT/CT vs standardized contrast enhanced 3T MRI in patients with endogenous hyperinsulinemic hypoglycemia. Preliminary results of an ongoing study are reported.

Methods and Materials: Twelve consecutive Patients with neuroglycopenic symptoms due to endogenous hyperinsulinemic hypoglycemia were enrolled. A standardized contrast enhanced 3T MRI was performed. Afterwards the patients received a SPECT/CT at 4 and 72 hours after injection of ^{111}In-DOTA-exendin-4 and a PET/CT 2,5 hours after injection of ^{68}Ga-DOTA-exendin-4 in a randomized order. Standard of comparison was the histological diagnosis after surgery.

Results: In 9 patients histological diagnosis confirmed benign insulinoma, 1 patient had adult nesidioblastosis. In 1 patient none of the imaging modalities were able to find any lesion. Another patient refused surgery despite a positive PET\CT scan. In 7/10 patients previously performed conventional imaging (CT/MRI) was not able to localize the insulinoma. Standardized 3T MRI was able to predict the exact localisation of the insulinoma in 7/10 patients. PET/CT correctly identified the insulinoma or nesidioblastosis in 10/10 patients whereas SPECT/CT correctly identified the insulinoma in 8/10 patients. PET/CT was the only modality which correctly identified the region of islet cell hyperplasia (adult nesidioblastosis) within the pancreas so far.

Conclusion: 1) These preliminary data suggest that PET/CT performs better as standardized MRI imaging and SPECT/CT at lower irradiation dose and much shorter investigation time than the latter. 2) Further studies will have to confirm whether PET/CT is able to localize adult nesidiblastosis.

NSS205

Clinical PET of neuroendocrine tumors (NET) with cyclotron produced 44Scandium: An alternative to short-lived 68Gallium

R. Schibli[1], N. van der Meulen[1], K. Domnanich[1], M. Bunka[1], A. Türler[1], I. Klette[2], A. Singh[2], N. Schäfer[3], R. P. Baum[2]; [1]Villigen PSI/CH, [2]Bad Berka/DE, [3]Zurich/CH

Purpose: ^{44}Sc is a promising λ+ emitter for PET ($t_{1/2}$ = 3.97 h, E_{β}+ 1475.4 keV, 94.34%) and could be an alternative to the currently-used short-lived ^{68}Ga ($t_{1/2}$ = 68 min). The aims of this study were to prove that ^{44}Sc can be routinely produced in amounts that allow the delivery of PET radiopharmaceuticals over long distances and to clinically assess ^{44}Sc-DOTATOC for the detection of NET.

Methods and Materials: The ^{44}Ca(p,n)^{44}Sc nuclear reaction was used (10 mg $^{44}CaCO_3$; 11.5 MeV, 75 µAh, 60 min) at the Paul Scherrer Institute. Separation was achieved via DGA and SCX cation exchange resins. $^{44}ScCl_3$ was shipped to the Zentralklinik Bad-Berka, Germany, where DOTATOC was radiolabeled according to the 68Ga-labeling procedure. ^{44}Sc-DOTATOC was applied in 3 patients with somatostatin receptor-positive hepatic metastases.

Results: Upto 2 GBq of ^{44}Sc (EOB) could be produced and isolated suitable for direct peptide radiolabeling. Quantitative radiolabeling was performed with 10 MBq ^{44}Sc/nmol of DOTATOC. Time-dependent whole-body PET/CT scans were performed at 10, 25, 60 min, 2, 4 16 and 23 h p.i. PET images allowed clear delineation of more metastases than detected by MRI and ultrasound (performed on the same day) as well as tiny new lesion, which were not detected by ^{68}Ga-DOTATOC.

Conclusion: The longer half-life of ^{44}Sc enables centralized production of peptide radiopharmaceuticals and delivery of multiple patient doses to remote PET centers. This, as well as the possibility of PET-scans at later time-point p.i. is an advantage compared to ^{68}Ga. Production scale-up is ongoing as well as dosimetric calculations.

NSS206

Prognostic value of GA-68-DOTA-TOC PET/CT prior to Y-90- or LU-177-Dota-Toc therapy in metastasized neuroendocrine tumour patients: Liver involvement predicts toxicity

Y. Anongpornjossakul[1], D. Wild[2], G. Nicolas[2]; [1]Bangkok/TH, [2]Basel/CH

Purpose: Peptide-receptor radionuclide therapy (PRRT) is efficient against metastatic neuroendocrine tumour (NET) but dose-limiting toxicities may occur. We therefore addressed the prognostic value of hepatic tumour load and its impact on hepatotoxicity after PRRT.

Methods and Materials: We included NET-patients treated with ^{90}Y-/^{177}Lu-DOTA-TOC and performed ^{68}Ga-DOTA-TOC PET/CT within 180 days before therapy start. Clinico-biochemical follow-up was obtained until death or at least 12 months after treatment. The onset of hepatotoxicity was characterized subacute or delayed when occurring within 3 or 12 months respectively. Hepatic tumour extension was assessed by 2 independent readers on ^{68}Ga-DOTA-TOC PET/CT and correlated with the severity of hepatotoxicity graded by CTCAE v4.0. Interobserver agreement was analysed.

Results: Fifty-eight patients were included (61 scans). Among patients with liver involvement <50% (n=50), 68% did not experience any subacute hepatotoxicity (grade 1: 18%, grade 2: 2%, grade 3: 6%, no grade 4). After a year of follow up (n=21), 62% showed no delayed toxicity (grade 1: 24%, grade 2: 14%, no grade 3 and 4). Patients with liver involvement >50% (n=11), 9% had no subacute hepatotoxicity (grade 1: 55%, grade 2: 18%, grade 3: 0% and grade 4: 9%). After a year, all available patients with liver involvement >50% (n=5) showed some degree of liver dysfunction with 3/5 patients (60%) grade 3-4 hepato-toxicity. Cohen's coefficient was >0,5.

Conclusion: Hepatic tumour burden >50% is associated with increased occurrence of subacute and delayed liver dysfunction after PRRT. Tumour load can be assessed visually with moderate interobserver-variability on pre-therapeutic ^{68}Ga-DOTA-TOC PET/CT.

NSS207

Comparison of FDG PET and CSF biomarkers diagnostic accuracy in clinical and preclinical Alzheimer's dementia

G. Amzalag, I. C. Mainta, O. Ratib, V. Garibotto; Geneva/CH

Purpose: Various biomarkers are used to support the diagnosis of Alzheimer's disease (AD), among these FDG PET imaging and the dosage of tau, phospho-tau and amyloid beta concentration in the CSF.
Aim of this study is to compare the diagnostic performance of these biomarkers in AD and in prodromal AD, i.e. MCI subjects converting to AD at 3 years follow-up.
Methods and Materials: We selected 45 healthy controls, 41 patients with prodromal AD and 51 patients with AD from the ADNI database. Among the subjects with prodromal AD, 14 converted to AD within 1 year (fast converters) and 27 converted within 3 years of follow up (slow converters).
In order to provide an objective metric of the presence of AD hypometabolism, we extracted mean relative glucose metabolism within a set of regions typically affected (metaROI), with a previously published approach (Landau et al., 2011). We used a Receiver Operating Characteristic (ROC) curve approach (Hanley et al., 1982).
Results: FDG PET and CSF -derived indices (tau/Abeta and phosphotau/Abeta) performed well to differentiate HC from clinical and preclinical AD, without statistically significant difference between the area under the curve (AUC) obtained by the different indices. The PET derived index had the best performance (AUC=.92) for fast converters.
Conclusion: FDG PET and CSF markers have a similar performance in identifying prodromal and clinical AD. FDG PET metrics perform especially well in MCI subjects 1 year or less before conversion, representing thus a very useful marker for short term cognitive deterioration.

NSS208

Prevalence of normal TSH levels in patients with thyroid autonomy detected by thyroid scintigraphy

G. Treglia[1], P. Trimboli[1], F. Verburg[2], L. Giovanella[1]; [1]Bellinzona/CH, [2]Aachen/DE

Purpose: International guidelines diverge significantly about the usefulness of thyroid scintigraphy (TS) in patients with nodular goiter. Particularly its role in detecting/excluding autonomously functioning thyroid nodules (AFTN) in patients with normal serum thyrotropin (TSH) is widely debated. Therefore we assessed the prevalence of normal TSH values among patients with AFTN detected by TS performed in our Center. Furthermore we carried out a meta-analysis of the literature to evaluate the usefulness of TS in European patients with AFTN and normal TSH values.
Methods and Materials: We included patients with AFTN detected by TS and enrolled at our Center. Pooled prevalence of AFTN with normal TSH values was calculated. Furthermore a comprehensive literature search of European studies published from 2000 up to 2014 on AFTN detected by TS was performed and a meta-analysis on the prevalence of patients with AFTN and normal TSH values was carried out.
Results: 110 patients with AFTN enrolled at our Center and 2662 European patients with AFTN described by six articles were selected for the meta-analysis. Prevalence of patients with AFTN and normal TSH was 35% in our Center. Pooled prevalence of AFTN detected by TS with normal TSH was 45% (95% confidence interval: 27-64%) on a per patient based analysis.
Conclusion: Serum TSH measurement is not an effective screening test to diagnose AFTN, at least in Europe, as a significant proportion of patients with AFTN detected by TS had a normal TSH value. TS remains the only technique that permits the diagnosis of thyroid autonomy which does not require invasive procedures.

NSS209

Potentiometric measurement of urinary iodine concentration in patients with thyroid diseases with and without previous exposure to nonradioactive iodine

G. Giovacchini[1], L. Giovanella[2], A. Haldemann[1], U. Staub[1], F.-G. Füchsel[1], P. Koch[1]; [1]Zurich/CH, [2]Bellinzona/CH

Purpose: Extensive application of measurement of urinary iodine concentration (UIC) in several benign and malignant thyroid diseases could profit by the availability of rapid and inexpensive measuring techniques. Aim of this study was to apply a simple and inexpensive commercially available potentiometric method for the quantification of UIC based on iodine-specific ion-selective electrodes (ISE) in patients with thyroid diseases.
Methods and Materials: This retrospective study included patients with differentiated thyroid cancer (n=286) and patients with hyperthyroidism of different etiologies (n=203). Within the whole sample (n=489) 20 patients had previously (1 week to 6 months) been exposed to iodine overload, either from contrast media (n=8) or amiodarone (n=12).
Results: In patients not exposed to iodine, the histogram showed that the distribution of UIC violated normality. The peak of the curve occurred between 5.0 mmol/L and 6.0 mmol/L. Variability was sizeable (percent coefficient of variation, %CV: 66%, 95% confidence interval: 1.48 –18.72 mmol/L). The group of exposed patients could be easily distinguished from not exposed patients (median UIC: 47.5 mmol/L vs. 5.42 mmol/L). UIC was significantly correlated to urinary creatinine concentration, but normalization to urinary creatinine increased the inter-subject variability of UIC (%CV = 96% vs. 66%). In test-retest studies (n=25) the intraclass correlation coefficient was 0.73 for UIC, 0.82 for creatinine and 0.64 for the UIC: creatinine ratio.
Conclusion: Iodine-specific ISE-based potentiometric methods can be successfully applied as an alternative to existing methods in patients with thyroid diseases. The promising characteristics of the method need to be confirmed in future larger prospective studies.

NSS210

Whole body Tc99m-HDP-SPECT/CT versus FDG-PET/CT for bone metastatic workup in breast cancer

S. Lee-Felker, C. Tabouret-Viaud, E. Felker, G. Amzalag, I. C. Mainta, O. Ratib, O. Rager; Geneva/CH

Purpose: Bone is the most common site of metastasis in breast cancer. Bone metastases are as well as or better detected using 18F-PET/CT than planar bone scan. The NCCN guideline proposes to get rid of bone scan when a 18F-PET/CT is performed. The aim of this study was to compare whole body SPECT/CT, to PET/CT in differentiating between benign and metastatic uptake on a per lesion and a per patient analysis.
Methods and Materials: 25 consecutive females (mean age (+/-SD): 55+/-13 y.o.) referred for a whole body SPECT-CT and a PET-CT of proven high risk breast cancer were included in this retrospective study. The findings from whole-body SPECT-CT, and PET-CT were compared with the results of imaging follow-up (median (+/-SD): 21 months+/-11.7).The free-response data were analysed by the jacknife free-response receiver operating characteristic (JAFROC) method and with the receiver operating characteristic (ROC) method.
Results: A total of 117 scored lesions were examined: 91 malignant, 24 benign and 2 excluded because of missing follow up data. In 2 by 2 comparisons, no difference was found significant in inferred ROC analysis whereas two differences were statistically significant in JAFROC analysis: the PET-CT figure-of-merit (FoM) was statistically significantly lower than the SPECT-CT (FoM difference = -0.11, 95%CI [-0.21;-0.02], p=0.021).
Conclusion: SPECT/CT was found to be more sensitive and more specific than PET/CT. Our results suggest that whole body SPECT/CT could be the modality of choice for metastatic workup in breast cancer.

NSS211

Acquisition and reconstruction optimisation in quantitative Y-90 PET/CT: An anthropomorphic phantom study

S. Gnesin, L. Paterne, A. Boubaker, S. Adib, M. Pappon, M. Kosinski, J. Prior, S. Baechler, F. R. Verdun; Lausanne/CH

Purpose: Post-radioembolization ^{90}Y biodistribution and dosimetry can be obtained from clinical quantitative ^{90}Y PET/CT to validate predictive dosimetry based on ^{99m}Tc-MAA SPECT/CT. The goal of this study was to determine optimal reconstruction parameters for quantitative ^{90}Y PET/CT acquisition of an anthropomorphic abdominal phantom

Methods and Materials: We performed time-repeated (1 per day, for 10 days) PET/CT scans (Discovery 690, GE-Healthcare) of an anthropomorphic abdominal phantom including a liver insert with 3 hot-spheres (20-30-40mm diameter). Hot-sphere to liver ^{90}Y activity concentration (AC_{bg}) ratio was 5:1. Initial liver background activity concentration was 1MBq/ml. The rest of the phantom volume was filled with water. AC_{bg} linearity as a function of time was assessed in the liver background. At each time point, recovery coefficients (RC, mean and max) and image noise (COV) was assessed as a function of reconstruction parameters: iterations (It=1, 2 and 3), frame duration (F_d=20, 30, and 45 min). The impact of Time-of-flight (TOF) information and point-spread-function (PSF) recovery where also assessed.

Results: TOF-based reconstructions provided AC_{bg} and RC convergence in 1 iteration, 2 iterations where required otherwise. Furthermore TOF reconstructions minimized spurious signal in region without activity concentration. Higher RCs were obtained for combined TOF+PSF reconstructions regardless other reconstruction parameter combinations (RC_{mean} from 0.45% in 20mm spheres to 0.65% in 40mm spheres). COV higher than 40% was found for AC_{bg}<200kBq/ml (F_d=30 min).

Conclusion: Combination of TOF and PSF optimize quantitative assessment in intrinsically low statistic ^{90}Y PET acquisitions. TOF-based reconstruction significantly reduced correlated noise and improves activity recovery convergence in clinical relevant conditions.

NSS212

18F-FDG-PET/CT for therapy control in vascular graft infections

B.-R. Sah, L. Husmann, D. Mayer, A. Scherrer, Z. Rancic, P. Stolzmann, R. Weber, B. Hasse; Zurich/CH

Purpose: The aim of this study was to evaluate the clinical value of positron emission tomography/computed tomography with ^{18}F-fluorodeoxyglucose (FDG-PET/CT) for therapy control in patients with prosthetic vascular graft infections (PVGI).

Methods and Materials: In this single center observational prospective cohort study, 19 patients were included who had a proven PVIG. Follow-up FDG-PET/CT was performed at a time interval of 170 ± 47 days after baseline examination. Two independent and blinded readers measured maximum standardized uptake values (SUVmax) to quantify metabolic activity and analysed whole body datasets for secondary diagnosis (i.e. other infectious foci). Metabolic activity of graft was correlated with laboratory biomarkers of inflammation (C-reactive protein and white blood cell count).

Results: FDG-PET/CT had an impact on patient management in all patients, as in 15/19 patients (79%) antibiotic treatment was not changed due to the results of follow-up FDG-PET/CT; in two patients (11%) treatment was stopped and in two patients (11%) antibiotic treatment was restarted. In six patients (32%) additional incidental findings were detected on follow-up FDG-PET/CT, which had further impact on patient management. Only in a subgroup of patients with a graft infection and no other sites of infection, a significant correlation between the difference in CRP at the time of baseline and follow-up FDG-PET/CT and the difference in SUVmax was detected ($n = 8$; $r = 0.84$; $P < 0.01$).

Conclusion: FDG-PET/CT allows for monitoring of PVGI and treatment response. It appears to be superior to blood biomarkers by suggesting alternative infectious sites impacting on therapeutic regimens.

PO01

Multi phase post mortem CT-Angiography (MPMCTA) versus MDCT to detect vascular bleeding source in patients with blunt pelvic trauma

M. Hussami, S. Grabherr, S. Schmidt, R. A. Meuli; Lausanne/CH

Learning Objectives: To compare intravenously contrast-enhanced multidetector CT (MDCT) with Multi-Phase Post-Mortem CT-Angiography (MPMCTA) for the detection of vascular pelvic bleeding.
Background: MDCT is the most common emergency examination to depict vascular lesions in polytrauma patients, often followed by immediate embolisation in case of contrast medium extravasation. Thus, the exact detection of vessel injury is mandatory.
MPMCTA has become a standardized technique for investigating vessel injuries in cadavers, mostly performed for medico legal reasons. Compared with clinical ante-mortem MDCT, MPMCTA is superior in detecting vascular bleeding, especially in venous lesions. This higher sensitivity is mainly related to the different injection conditions and acquisition parameters.
Imaging Findings or Procedure Details: The femoral cannulae are broader than the classical peripheral venous catheters allowing for higher pressure during contrast medium injection. Furthermore, a modified heart-lung machine clearly enables the administration of a higher volume of contrast agent composed of iodinated contrast media and paraffin oil, to keep the contrast media within the vessels and to clear the vessels from post-mortem clots. Finally, by performing 4 acquisitions, a non-enhanced, arterial, venous and dynamic phase, we obtain complete arterial and venous filling.
In MDCT, general vasoconstriction with other hemodynamic alterations occurring in polytrauma patients often hampers the clear visualisation of vascular injuries.
Conclusion: In blunt pelvic trauma situations, the venous and arterial pelvic bleeding sites are more precisely depicted by MPMCTA than by clinical ante-mortem MDCT. Nevertheless, using MPMCTA several limitations and artifacts need to be kept in mind.

PO02

Mp-MRI of the prostate in the detection of cancer

M. Martins Favre, S. Ropraz, P. Peteut, C. Colonneau, D. Flagner, B. Leffe, S. Regusci; Geneva/CH

Learning Objectives: To know how to perform a multiparametric MRI of the prostate.To demonstrate the useful of the PIRADS score.
Background: Prostate MRI has become an increasingly common adjunctive procedure in the detection of prostate cancer. This exam is mainly used in patients with prior negative biopsies and/or abnormal or increasing PSA levels, or before selected biopsy.
Imaging Findings or Procedure Details: The procedure of choice is multiparametric MRI, a combination of high-resolution T2-weighted (T2w) morphological sequences and the multiparametric techniques of diffusion-weighted MRI (DWI) and dynamic contrast-enhanced MRI (DCE-MRI). To improve the quality of the procedure and reporting, a group of experts of the European Society of Urogenital Radiology (ESUR) has recently published a guideline for MRI of the prostate. In addition to providing recommendations relating to indications and minimum standards for MR protocols, the guideline describes PI-RADS Classification: a structured reporting scheme based on the BI-RADS classification for breast imaging. This is based on a Likert scale with scores ranging from 1 to 5.
Conclusion: The main of this presentation is to demonstrate the performance of this exam in a private practice and the importance to work together with the urologist in order to improve the results of the biopsy and to propose the best treatment for the patient.

PO03

Percutaneous ultrasound-guided radiofrequency ablation (RFA) of pancreatic ductal adenocarcinoma

M. Pregarz[1], P. Tinazzi Martini[1], E. Barbi[1], R. Girelli[1], A. Giardino[1], S. Gobbo[1], R. de Robertis[2], M. D'Onofrio[2]; [1]Peschiera del Garda/IT, [2]Verona/IT

Purpose: The aims of the study are to evaluate the feasibility and the safety of percutaneous US-guided RFA of locally advanced non-resectable non-metastatic pancreatic ductal adenocarcinoma; to identify a follow-up program able to evaluate necrosis and cytoreduction effects induced by the procedure in the neoplastic tissue and to evaluate the quality of life and the survival rate of treated patients.
Methods and Materials: Fourteen patients with locally advanced pancreatic ductal adenocarcinoma of the pancreatic body have prospectically been treated with RFA. In every case the procedure has been performed by US-guided percutaneous approach. Every patient has been evaluated the day before, the day after and one month after the procedure by means of abdominal CT scan and serum level assessment of tumoral marker Ca 19-9.
Results: RFA procedure has been feasible in all cases. There were no post-procedural complications. In every case a complete necrosis has been obtained in the treated portion of the neoplastic tissue; necrosis extension was more than 50% of the whole tumor in 93% of cases, thus configuring a technical success. The mean extension of the necrotic area has been 70% of the whole tumor. The cytoreduction effect assessed by reduction/stability of tumoral marker Ca 19-9 has been obtained in more than 80% of the cases.
Conclusion: Percutaneous US-guided RFA of ductal adenocarcinoma has been proved a feasible and safe interventional procedure, resulting in possible neoplastic cytoreduction to be applied in a multimodality therapeutic approach for unresectable non-metastatic pancreatic ductal adenocarcinoma.

PO04

Renal volume measurements in polycystic kidney disease: intraobserver, interobserver variability and accuracy of MR segmentation algorithms

G. Wegmüller[1], A. Serra[2], J.-Y. Meuwly[1]; [1]Lausanne/CH, [2]Zurich/CH

Purpose: Total renal volume and enlargement of cyst-filled kidneys are reliable surrogate markers of the evolution of renal function in ADPKD. Renal volume measurements with MRI are performed in clinical practice in order to predict disease progression. The aim of our study was to evaluate the accuracy, intraobserver and interobserver variability of volume measurement of polycystic kidneys using segmentation algorithms currently used in clinical practice.
Methods and Materials: The volume of a homemade polycystic kidney phantom was segmented from transverse and coronal HASTE and T1 coronal images acquired at 1.5 and 3 Tesla. The volume of the 2 kidneys of the 37 patients were measured by one observer with the same algorithm and compared to the measurements obtained in clinical routine. Agreements were calculated with the Bland-Altman technique.
Results: All the algorithms produced bias in measurement. Measurements at 1.5T were more accurate than at 3.0T ($p<0.02$). Intraobserver analysis showed a concordance of 99.4%. Limits of agreement (LoA) were -70.20; 86.78 milliliters. Interobserver analysis demonstrated a concordance of 99.7%. A systematic bias of 8.84 milliliters was observed. Limits of agreement (LoA) were -72.32; 90.00 milliliters. Accuracy of measurements was higher for kidney <600 milliliters.
Conclusion: Accuracy of volume measurement of kidney in ADPKD with MRI is highly dependent of the segmentation method used. In order to lower the variability of the sequential measurements, the same technique has to be used for each subsequent control. Even with the best measurement method, LoA remains in a 90 milliliters range, what may decrease the objective sensitivity to renal enlargement

PO05

Dual-source single-energy computed tomography for tube voltage and contrast media dose reduction in varying abdominal sizes – A phantom study

D. Thor[2], A. Svensson[2], T. B. Brismar[2], M. A. Fischer[1]; [1]Zurich/CH, [2]Stockholm/SE

Purpose: To evaluate the potential of dual-source (DS) single-energy CT for reduction of tube voltage and contrast media (CM) dose while maintaining constant contrast-to-noise ratio (CNR) in comparison to single-source (SS) single-energy CT.
Methods and Materials: Four abdominal phantoms simulating a body-mass index (BMI) of 16 to 35 kg/m^2 were inserted with test tubes with varying CM concentrations and scanned using a 64-slice DS-CT scanner. Four low kV-protocols (70kV / 80kV) at SS and DS mode and eight different dose levels were designed to match a 120kV SS reference protocol.
Results: The potential CM reductions were determined to be approximately 53% for DS 70 kV, 51% for SS 70 kV, 44% for DS 80 kV and 40% for SS 80 kV (all differences were significant, P < 0.05). Constant CNR could be achieved by using DS 70 kV for small to medium phantom sizes (16-26 kg/m^2) and for all sizes (16-35 kg/m^2) when using DS 80 kV. Corresponding radiation doses increased of 60-107% and 23-83% respectively.
Conclusion: DS-CT can be used to reduce tube-voltage and therefore CM-dose in adult abdominal examinations, at the cost of an increased radiation dose. Thus, DS-CT might be suitable in minimizing CM-induced nephropathy in elderly patients; for whom an increased radiation dose could be of less concern.

PO06

Prostate MRI: Current Practice and Adherence to European Guidelines in Switzerland

B. Barth[1], A. Cornelius[2], S. T. Schindera[3], G. Bongartz[3], O. F. Donati[1]; [1]Zurich/CH, [2]Aarau/CH, [3]Basel/CH

Purpose: In order to strengthen its role in the diagnostic and therapeutic management of men with suspicion of prostate cancer, multiparametric magnetic resonance imaging (MRI) of the prostate should be acquired, interpreted and reported in a standardized manner. The purpose of this study was to analyze the current practice of prostate MRI in Switzerland and to establish its adherence to European guidelines.
Methods and Materials: A phone-based survey was conducted, contacting 118 radiologic institutes in the German-speaking part of Switzerland. Each survey was answered by one of the radiologists responsible for the MRI department. The survey consisted of questions regarding quantity, acquisition technique, interpretation and reporting of prostate MRI.
Results: Of the 69/118 (59%) radiologic institutions who completed the survey, 3 (4%) were university hospitals, 26 (38%) were public hospitals and 40 (58%) were private hospitals/institutes. Fifty-five of 69 (80%) institutions are performing prostate MRI examinations. Most of them (55%) perform 1-5 examinations per month. In 67% of cases, prostate MRI is performed using 3T and in 74%, no endorectal coils is used. In 80% of cases, the ESUR guidelines regarding prostate MRI are known and in 76% they are applied at least to a certain extent. Prostate MRI studies are reported in a standardized manner in 48% of institutions. Almost 80% of interviewed radiologists would be willing to participate in standardization of prostate MRI in Switzerland.
Conclusion: Acquisition, interpretation and reporting of prostate MRI in Switzerland is heterogeneous and there is a demand among Swiss radiologists for standardization of this examination.

PO07

Advanced virtual monoenergetic CT in hyper- and hypoattenuating liver lesions: Ex-vivo and patient experience in various body sizes

D. B. Husarik[1], S. Gordic[1], L. Desbiolles[2], S. Wildermuth[2], H. Alkadhi[1], S. Leschka[2]; [1]Zurich/CH, [2]St. Gallen/CH

Purpose: To compare attenuation, noise, CNR, and liver lesion conspicuity on advanced monoenergetic images(mono+) from dual-energy CT(DECT) in phantoms and in patients with HCC in comparison with standard monoenergetic images(mono).
Methods and Materials: Four anthropomorphic phantoms (S-XL) with a liver insert with iodine containing hyper- and hypoattenuating lesions were imaged with dual energy (100/150Sn kVp; 240/120 ref.mAs). Additionally four patients with HCC were imaged. Images were reconstructed with mono and mono+ at 10 kiloelectron volt (keV) intervals (40keV-190keV). Liver and lesion attenuation and noise were measured. CNRs were calculated. Lesion conspicuity was rated by two readers (1:lowest-5:highest conspicuity).
Results: Attenuation did not differ between mono and mono+ (p=0.41-0.49). Noise was significantly lower for mono+ (p<0.05). Hyperattenuating lesion CNR was highest for mono+ at 40keV and significantly higher for mono+ than mono in all phantoms (S:6.73 vs. 5.73-XL:1.89 vs. 1.37, all p<0.001). Hypoattenuating lesion CNR was highest for high-keV mono+ and significantly higher for mono+ than mono (S:3.12 vs. 2.41-L: 2.29 vs. 1.85, all p<0.001). In the XL phantom hypoattenuationg lesion CNR was significantly higher for mono. In patients, CNR curves of hyperattenuating HCC were in accordance with phantom data. Hypoattenuating lesions demonstrated varying curves. Interreader agreement for conspicuity was very good (ICC=0.95), with higher conspicuity for mono+ than mono.
Conclusion: Ex-vivo and patient data demonstrate stable attenuation, decreased noise, and increased CNR and lesion conspicuity on advanced virtual monoenergetic CT-images in small to large bodies with limitations in extra large bodies.

PO08

Reporting of hepatocellular carcinoma: comparison of interreader agreement between LI-RADS and standard Likert-scale in patients at risk for hepatocellular carcinoma

B. Barth, O. F. Donati, M. Fischer, E. J. Ulbrich, C. S. Reiner; Zurich/CH

Purpose: To assess interreader agreement in reporting of liver observations in patients at risk for hepatocellular carcinoma (HCC) using fixed Liver Imaging Reporting and Data System (LI-RADS) criteria or a Likert-scale (LIKERT) based on reader's impression.
Methods and Materials: The local ethics committee approved this HIPAA-compliant retrospective study. Eighty-four patients at risk for HCC with Gd-DOTA-enhanced liver MRI between 2005 and 2013 were included in this retrospective study. Four readers rated the likelihood of HCC for 104 liver observations using fixed LI-RADS criteria (LR1-LR5) and a 5-point LIKERT based on overall impression in two separate reading sessions. Major features (arterial-phase hyper-enhancement, washout, capsule appearance, threshold growth) were recorded. Interreader agreement was assessed using kappa-statistics (κ). Histopathology and imaging follow-up were used as reference standard.
Results: LI-RADS showed higher overall interreader agreement compared to LIKERT (κ, 0.44 and 0.35). For both LI-RADS and LIKERT experienced readers showed higher interreader agreement (κ, 0.58 and 0.41) than less experienced readers (κ, 0.39 and 0.25). Interreader agreement was moderate for arterial-phase hyper-enhancement (κ, 0.46), washout (κ, 0.48), capsule appearance (κ, 0.41) and threshold growth (κ, 0.43). HCC observations (n=55) were rated LR1 or LR2 in 6.4% (14/220), whereas 10% (22/220) were assigned LIKERT-scores 1 or 2. Non-HCC observations (n=49) were rated LR4 or LR5 in 25.6% (50/196), whereas 22.9% (45/196) were assigned LIKERT-scores 4 or 5.
Conclusion: LI-RADS shows higher interreader agreement than LIKERT and may therefore reduce variability in reporting of HCC.

PO09

Diffusion-weighted imaging of the prostate: Comparison of readout-segmented DWI and parallel-transmit-accelerated selective excitation DWI regarding image quality and distortion

B. Barth[1], A. Cornelius[2], D. Nanz[1], D. Eberli[1], O. F. Donati[1]; [1]Zurich/CH, [2]Aarau/CH

Purpose: To compare image quality and geometric distortion between readout-segmented DWI(rs-DWI) and parallel-transmit-accelerated reduced-FOV DWI(pTX-DWI) of the prostate.

Methods and Materials: Sixty-five patients underwent 3T-MRI of the prostate including rs-DWI and pTX-DWI (b-values,0,50,1000 s/mm²; ST, 3mm; in-plane resolution, 1.3x1.3mm²; acquisition time, 8:18min and 1:37min). Two readers assessed overall image quality(IQ), resolution, depiction of zonal anatomy and geometric distortion subjectively on a 5-point Likert scale. Quantitative analysis of geometric distortion was assessed by measurements of sagittal and coronal diameters on both DWI-sequences and compared to TSE-T2w.

Results: There were no significant differences regarding overall IQ (4.09±.66vs4.03±.79;p=433 and 3.86±.66vs3.80±.74;p=.465 for readers 1 and 2 respectively), image resolution (3.95±.65vs3.75±.94;p=.144 and 4.17±.73 vs4.02±.73;p=.111) or depiction of zonal anatomy (3.71±0.84vs3.75±0.94;p=.577 and 3.48±0.89vs3.62±0.84;p=.095) between rs-DWI and pTX-DWI, respectively. Geometric distortion was significantly lower on rs-DWI than on pTX-DWI (0.74±0.67vs1.17±0.84;p<0.001 and 0.55±0.64vs1.09±0.95;p<0.001 for readers 1 and 2 respectively). Sagittal and coronal diameters measured on rs-DWI correlated better with TSE-T2w-images (ICC,0.96 and 0.98) than pTX-DWI (ICC,0.89 and 0.96). On side-by-side analysis, rs-DWI was preferred in 57.7% of cases.

Conclusion: Despite a more than 5-fold shorter acquisition time of pTX-DWI, there was no significant difference in subjective IQ when compared to rs-DWI. However geometric distortion was significantly higher on PTX-DWI than on rs-DWI.

PO10

Advanced modelled iterative reconstruction for abdominal CT: Qualitative and quantitative evaluation

S. Gordic[1], L. Desbiolles[2], P. Stolzmann[1], S. Leschka[2], D. B. Husarik[1], H. Alkadhi[1]; [1]Zurich/CH, [2]St. Gallen/CH

Purpose: To determine qualitative and quantitative image-quality parameters in abdominal imaging using advanced modelled iterative reconstruction (ADMIRE) with third-generation dual-source 192 section CT.

Methods and Materials: Forty patients undergoing abdominal portal-venous CT at different tube voltage levels (90, 100, 110, and 120 kVp, n=10 each) and 10 consecutive patients undergoing abdominal non-enhanced low-dose CT (100 kVp, 60 mAs) in single-source mode were included. Images were reconstructed with FBP and ADMIRE (strength levels 1-5). Two blinded, independent readers subjectively determined image noise, artefacts, visibility of small structures, and image contrast, and measured attenuation in the liver, spleen, kidney, muscle, fat, and urinary bladder, and objective image noise.

Results: Subjective noise was significantly lower and image contrast significantly higher for each increasing ADMIRE strength level and also for ADMIRE 1 compared to FBP (all,P<.001). No significant differences were found for artefact and visibility ratings among image sets (all,P>.05). Attenuation was similar across tube voltage-image datasets in all anatomical regions (all,P>.05). Objective noise was significantly lower for each increasing ADMIRE strength level, and for ADMIRE 1 compared to FBP (all,P<.001, maximal reduction 53%). Independent predictors of noise were tube voltage (P<.05) and current (P<.001), diameter (P<.05), and reconstruction algorithm (P<.001); the amount of noise reduction was related only to the reconstruction algorithm (P<.001).

Conclusion: Abdominal CT using ADMIRE results in an improved image quality with lower image noise as compared with FBP, while the attenuation of various anatomical regions remains constant among reconstruction algorithms.

PO11

Non-invasive assessment of fibrosis and inflammation in rat kidney models with diffusion-weighted MRI

L. A. Crowe, I. Friedli, C. Vesin, L. Berchtold, P. Y. Martin, S. de Seigneux, J.-P. Vallee; Geneva/CH

Purpose: Chronic kidney disease (CKD) evolution is associated with renal fibrosis. We propose non-contrast MRI fibrosis assessment to potentially reduce the number of necessary renal biopsies. This animal study introduces pathology (after phantom/volunteer: ISMRM 2014) to evaluate Readout-Segmentation-Of-Long-Variable-Echo-Train (RESOLVE) diffusion-weighted-imaging (DWI) in well-controlled models, using clinical 3T MR.

Methods and Materials: The severe unilateral ureteral obstruction (UUO) model included 16 rats (internal control) and moderate interstitial inflammatory nephritis with bovine serum albumin (BSA) protein-overload, 8 rats (external control) with imaging up to 3 weeks later.

'RESOLVE' DWI measuring cortical ADC with 10 b-values, resolution 1.2*1.2*2.2mm, was compared to optimised single-shot-EPI. Correlations (Pearson's) were assessed with automated histological fibrosis quantification (Sirius Red, Imaris) and cellular infiltration H&E nuclei. ANOVA was statistically significant with p<0.05.

Results: Single-shot-EPI shows severe distortion (14% of kidneys not analysable). From RESOLVE, UUO had strong correlation between ADC and fibrosis (R2=0.7) and cellular infiltration (R2=0.9). There was no cellular infiltration correlation for BSA, but R2=0.4 with fibrosis. A significant difference is seen between control and UUO (p<0.03). For BSA, less histological fibrosis still gave significantly different ADC between groups (p=0.007), showing a low-detection limit sensitive to fibrosis <20%. Both models showed histologically different fibrosis with controls and UUO for cellular infiltration.

Conclusion: We overcame challenges to measure diffusion in rodent at 3T, an important translational step from model to clinic. RESOLVE considerably limits distortions that make standard diffusion non-exploitable. We demonstrated the new RESOLVE strategy with histological validation as strong incentive to apply RESOLVE to renal patients.

PO12

Renal versus splenic maximum slope based perfusion CT modeling in patients with liver cirrhosis and portal-hypertension

M. A. Fischer[1], K. Brehmer[2], A. Svensson[2], P. Aspelin[2], T. B. Brismar[2]; [1]Zurich/CH, [2]Stockholm/SE

Purpose: At maximum-slope based perfusion CT (P-CT) the time of peak splenic enhancement (PSE) is commonly used to define arterial (ALP) and portal liver-perfusion (PLP). However, PSE might be delayed in patients with portal-venous hypertension (PVH), while peak renal enhancement (PRE) should be insensitive to PVH. Thus, we aimed to evaluate time-to-peak of splenic ($TTP_{splenic}$) versus renal (TTP_{renal}) enhancement and P-CT parameters derived from PSE- versus PRE-based modeling in cirrhotic patients with different levels of PVH.

Methods and Materials: 24 cirrhotic patients (16 men; mean age 68±10), who underwent dynamic P-CT for evaluation of hepatocellular carcinoma (HCC) were retrospectively depicted to form three groups, (A) with-out PVH (n=8), (B) with PVH (n=8), and (C) with PVH and thrombosis (n=8). $TTP_{splenic}$ and TTP_{renal} were determined from the time-resolved data-set. ALP, PLP and hepatic perfusion-index (HPI) of the liver and HCC were determined using both PSE- and PRE-based modeling.

Results: TTP_{renal} was similar in groups-A/B/C (P>0.05), whereas $TTP_{splenic}$ was significantly longer in the PVH groups-B/C (P=0.02). In group-A, perfusion parameters (liver and HCC) were similar for PSE- and PNE-based modeling (all, P>0.05), whereas significant differences were seen for PLP and HPI in group-B and ALP in group-C respectively (all, P<.05).

Conclusion: $TTP_{splenic}$ is prolonged in patients with PVH, resulting in significantly different P-CT parameters of PSE- as compared to PNE-based modeling. Accordingly, $TTP_{splenic}$ might serve as a non-invasive biomarker of PVH, whereas maximum-slope based P-CT might be improved in patients with liver cirrhosis by replacing PSE with PNE.

PO13

In-vitro evaluation of a novel single-source dual-energy CT for urolithiasis: Comparison with dual-source dual-energy CT in material characterization and radiation dose

C. Zähringer[1], A. Parakh[1], A. Euler[1], F. Morsbach[2], D. Müller[2], G. Stadelmann[1], S. T. Schindera[1]; [1]Basel/CH, [2]Zurich/CH

Purpose: To assess the efficacy of renal stone characterization by a single-source dual energy CT (SS-DECT) using a gold and tin filter (TwinBeam Dual Energy, Siemens) compared to existing dual-source dual-energy CT (DS-DECT) in a phantom with standard and dose-optimized protocols.
Methods and Materials: Twelve urinary stones (diameter: 1-7 mm; chemical composition: six calcium, five uric acid and one cystine) were set in jelly-based phantom and placed in a water-containing cylinder simulating an intermediate-sized patient. Scans with dose-optimized and vendor-recommended protocols were performed on DS-DECT (Flash, Siemens; protocol A (dose-optimized) tube A, 100kVp, 90 reference mAs; tube B, 140kVp, 70 reference mAs; protocol B (standard) tube A, 100kVp, 210 reference mAs; tube B, 140kVp,162 reference mAs) and SS-DECT (Edge, Siemens; protocol C (dose-optimized) AuSn 120kVp, 258 reference mAs; protocol D (standard) AuSn 120kVp, 672 reference mAs). Images were evaluated using dedicated post-processing software. The detection and radiation dose were also analyzed.
Results: The accuracy for renal stone detection with protocols A-D was identical (nine out of twelve stones). Both dual-energy techniques characterized 77% of the detected stones correctly (seven out of nine). All protocols failed to characterize the visualized 2mm-sized uric acid and cystine stones, probably due to their small size. There was a reduction in radiation dose ($CTDI_{vol}$) between protocols A (4.4mGy) and B (10.3mGy) by 57 % and protocols C (5.07mGy) and D (10.6mGy) by 52 %.
Conclusion: The SS-DECT demonstrates same efficacy for renal stone characterization and detection as DS-DECT at similar radiation dose, even in dose-optimized protocols.

PO14

Can an advanced model iterative reconstruction technique improve the diagnostic accuracy of low-contrast lesions in abdominal CT at different tube voltages and sizes?

A. Euler[1], C. Zähringer[1], A. Hirschmann[1], C. Reisinger[1], R. Eichenberger[1], S. Kopp[1], D. Bürgler[1], A. Kircher[1], M. Streif[1], L. D'Errico[1], Z. Szuecs-Farkas[2], S. T. Schindera[1]; [1]Basel/CH, [2]Biel/CH

Purpose: To assess the low-contrast-lesion detectability and image quality of a novel iterative reconstruction technique (ADMIRE, Siemens) compared with filtered back projection (FBP) at four different tube voltages in abdominal CT of simulated intermediate sized and obese patients.
Methods and Materials: A custom liver phantom with 45 hypoattenuating lesions containing iodine (diameters: 5-15 mm; lesion-to-liver contrast: 10-50 HU) was placed in water containers mimicking an intermediate sized and obese patient (diameter: 30 and 40 cm). Scans were performed at 70, 80, 100 and 120 kVp (SOMATOM Force, Siemens). The 120 kVp protocol served as the reference protocol and the mAs of the other protocols were adjusted to keep the $CTDI_{vol}$ constant. The datasets were reconstructed using ADMIRE (strength 3) and FBP. Tumor detection was independently assessed by nine radiologists. CNR was calculated. Descriptive statistics and Fisher exact test were applied.
Results: The CNR was on average 28% higher for the intermediate and 34% higher for the obese phantom with ADMIRE compared with FBP. There was no significant difference in detection rate between ADMIRE (intermediate: 81.5%, 80.7%, 80%, 80.7%; obese: 56.7%, 64.1%, 63%, 64%) and FBP (intermediate: 80%, 80.7%, 79.3%, 79.3%; obese: 60.7%, 64.8%, 65.2%, 61.5%) at 70, 80, 100 and 120 kVp, respectively (p-value range: 0.43 to 1). Interobserver agreement was very good for both groups (λ-range: 0.81 to 0.9).
Conclusion: While ADMIRE improves substantially the quantitative image quality compared with FBP, there is no difference in the diagnostic accuracy at different tube voltages and sizes.

PO15

Analysis of image quality in thoraco-abdominal CT in new generation iterative reconstruction

S. Toso, A. Neroladaki, D. Botsikas, A.-L. Hachulla, C. D. Becker, X. Montet; Geneva/CH,

Purpose: To compare the effect of adaptive statistical iterative reconstruction at 40% (ASIR-40) and 100% (ASIR-100) and model based iterative reconstruction (MBIR) on image quality at decreased mA level and 100kVp.
Methods and Materials: A total of 286 adult patients underwent thoraco-abdominal CT between March and December 2012 for oncologic follow-up. CT was performed using routine protocols on a GE 750HD scanner. Dose was reduced incrementally every 20 patients by increasing the noise index. Data was reconstructed with ASIR-40, ASIR-100 and MBIR . Subjective analysis of overall image noise, lesion/organ conspicuity and overall image quality was performed by two radiologist, using an ordinal likert scale. Data was analysed using the Kruskal-Wallis test for non-parametric data. Objective analysis of constrast-to-noise ratio was assessed.
Results: Overall noise was unchanged for the thoracic CT component, even with dose reductions up to 50 %. Subjective noise and constrast-to-noise was significantly improved for the MBIR compared to ASIR for the abdomen, with dose reduction up to 50%, $p<0.05$. Lesion conspicuity was unchanged with dose reduction up to 50 % in thoracic CT but resulted in uninterpretable images using ASIR and diagnostic using MBIR in the abdomen. Lesion conspicuity was improved with MBIR at all dose levels compared to ASIR.
Conclusion: Lowering the dose of thoracic CT does not appear to effect image quality across the iterative reconstructive methods. With dose reduction in abdominal CT, overall noise and lesion detection are significantly improved with MBIR compared to ASIR-40 and ASIR-100 with dose reductions up to 50%.

PO16

Prognostic stratification and therapeutic response assessment in liver and pancreatic tumors: The new imaging

M. Pregarz[1], P. Tinazzi Martini[1], R. de Robertis[2], S. Gobbo[1], F. Scopelliti[1], P. Regi[1], I. Frigerio[1], M. D'Onofrio[2]; [1]Peschiera del Garda/IT, [2]Verona/IT

Purpose: To show and discuss possible applications of contrast-enhanced ultrasound (CEUS) quantification perfusion analysis, perfusion CT (pCT) quantification perfusion analysis and diffusion-weighted imaging (DWI) for the study of liver and pancreatic tumors for prognostic stratification and therapeutic response assessment.
Methods and Materials: Many authors have reported the usefulness of CEUS and pCT with enhancement quantification analysis for either prognostic stratification or therapeutic response assessment in the study of liver and pancreatic tumors. More recently DWI in the MRI evaluation of liver and pancreatic tumors demonstrated its capability for prediction and assessment of therapeutic responses.
Results: The use of CEUS, pCT and DWI in the liver can give added value to the study of hepatocellular carcinoma and hypervascular metastatic diseases while in the pancreas can add useful information in the study of ductal adenocarcinoma and neuroendocrine tumors.
Possible applications of CEUS quantification perfusion analysis, pCT quantification perfusion analysis and DWI in studying liver and pancreatic tumors for prognostic stratification and therapeutic response assessment, emblematic cases, imaging-pathologic correlations will be presented. Moreover a review of the most recent literature will be provided.
Conclusion: CEUS, pCT and DWI are attractive relatively new techniques giving to the imaging oncologic studies new possibilities of analysis able to provide not only morphological but function profiles of the liver and pancreatic tumors.

PO17

Pelvic MRI: Endometriosis, development and prospects

D. Keskin[3], A. Stolz[1], K. Kinkel[2]; [1]Geneva/CH, [2]Chêne-Bougeries/CH, [3]Neuchâtel/CH

Learning Objectives: We recall MRI techniques which can be useful in the endometriosis assessment.

Background: From a review of literature we propose a focus on technical advances in pelvic and abdominal MRI and their applications for endometriosis.

Imaging Findings or Procedure Details: Generally, standard protocol starts with 2D T2-weighted sequences in three different planes. The advent of 3D MR sequences involves evaluating its usefulness in deep endometriosis.

Then, two T1-weighted sequences, with and without saturation of fat are carried out systematically. It may be replaced by the simple DIXON sequence, based on the chemical shift.

Additional sequences: the diffusion imaging has, for the moment, limited value in the balance sheet of endometriosis. However it can be used to differenciate infiltrative digestive endometriosis of the colorectal carcinoma.

Diffusion tendor imaging (DTI) with tractography can reveal sacral root abnormalities in patients with endometriosis-associated pain.

As far as the assessment of endometriosis extension in the bowel, is concerned. The current gold standard, abdominal CT with intravenous injection of iodinated contrasted product, tends to be replaced by the contrast enhanced MR colography.

Also, MR urography has its place in the case of bladder and ureteral involvement.

Some authors consider contrast enhanced MR to have an additional diagnostic value in the intestinal endometriosis assessment. Dynamic MR imaging may be used to differentiate nodular endometriosis from other pathologic conditions of the abdominal wall and pelvis.

Conclusion: Multimodal MRI provides a reliable study in the various location of endometriosis, which are sub-peritoneal, pelvic, digestive, urinary and nervous.

PO18

Rare causes of dementia

J. Lieb, P. Hafner, J. Kuhle, M. Sollberger, C. Stippich; Basel/CH

Learning Objectives: The most common cause of « dementia » are neurodegenerative diseases, the most common one is Alzheimer`s. Beside second common causes such as vascular disease or normal pressure hydrocephalus, there are rare causes left in less than 5 % of patients, that might not be considered in dementia workup. Many of these rare causes can be treated.

Background: « Rare causes » of dementia are heterogeneous in origin consisting of infectious, inflammatory/autoimmune, toxic, inherited, metabolic, traumatic or neoplastic diseases. Only some of them present with specific imaging findings. Cognitive symptoms, clinical course, symptom onset and imaging findings differ from typical neurodegenerative disease, which makes the correct diagnosis more difficult and may lead to a substantial delay in treatment.

Imaging Findings or Procedure Details: We present an overview of rare causes of dementia to be considered in patients with « atypical » symptoms, young age of symptom onset or nonspecific imaging findings. This includes both, rare disorders that commonly cause dementia and more common disorders that rarely cause dementia. The presentation is completed with selected illustrative cases of rare causes of dementia with specific and nonspecific neuroimaging findings that have been collected from clinical routine.

Conclusion: Radiologists should be aware, that rare causes of dementia exist (other than Alzheimer`s or vascular disease) and that these disorders can present with atypical symptoms at younger age and various neuroimaging findings ranging from obvious to very subtle. In this context Neuroimaging can contribute substantially to a timely diagnosis and efficient treatment.

PO19

Brain morphometry in atypical parkinsonian syndromes: current status and new developments

M. Babaker[1], J. M. Grimm[1], C. Federau[2], R. A. Meuli[1], P. Hagmann[1], P. Maeder[1]; [1]Lausanne/CH, [2]Zurich/CH

Learning Objectives: The purpose of this poster is to review the current status of manual and automatic cerebral morphometric measurements and current knowledge about significant morphometric findings and their correlation in Parkinson Disease(PD), multiple system atrophy (MSA) and progressive supranuclear palsy (PSP).

Background: Clinical differentiation between PD, MSA and PSP may prove difficult, especially in the early stages of atypical parkinsonian syndromes. While still a developing field especially regarding automatic morphometry, studies have shown specific patterns in each condition that correlate with the clinical diagnosis.

Imaging Findings or Procedure Details: Pathological and MR imaging evidence has shown that the midbrain and the superior cerebellar peduncles(SCPs) are atrophic in PSP, whereas the middle cerebellar peduncles(MCPs) and the pons are mainly involved in MSA. Manual morphometry has been attempted by drawing anatomical reference lines in MR images; measurements of the midbrain area and SCP width in patients with PSP were significantly smaller than in patients with PD, with MSA-P and control participants. Automatic voxel-based brain morphometry has shown a cortical atrophy pattern, as well as subcortical atrophy in caudate nuclei, putamen and in the midbrain, in MSA-P compared to PD.

Volume-based morphometry is currently being evaluated in brainstem and striatum measurements in PD, MSA and PSP.

Conclusion: Manual and automatic brain morphometry measurements have shown significant correlation and differentiation between atypical parkinsonian syndromes, and are a useful tool especially when clinical differentiation proves difficult. Automatic morphometry is a promising tool that can easily be used in clinical practice; further developments, such as the use of voxel-based morphometry, are currently being studied.

PO20

Neurovascular compression of cranial nerves

L. Etienne[1], S. Haller[2]; [1]Geneva/CH, [2]Commugny/CH

Learning Objectives: To expose current knowledge of neurovascular compression syndromes.

Background: Neurovascular compression syndromes (NVCS) are caused by blood vessels, typically arteries, that have a direct contact and consequent irritation of cranial nerves. Not all cases of neurovascular contact are clinically symptomatic. We systematically review the transition zone between the central and peripheral myelin, which is the most vulnerable region for a symptomatic neurovascular compression syndrome.

Imaging Findings or Procedure Details: Systematic of the literature, illustration of normal anatomy and cases with neurovascular compression of the cranial nerves V, VII, VIII and IX

Conclusion: The exact anatomic knowledge of the transition zone between central and peripheral myelin is essential for the interpretation of neurovascular compression syndromes.

PO21

Differences in clinical characteristics of certain forms of temporomandibular joint disc displacement

T. Badel[1], M. Laškarin[2], D. Zadravec[1], S. Cimic[1]; [1]Zagreb/HR, [2]Šibenik/HR

Purpose: To compare clinical characteristics of partial disc displacement (DD) with other forms of DD of temporomandibular joint (TMJ).

Methods and Materials: A study included 92 patients (mean age 33.97, 80.4% female) with anterior DD of TMJ. There were 74 patients in the comparison of clinical characteristics of certain diagnoses of DD and they were required to have the same diagnosis of disc displacement in the left and right TMJ or just unilateral DD. Clinical diagnostics was confirmed by magnetic resonance imaging (MRI). Pain intensity was rated on a visual-analogue scale (VAS 1-10).

Results: The distribution of certain diagnoses of DD was balanced: partial DD with reduction (32.4%), total DD with reduction (32.4%) and total DD without reduction (35.2%). Pain on VAS was statistically higher on palpation in DD without reduction ($p=0.028$). Active mouth opening was significantly larger in joints with partial DD with reduction ($p=0.04$) than in other diagnoses of DD. However, in 30% of joints, both with diagnoses of DD with reduction there was no noise. Noise on palpation during mouth opening was statistically significant in comparison of all diagnoses of DD ($p=0.04$): clicking was more frequent in joints with reduction and it was not present in DD without reduction.

Conclusion: In this study significance was found for the following variables: pain intensity on palpation of TMJs, active mouth opening and noise in the joints. The use of MRI is needed to differentiate clinical symptomatology of other forms of DD.

PO22

Experimental setup of MR-compatible automated gait analysis

C. N. Bürki, J. Reinhardt, J. Benner, S. Bridenbaugh, R. W. Kressig, C. Stippich, M. Blatow; Basel/CH

Purpose: Normally, walking is a mostly automated behavior requiring minimal attention. Gait alterations under a dual task condition, i.e., walking while simultaneously performing a cognitive task, provide an indicator for changes in attentional processes. In geriatric clinical diagnostics electronic gait analysis with dual task is used to predict falling risk and cognitive decline. However, to date the neural correlates of divided attention processes in cognitive-motor dual tasks are not fully understood.
Methods and Materials: We designed an fMRI paradigm to reproduce as accurately as possible the electronic gait analysis and developed an fMRI compatible stepping device which allows recording stepping velocity and variability. In the motor single task condition participants lying in the scanner were asked to step on the device while mentally imaging that they were walking. Two cognitive single task conditions were included, a semantic memory task (word generation) and a working memory task (counting backwards). In the dual task conditions the motor task was performed simultaneously with the semantic memory task or with the working memory task.
Results: Results from 13 volunteers suggest that during the dual task conditions compared to the single task conditions primary motor areas are down-regulated while parietal regions are more activated.
Conclusion: We hypothesize that the latter pattern represents divided attention processes specific to cognitive-motor dual tasking. In a further study we aim at comparing the present findings to a sample of older adults. The long-term goal is to develop an fMRI tool for clinical diagnostics of cognitive disorders in aging.

PO23

Treatment of Distal Anterior Cerebral Artery Aneurysms using Minimally Porous Endoluminal Devices

D. W. Zumofen[1], E. Nossek[2], C. Stippich[1]; [1]Basel/CH, [2]New York/US

Purpose: Coil-embolization of wide-neck aneurysms often requires adjunct devices such as balloons- or stents. However, the use of adjunct devices is limited in the distal ACA due to the small diameter of the parent artery.
Methods and Materials: We have treated four unruptured distal ACA aneurysms by endoluminal reconstruction using the PED.
Results: Three aneurysms were of saccular configuration, and were judged inappropriate for classic surgical or endovascular strategies based on their geometry. The fourth was of fusiform shape, and had previously aborted clip reconstruction. The mean diameter of the ACA immediately distal to the AcomA was 2.6mm (1.7-3.7mm). The diameter tapered to 1.9mm (0.9-2.6mm) distal to the take-off of the pericallosal artery. A single PED was the sole treatment in three cases. Two telescoped PEDs were used in the fourth case. There were no new neurological deficits or radiographic evidence of ischemia. There was no artery occlusion of either of the parent vessel or of the associated branch vessel, which was covered in all cases. One patient showed immediate complete aneurysm occlusion confirmed on 3-month follow-up MRA. Two patients showed significant angiographic reduction of intra-aneurysmal flow immediately following PED deployment, resulting in complete angiographic aneurysm occlusion at 1year. The remaining patient showed immediate intra-aneurysmal contrast-stasis following PED deployment. This patient has not reached yet his fist angiographic follow-up interval.
Conclusion: Endoluminal reconstruction is a safe and effective treatment alternative for a carefully selected subset of distal ACA aneurysms. We advocate that the current generation of PED can be safely deployed in vessel smaller than 2mm.

PO24

Comparison of multi-institutional standardised presurgical language fMRI protocols

A. J. Tyndall, V. Epple, M. Blatow, J. Reinhardt, C. Stippich; Basel/CH

Purpose: FMRI is valid to localize and lateralize language function prior to brain tumor surgery. Still, imaging protocols and data processing are highly variable between medical centers limiting the comparability of clinical and research fMRI-data.
Methods and Materials: In a transatlantic multicenter trial 15 consecutive patients with language relevant brain tumors scheduled for presurgical fMRI were investigated prospectively using two different standardised imaging protocols employed in the US and Switzerland. Functional localisations (BOLD-signal characteristics, anatomical correlates, euclidean coordinates) and language lateralisation indices were analysed on an individual basis using BrainVoyager® and fMRI results from the different protocols were correlated statistically.
Results: Diagnostic BOLD-activation rates ranged between 97% (word generation US) and 78% (sentence generation CH). Functional localisations of Broca's and Wernicke's language areas and their right hemispheric anatomical homologues were highly congruent between protocols, except for 5 / 72 comparisons (7%). Language lateralisation in the 12 right-handers was also congruent except 2 patients for Wernicke's area.
Conclusion: Both, the US and Swiss standardised presurgical language fMRI protocols provided overall congruent information. Regarding language localisation the differences were close to chance-level. Differences in language lateralisation occurred in one patient between two US paradigms and in the other patient between a Swiss and US paradigm.

PO25

Traumatic aortic injury – What the radiologist needs to know

A. Kalovidouri, A. Platon, P.-A. Poletti, M. Scheffler; Geneva/CH

Learning Objectives: Pathophysiology of Traumatic aortic injury (TAI) involves application of shearing forces, bending, hydrostatic stress, and osseous pinch, resulting in transection, pseudoaneurysm formation, intramural hematoma, or focal intimal laceration. The most frequently affected part of the aorta is the isthmus.
Complications of TAI include hemomediastinum, hemothorax, and hemopericardium.
Radiographic findings of TAI without blunt aortic rupture are neither sensitive nor specific, but allow to rule out other life threatening conditions, such as tension pneumothorax.
Contrast-enhanced computed tomography (CT) is the imaging method of choice, with a sensitivity of 92-100% and a specificity of 62-100%. CT findings of TAI are intimal flap, focal intraluminal thombus, pseudocoarctation, focal bulging, and active contrast extravasation. Findings may be subtle in intramural hematoma or in moderate hemomediastinum, showing only periaortic fat stranding. Confirmed TAI is a surgical emergency. CT provides the surgeon with multiplanar reformations for treatment such as open surgery or endovascular stent graft placement.
Background: TAI is a frequent cause of death after rapid deceleration injury, as in motor vehicle accidents or fall from height. In patients surviving transport to the hospital, rapid diagnosis of TAI is lifesaving.
Imaging Findings or Procedure Details: The poster shows examples of each subtype of TAI from cases admitted to our institution during the last ten years.
Conclusion: TAI is a life threatening condition after rapid deceleration injury that demands immediate diagnosis and management. The gold standard for diagnosis is CT. The emergency radiologist must be familiar with the different subtypes of TAI, some of which may present only subtle findings on CT.

PO26

Modified contrast agent injection protocol using a multibolus technique for CT angiography: Impact on the aortic enhancement curve profile

M. Benz[1], J. Steinhauser[2], J. M. Fröhlich[2], G. Stadelmann[1], A. Willmes[3], A. Euler[1], G. Bongartz[1], S. T. Schindera[1]; [1]Basel/CH, [2]Zurich/CH, [3]Ulm/DE

Purpose: State of the art CT contrast agent (CA) power injectors are designed to enable multiboli injection protocols. The purpose of this study was to analyze the effects of various injection protocols on aortic enhancement curve profile in CT angiography (CTA).
Methods and Materials: A custom made physiologic flow-phantom was designed to mimic the cardiovascular system in an intermediate-sized patient. 80ml of Xenetix 350 (Iobitridol, Guerbet) were injected (CT-Motion, Ulrich Medical) according to a standard single-bolus injection protocol with a fixed flow-rate of 4ml/s (protocol A), a previously introduced protocol using exponentially decreasing CA flow-rates (4exp(-0.01t) mL/s) (protocol B), and a protocol with rapid intermittent administration of CA and saline boli (an initial CA bolus of 40ml was followed by intermittent administration of 8x5ml of CA and 8x5ml of saline) (protocol C). Dynamic CT-images (80 kVp, 200 mAs) were acquired after CA injection. Peak aortic enhancement (PAE) [HU], the duration of diagnostic aortic enhancement ≥200HU (t200) [sec.], and the area under the curve ≥200HU (AUC200) were recorded.
Results: Using optimized multiboli injection the duration of a diagnostic enhancement increased by 25% (A vs. C) while the PAE decreased (t200 averaged 24.6±0.3, 27.6±0.0, and 30.7±0.3sec., and PAE averaged 534.7±13.9, 431.7±4.5, and 391.0±3.6HU, for protocol A, B, and C, respectively). The AUC200 was comparable between protocols (9361.0±123.0, 9369.7±108.0, and 9385.0±62.6 for protocol A, B, and C, respectively).
Conclusion: Modified CA injection protocols using a multiboli technique substantially increase the duration of diagnostic aortic enhancement in comparison to a fixed injection-rate.

PO27

Tube voltage–adapted intravenous contrast media reduction in patients undergoing thoracoabdominal 192–slice CT–angiography

K. Higashigaito, T. Schmid-Rüegger, G. Puippe, T. Frauenfelder, T. Pfammatter, H. Alkadhi, D. B. Husarik; Zurich/CH

Purpose: To prospectively assess quantitative and qualitative image quality of thoracoabdominal CT-angiography (CTA) using automated attenuation-based tube voltage selection (ATVS) and tube voltage-adapted intravenous contrast media reduction.
Methods and Materials: 131 patients (69±11.7 years) underwent thoracoabdominal CTA with ATVS (ref.kVp=100, ref.mAs=130) with 192-slice dual-source CT. Intravenous contrast media (CM) volume was reduced depending on the automatically preselected tube voltage according to iodine attenuation curves derived from a phantom study (tube voltages from 70-150kVp at 10kVp intervals). CM volume and injection rate ranged from 75ml at 4ml/s at 120kVp to 40 ml at 2ml/s at 70kVp. Subjective (5-point Likert-scale: 5:excellent; 1:non-diagnostic) and objective image quality (aortic attenuation, noise and contrast-to-noise ratio [CNR]) were assessed. CT-dose-index ($CTDI_{vol}$) and dose-length product (DLP) were recorded.
Results: Four patients were imaged at 70kVp, 48 at 80kVp, 55 at 90kVp, 17 at 100kVp, 5 at 110kVp, and 2 at 120kVp. Diagnostic image quality was achieved in 97.7% of patients (excellent n=85; good n=37; moderate n=6, poor n=3). Mean aortic attenuation and CNR were 419.9±95 HU and 20±6.9, respectively, showing higher values at lower tube voltages (r = -0.39 and -0.40 respectively, both $p<0.05$). Mean CTDI and DLP were 2.8±0.9 mGy and 195.6±69.0 mGy*cm, respectively. Both values positively correlated with increasing tube voltage (r = 0.85 and r = 0.86 respectively, both $p<0.05$).
Conclusion: The combination of ATVS and tube voltage-adapted contrast media administration allows for considerable contrast and radiation dose reduction in thoracoabdominal CTA, while image quality remains diagnostic.

PO28

Tube voltage–dependent contrast media reduction in CT–angiography of coronary artery bypass grafts

K. Higashigaito, A. Plass, D. B. Husarik, F. Maisano, H. Alkadhi; Zurich/CH

Purpose: To evaluate tube voltage-dependent contrast media (CM) reduction in CT angiography (CTA) of coronary artery bypass grafts with automated attenuation-based tube voltage selection (ATVS).
Methods and Materials: Twenty consecutive patients (mean age 70±8.4 years) with a total of 63 bypass grafts underwent CTA with ATVS (ref.kVp=100, ref.mAs=200) with 192-slice dual-source CT. Intravenous CM volume was reduced depending on the selected tube voltage according to iodine attenuation curves derived from a phantom study. In-vivo, CM volume and injection rate ranged from 80ml at 7ml/s at 120kVp to 57 ml at 5ml/s at 90kVp. Image quality of proximal anastomosis, graft body, distal anastomosis and postanastomotic coronary artery was evaluated and objective image quality (attenuation, noise, and CNR) determined. $CTDI_{vol}$ and DLP were noted.
Results: Ten patients were imaged at 90kVp, two at 100kVp, two at 110kVp, and 6 at 120kVp. Diagnostic image quality was achieved in 97.5% bypass segments (excellent n=194; moderate n=21; poor n=3). Mean vessel attenuation and noise were 419.6±117 and 26±5 HU, respectively. CNR was significantly higher at lower tube voltages (r=-0.50 $p<0.05$). Mean $CTDI_{vol}$ and DLP were 4.2±0.9 mGy and 138.0±32.8 mGy*cm, correlating positively with higher tube voltages (r=0.62 and r=0.76 respectively, both $p<0.05$).
Conclusion: Combining ATVS and tube voltage-adapted CM administration allows for considerable contrast and radiation dose reduction in CTA of coronary bypass grafts.

PO29

Progression of thoracic aorta dilation in Fabry disease: a follow-up study

S. Hajdu, F. Barbey, A.-M. Jouannic, C. Beigelman, S. D. Qanadli; Lausanne/CH

Purpose: To evaluate the progression of thoracic aortic remodelling in patients with Fabry disease (FD).

Methods and Materials: 10 males (42±14 years) and 5 females (47±16 years) with FD studied at three time points (5±2 years and 8±3 years at first and second follow-up respectively) using serial cardiac magnetic resonance imaging (CMR) exams were included in our study. Average thoracic aorta diameter was measured at three anatomical levels: sinotubular junction (STJ), ascending aorta (AA), and brachiocephalic artery (BCA). Averages were compared and analyzed for statistical significance.

Results: Concomitant aortic dilation (>35 mm for males, >32 mm for females) in all three regions was observed in 5 male patients. Concomitant AA and BCA dilatation and isolated AA dilation was observed in 2 and 1 female patients respectively.

Initial and follow-up aortic diameters at the STJ were 30.9±4.0 mm (95% CI), 32.6±3.8 mm and 34.6±3.8 mm for males and 28.0±2.3 mm, 28.4±0.8 mm and 29.3±1.4 mm for females.

At the same time points, the diameters of the AA were 31.2±4.6 mm, 32.2±4.3 mm and 33.9±4.3 mm in males and 31.0±2.7 mm, 30.8±2.1 mm and 31.6±2.3 mm for females.

Aortic diameters at the level of the BCA were 30.0±4.4 mm, 31.3±4.0 mm and 33.1±4.1 mm for males and 30.5±4.2 mm, 30.4±3.2 mm and 30.1±3.2 mm for females.

Conclusion: Thoracic aortic diameter increase is observed on serial CMR at the STJ, AA and at the BCA exclusively in male patients with FD. A larger cohort would show statistical significance. No thoracic aorta increase was observed in their female counterparts.

PO30

Update in pulmonary aspergillosis syndrome

S. Hajdu, R. Vilarino, R. A. Meuli, S. D. Qanadli, C. Beigelman; Lausanne/CH

Learning Objectives: The diagnosis of pulmonary aspergillosis syndrome (PAS), a potentially life-threatening infection, is challenging due to its spectrum of radiological appearances that may alternate from one form to another. A review of the major computed tomography (CT) imaging characteristics of the three forms of PAS and their subtypes is presented.
Background: Various radiological appearances of PAS are observed primarily relating to immune status. The risk for invasive PAS, primarily described in patients with hematologic malignancy or leucopenia, is currently extended to other conditions such as transplant recipients, inherited immunodeficiencies, connective tissue diseases, end-stage liver disease, alcoholic hepatitis and illnesses requiring intensive care. Patients moderately immunocompromised or with underlying cavitary lesions such as tuberculosis may be at risk for chronic PAS. Asthmatics and patients with cystic fibrosis are mainly at risk for allergic bronchopulmonary aspergillosis.
Imaging Findings or Procedure Details:
1. Invasive PAS includes angio-invasive (AI) and bronchial-invasive (BI) forms.
   a. AI PAS may present as nodules with or without halo sign, wedge-shaped nodules, consolidation, with or without air-crescent sign.
   b. BI-PAS produces findings centered on airways.
2. Chronic PAS includes simple aspergilloma (SA) and chronic cavitary (CC) form.
   a. SA-PAS appears as a fungus ball within a cavity with thin walls.
   b. CC-PAS typically presents with thick-wall cavities and pleural thickening with or without fungus ball.
3. Allergic bronchopulmonary aspergillosis (ABPA) is characterized by proximal bronchiectasis occasionally with high-attenuated mucus plugs.

Conclusion: Understanding the CT aspects of PAS according to the patients' immune status and their alternating potential is valuable in routine practice.

PO31

Dual-energy CT imaging of pulmonary hypertension

A.-L. Hachulla, F. Lador, J. Gariani, C. D. Becker, M. Beghetti, X. Montet; Geneva/CH

Learning Objectives: To recognize signs of pulmonary hypertension (PH) on chest CT, appreciate the severity and allow follow-up under treatment.
To diagnose and characterize a potential underlying disease.
To assess lung perfusion using iodine maps provided by Dual-Energy CT (DE-CT).
Background: PH is a life-threating condition with an insidious onset. Patients have non-specific symptoms and always undergo a chest CT as part of their work-up.
Dual-Energy Chest CT is also an essential tool to characterize the cardiovascular and parenchymal changes of PH.
Imaging Findings or Procedure Details: Morphological signs of PH on enhanced chest CT include a) an increased diameter of the proximal pulmonary arteries with diminished peripheral vessels, b) mosaic lung perfusion, c) dilatation of bronchi, d) systemic arterial hypertrophy and shunts, and e) right cardiac changes.
Chronic thromboembolic pulmonary hypertension, or lung diseases such as pulmonary fibrosis or chronic obstructive pulmonary disease are important underlying causes of PH, identifiable on CT.
Dual-energy CT with functional analysis permits additional qualitative and quantitative insights of pulmonary perfusion by implementation of iodine maps, especially in the depiction of systematized perfusion defects or perfusion heterogeneity.
Conclusion: Chest DE-CT enables the simultaneous assessment of vascular anatomy, parenchymal morphology, cardiac changes and functional pulmonary imaging in PH.

PO32

Comparison of two-dimensional galactography versus galactography performed with tomosynthesis

F. Tobalem, C. Flick, C. Nakajo, L. Alamo, J.-Y. Meuwly; Lausanne/CH

Learning Objectives: To compare the diagnostic performance and image conspicuity of 2D galactography to galactography performed with tomosynthesis (3D).
Background: Twelve galactographies in 10 women with bloody or serous nipple discharge examined between June 2014 and December 2014 were retrospectively reviewed. Craniocaudal (CC) and mediolateral (ML) view of symptomatic breast were performed in tomosynthesis with synthetic reconstruction of 2D images after contrast injection in the discharging duct. Five radiologists independently reviewed the 2D and 3D images. Changes in diagnostic assessment and conspicuity of findings were evaluated. Wilcoxon sign rank test and kappa test were used for statistical evaluation.
Results: The mean age was 48 years [range 39-71]. Tomosynthesis did not change the diagnostic assessment. Conspicuity of findings was significantly improved with 3D imaging ($p<0.05$). Interobserver agreement was improved with 3D imaging ($k=0.4714$ for 2D, $k=0.6792$ for 3D).
Conclusion: Conspicuity of findings in galactography was significantly improved with tomosynthesis. Furthermore, interobserver agreement increased with 3D imaging.

PO33

Anti-allergic premedication in patients with contrast-medium-induced hypersensitivity: a view insight

I. Böhm, J. Heverhagen; Bern/CH

Learning Objectives: Clinical experience shows that anti-allergic premedication given to patients with a history of a contrast medium (CM)-related hypersensitivity reaction sometimes works, and sometimes not. Thereby, the question arises: why does it sometimes work, and why not?
Background: In order to answer these questions patients who received a premedication before they were given the CM were carefully retrospectively and qualitatively analyzed. In parallel we analyzed the available literature.
Imaging Findings or Procedure Details: In category I (premedication works) we identified at least two groups of patients: a) patients in whom the premedication successfully suppressed the CM-induced hypersensitivity, and b) patients who had tolerated the CM-injected even without a premedication. In category II (premedication does not work) we detected the following three subgroups: c) severe hypersensitivity that was not completely suppressed by the premedication, d) reactions that did not respond to the applied premedication (e.g. heat feeling, erythema, fixed drug eruption), and e) reactions which were not induced by the CM but by the drugs given as premedication or by other compounds and did not respond to the premedication.
Conclusion: We recommend the following points for a safe and effective application of a premedication: a causal analysis of the culprit agent, and a symptom-oriented premedication.

PO34

SOCRATES – a web-based standardized evaluation system to assess and advance competency and professionalism of radiology trainees

O. Kolokythas, M. Straka, R. Patzwahl, C. A. Binkert; Winterthur/CH

Learning Objectives: To introduce a standardized evaluation system for the promotion of competency and professionalism of radiology trainees. To shows its impact in the assessment of radiology trainees in a midsize teaching hospital.
Background: Developing competency in both specialty and professionalism is of pivotal importance for radiology trainees. Objective assessment and feedback during education and support of their development process is often hampered by absence of directives, uncertainty about assessment criteria and by lack of objectivism.
Imaging Findings or Procedure Details: SOCRATES (Standardized Online Competency Review and Advancement of Trainee Evaluation System) was developed to allow peers and trainees to rate performance and professionalism using a web-based standardized scoring system. Seven sections on medical knowledge, patient care, report creation, technical skills, professionalism, personal development and on-call performance are being addressed with a ten-point scale and by free text. The self-assessment module is displayed next to the peers' assessment for comparison. Longitudinal and horizontal personal and departmental tracking allow more objective and quantitative assessment of personal development. User access may be adjusted to allow for adequate confidentiality and transparency. After implementation over one year the system was shown to increase in the annual Swiss residency survey 2014 the frequency of feedback by peers: ratings increased from average of 5.1 (max. 6.0) in 2012 and 4.9 in 2013 to 5.9 in 2014, compared to national average of 4.9, 4.9 and 5.1.
Conclusion: The evaluation system allows an objective assessment for peers and self-assessment tool for radiology trainees to promote radiological education and professional development.

PO35

Experience in CT-guided interventions – an analysis of > 1000 procedures over an 18 month period

M. Pradella[1], T. Heye[1], C. Trumm[2], M. T.-L. Takes[1], A. Kircher[1], C. J. Zech[1]; [1]Basel/CH, [2]Munich/DE

Purpose: CT-guided biopsies and drainages are well established techniques most radiologists have been trained in. We investigated 1024 procedures in order to investigate the main factors that were influencing our results.

Methods and Materials: For every procedure we evaluated lesion size, distance from skin, procedure duration, radiation exposure and clinical success. Thereafter, all procedures were subdivided into biopsies of different regions: liver, abdomen (excl. liver), thorax and musculoskeletal system (MSK) or drainages from any site and grouped experienced versus inexperienced operators (under supervision) for further statistical analysis.

Results: The overall success rate was 93.6% and the success rate was not different for experienced versus inexperienced operators. In total, successful procedures were less difficult than unsuccessful ones although success did not generally transpose into a higher efficiency ($p<0.05$, $p=0.17$). Successful liver biopsies were more efficient due to the significantly smaller radiation dose ($p=0.006$, $p<0.05$ respectively). Furthermore, MSK biopsies and drainages had a smaller distance from skin / shorter procedure duration ($p=0.04$, $p=0.03$) which did not result in higher difficulty / efficiency ($p=0.72$, $p=0.80$).

Comparison of operators' experience revealed that experienced operators performed drainages more effectively ($p=0.02$) due to less radiation use ($p=0.004$). They also needed significantly less time for liver procedures ($p=0.005$), although they were facing smaller lesions ($p=0.03$). In failures their thorax lesions were significantly smaller in size ($p=0.04$).

Conclusion: CT-guided interventions offer high clinical success rates in various anatomical areas of the body. Though inexperienced radiologists showed that they need more time or radiation in some situations, they still perform as reliable as experienced operators.

PO36

Movement of steel-jacketed projectiles in 1.5 and 3 T MRI units

S. Eggert[1], R. A. Kubik-Huch[2], J. M. Fröhlich[1], D. Gascho[1], M. Thali[1], S. Bolliger[1]; [1]Zurich/CH, [2]Baden/CH

Purpose: Ferromagnetic bullets subjected to the static magnetic field of magnetic resonance (MR) units have shown dislodgment in air or gelatine. In MR scanning of deceased victims of gunshot injuries, the retained bullets did not always present consistent movement. We therefore examined further factors affecting ferromagnetic projectile movement in the magnetic field of not only 1.5 T, but also 3 T MR units focussing on the steel-jacketed Swiss ordnance ammunition 7.5 mm GP 11 Suisse.
Methods and Materials: Five 7.5 mm GP 11 bullets were embedded horizontally and vertically in 10% ordnance gelatine phantoms and then scanned with a 1.5 T and 3 T MR unit. Before and after each MR scan a CT scan was done and the movement of the bullets was measured. Magnetic polarisation of the bullets was measured by a needle compass.
Results: Movement of the bullets increased when subjected to a stronger magnetic field (max. absolute movement 1.5T: 24.4 mm vs. 3T: 101.5 mm). The orientation of the bullet towards the gantry influenced its mobility (horizontally embedded projectiles showed poor movement, vertically embedded ones strong movement). One of the bullets showed an 180° flipping due to the 3 T magnetic field. Magnetisation and changing the polarization of these ferromagnetic bullets is possible.
Conclusion: Not only the location of a bullet within a patient, but also its orientation toward the gantry must be taken into account for when assessing the risk of performing an MR examination on a gunshot victim.

PO37

Proposal and evaluation of a parameter free segmented multistep algorithm to assess diffusion data with a combined IVIM-DKI Model

L. Filli, M. Wurnig, D. Kenkel, A. Boss; Zurich/CH

Purpose: Recently a parameter-free version of the very commonly used segmented multistep-procedure for analysis of the intra-voxel incoherent motion model (IVIM) was proposed. In this study we expanded the proposed algorithm for a combined IVIM-diffusion-kurtosis-imaging (DKI) model of diffusion and evaluated its performance regarding the resulting goodness-of-fit.
Methods and Materials: Diffusion data-sets of 6 healthy subjects were acquired in a 3T MR scanner using 16 different b-values during free breathing. Signal-intensity-curves as a function of the b-value were obtained in liver, pancreas, spleen, kidneys and skeletal muscle via ROI-analysis. For analysis an expanded version of the recently described parameter-free segmented approach was used. Goodness-of-fit was assessed using Akaike's Information-Criterion (AIC). Furthermore parametrical-maps for the different parameters of the assessed diffusion-models were computed.
Results: Mean D-values significantly increased in all assessed organs when using the IVIM-DKI-model in comparison with the simpler IVIM-model (all $p<0.02$). AIC values indicated a significantly better fitting-curve in liver, pancreas and renal medulla (all $p<0.02$). No significantly different fitting-curve could be found in renal cortex, spleen and skeletal muscle. Parametrical-maps for all free parameters of the evaluated diffusion-models could be obtained in appropriate image quality.
Conclusion: We could show that usage of a combined IVIM-DKI-diffusion-model leads to significantly better fitted signal- decay-curves in tissues such as liver and pancreas when compared to the simpler IVIM-model. Therefore we conclude that this model more accurately describes the behavior of tissue in diffusion experiments and might be used in the future for more precise tissue characterization including non-Gaussian diffusion behaviour without organ-specific adaptations.

PO38

Risk factors for contrast-induced nephropathy: Results of a prospective CT-study

I. Böhm[1], M. Gurschi[2], A.-C. Stamm[1], K. J. Klose[2], J. Heverhagen[1], H. Alfke[3]; [1]Bern/CH, [2]Marburg/DE, [3]Lüdenscheid/DE

Purpose: To analyse the frequency of contrast-induced nephropathy (CIN), to detect risk markers and to provide risk assessment for contrast medium (CM)-enhanced computed tomography (CT).
Methods and Materials: Adult patients were prospectively enrolled. Data collection comprised of patients' demographics, their medication, applied CM and dose. In pre- and post CM-dose (48h and 7 days) blood samples we measured serum creatinine (SCr), blood urea nitrogen (BUN), and others. Creatinine clearance (CrCl) was calculated by the Cockcroft-Gault, and eGFR by the MDRD equation.
Results: 200 patients were evaluated. 48h after CM-administration CIN (SCr increase ≥ 25%) occurred in 12 (6.5%) patients. Eight patients were classified as mild (grade I), and four as moderate CIN (grade II); severe CIN (grade III) did not occur. As relevant risks we identified proteinuria ($p < 0.005$), nephrotoxic medication ($p < 0.003$), high single CM-dose > 2.2 mL/kg ($p < 0.005$), Cigarroa > 2 ($p < 0.02$) and CM-double-dose (i.v. and oral) ($p < 0.0003$).
Conclusion: This study for the first time highlighted nephrotoxic medication and CM double dose as relevant risks for CIN, and introduced a severity grading for CIN. To prevent CIN in patients at risk it is recommended a) to carefully screen for CIN relevant risk factors, b) to exactly document the patients' complete medication, c) if indicated and possible to stop nephrotoxic medication for 2-3 days after CM-injection, and/or d) to possibly omit both high single and CM double doses.

PO39

Comparative patient dosimetric estimates for different radiological facilities when performing maxillofacial examinations

M. Sans Merce[1], J. Damet[1], M. Becker[2]; [1]Lausanne/CH, [2]Geneva/CH

Purpose: Maxillofacial radiologic examinations often result in irradiation of the thyroid gland, parotid glands and lens due to primary exposure or radiation scatter. Organ exposure depends on imaging modalities and protocols. The purpose of this investigation was to evaluate radiation doses to the above-mentioned organs for CT, cone beam CT (CBCT) and panoramic radiographs (orthopantomography, OPT).
Methods and Materials: The absorbed dose was measured on the surface of a head phantom with thermoluminescence dosimeters. The phantom was imaged with CT, CBCT and OPT using standardized protocols employed in clinical routine. The areas examined included the paranasal sinuses, the entire head and the mandible depending on the protocol used. Dose measurements were performed individually for each modality and each protocol.
Results: Doses to the thyroid gland when located outside the area of interest were lowest for all modalities (range: 0.01-1.22mGy; measurement uncertainty: 10% at $k=2$). Depending on the examination protocol, doses to the eye lens (due to primary beam or scattered radiation) showed wide variability (range: 0.02 - 26.22mGy). The parotid glands were the only organs systematically placed in the primary beam for all modalities and protocols. Values ranged from 1.40-29.11mGy with the highest values for CT examinations. For OPT, doses to the parotid glands were strongly inhomogeneous due to its operating mode.
Conclusion: CT was the most irradiating modality. The mean doses to the parotid glands were similar for CBCT and OPT, while doses to organs in the scattered field were systematically higher for CBCT than OPT.

PO40

Towards an objective way to assess image quality in CT

D. Racine, N. Ryckx, A. Ba, J. Ott, F. Bochud, F. R. Verdun; Lausanne/CH

Purpose: Patient dose optimization in Computed Tomography (CT) has to be done using clinically relevant tasks when dealing with image quality assessments. We will report the performances of more than 50 CT unit installed in Switzerland, using a model observer (MO) that mimics human detection of low contrast targets.
Methods and Materials: A dedicated phantom (QRM, Moehrendorf, Germany) containing spheres (5 and 8 mm diameter; 10 and 20HU at 120kV) was scanned on 53 CT units, at a $CTDI_{vol}$ level of 15 mGy. Images were reconstructed with a nominal thickness of 2.5 mm or 2mm and using only filtered back-projection and assessed using a MO. We used the Channelized Hotelling Observer with dense difference of Gaussian channels. The results were computed by performing Receiver Operating Characteristics analysis and using the area under the curve (AUC) as a figure of merit (FOM).
Results: Our results showed a small disparity depending on the CT units. For the 8 mm target the average of the AUCs were 0.998 ± 0.006 at 20HU, and 0.945 ± 0.027 at 10HU. For the 5 mm target the averaged AUCs were 0.967 ± 0.031, and 0.719 ± 0.071 respectively 20 and 10HU contrast.
Conclusion: Thus, showing the reliability of the CHO model, this investigation opens the way for CT benchmarking, when varying the dose settings or reconstruction strategies.
In the future, a FOM which represents an expected level of low contrast detectability should be issued to ensure that dose reduction does not impair diagnosis.

PO41

Clarity upgrade on Philips Allura FD20 angiography systems: Effects on patient dose and image quality

N. Ryckx[1], M. Sans-Merce[2], F. R. Verdun[1]; [1]Lausanne/CH, [2]Geneva/CH

Purpose: The extensive use of fluoroscopy in interventional radiology/cardiology can lead to high patient skin doses, increasing the risk of deterministic effects such as epilation, skin and subcutaneous tissue damage. To tackle this problem, Philips Healthcare recently commercialized a new system upgrade (Clarity), claiming to reduce patient exposure while maintaining sufficient image quality.
Methods and Materials: Two Allura FD20 flat-panel angiography systems, one of which was updated with Clarity, were assessed, and the collected data was compared for the main clinical protocols: low, medium and high quality fluoroscopy, and abdominal and thigh digital subtraction angiography (DSA). We used 5cm PMMA slabs to simulate patient thickness with values ranging from 5 to 20cm. A 6cc ionization chamber (Radcal, USA) located at 75cm from the focal spot was used to determine patient entrance skin dose. A TOR-CDR phantom (Leeds Test Objects, UK) was used to assess low-contrast detectability (LCD) and spatial resolution.
Results: For the fluoroscopy modes, average dose reductions of 25% (low), 44% (medium) and 35% (high) were measured. The dose per image for DSA runs was reduced by 70% (abdomen) and even 84% (thigh). No significant decrease in image quality was observed for both the LCD and the spatial resolution.
Conclusion: The Clarity upgrade for Philips angiography systems seems to be an efficient way to reduce patient exposure, and thus radiation risks. Further investigation should be made for what concerns the dynamic response, which should be assessed using a high-contrast moving objet. Moreover, further effort should be put into estimating the gain in staff exposure.

PO42

Effect of CT image metallic artifact on accuracy of organ delineation and dose calculations in treatment planning of spinal radiation fields

P. Shokrani[1], M. Alinejad[2], A. Amooheidari[1], M. Atarod[1], A. Pourmoghadas[3]; [1]Isfahan/IR, [2]Rasht/IR, [3]Ottawa/CA

Purpose: In radiation treatment planning, Hounsfield unit (HU) values from CT images are converted to electron density (ρ_e) values for organ delineation and dose calculations. Metallic artifacts may change HU and therefore ρ_e values. The tolerance for change in ρ_e, ($\Delta\rho_e$), to maintain 2% dose calculation accuracy is a function of tissue type, depth and treatment beam type and energy. The aim of this research was to evaluate the effect of metallic artifacts on the accuracy of organ delineation and dose calculations in treatment planning of spinal radiation fields using Monte Carlo calculations.
Methods and Materials: CT images (Siemens, Somatom Sensation 40/64) of a Plexiglas phantom containing a vertebral column with and without Titanium implants were used to calculate artifact related $\Delta\rho_e$ for different tissues. A Siemens Oncor linear accelerator (6MV photon beam) and the Plexiglas phantom were simulated using EGSnrc user codes: BEAMnrc and DOSXYZnrc/CTCREATE. Dose distributions with and without implants were calculated using the Plexiglas phantom CT images.
Results: For different tissues and depths, $\Delta\rho_e$ tolerance resulting in a planning dose error of 2% was determined. Backscattered electrons from metal increased $\Delta\rho_e$ tolerance at tissue metal interface. Maximum error in calculated dose due to artifact was 17%. The requirements for organ delineation accuracy were not affected by metallic artifact.
Conclusion: Metallic artifact did not affect organ delineation accuracy, due to high subject contrast of vertebral column. However, significant reduction in calculated dose due to artifact showed that application of artifact reduction algorithms is necessary when imaging patients with spinal implants for treatment planning purposes.

PO43

Hip pain: Imaging pearls of the hip and pelvis – A systematic approach

T. Fischer, T. Bühler, R. A. Kubik-Huch, S. Anderson; Baden/CH

Learning Objectives: 1. Improved understanding of pelvic pathologies and typical differential diagnoses.
2. Systematic approach to MRI imaging with radiological check list.
3. Correlating imaging findings with clinical aspects and impact on therapy.

Background: Improved standards of life as well as the general demographic shift in modern societies contribute to the increasing importance of hip and pelvic pain. The overall self-reported prevalence of intermediate or chronic hip pain is approximately 20%[1] and therefore has become a major factor in public health costs. Although in older people most hip pain relates to osteoarthritis, a thorough imaging analysis is critical to ensure accurate diagnosis and therapy.

Imaging Findings or Procedure Details: We will demonstrate the educational anatomical check list chart for a systematic approach to imaging of hip and pelvis. Furthermore multimodality imaging with an emphasis on MRI will depict specific pathologies. Surgical insights will be given.

Concrete clinical case examples will demonstrate the use of the check list and show the benefit for clinical colleagues in regard to the diagnostic and therapeutic impact.

Conclusion: For optimal patient care, a systematic approach to imaging as well as evaluation of the clinically relevant features is essential. This educational poster is intended to help colleagues with an approach to hip and pelvic problems and interpret their findings in an interdisciplinary setting.

1Dawson J, Linsell L, Zondervan K, Rose P, Randall T, Carr A, Fitzpatrick R. Epidemiology of hip and knee pain and its impact on overall health status in older adults. Rheumatology (Oxford). 2004 Apr 43(4):497-504.

PO44

Spinal disorders mimicking infection

S. Boudabbous, A. Neroladaki, M. Sahin, A. M. Korchi, C. D. Becker, M.-I. Vargas; Geneva/CH

Learning Objectives: The aim of this study is to illustrate spinal diseases mimicking an infection and to define characteristic MR imaging features allowing distinction of these different disco-vertebral disorders.

Background: Typical findings like endplate bone marrow hypo intensity on T1, disk signal abscess on T2 associated with enhancement after contrast injection in magnetic resonance imaging (MRI) are highly suggestive of spinal infection. However several spinal disorders may mimic infection mainly when underlying spinal disease is present. Furthermore, atypical patterns of spinal infection are frequent and difficult to rule out. Thus establishment of the diagnosis of spondylodiscitis necessitate mostly vertebral biopsy to avoid an inappropriate treatment.

Imaging Findings or Procedure Details: We realized a retrospective study using a keyword search (MRI, spondylodiscitis) in our institutional database of all patients from 2004 to 2014(1441MRI/836patients)undergoing spinal imaging with the identified endplate and disk abnormalities described in the definitive report. The results of MRI were analyzed and evaluated in confrontation with clinical and radiological follow up and/ or biopsies when performed.

Several diseases are mistaken for spinal infection and include, Modic I endoplate change, cristallin-induced discopathy (chondrocalcinosis and gout), neuropathic arthropathy of the spine, acute Schmorl nodes, pseudoarthrosis associated with ankylosing conditions such as ankylosing spondylitis and three-column fractures on degenerative spine.

The most relevant pathologies are illustrated in this work.

Conclusion: MRI features of disco-vertebral disorders must be crossed with clinical context, laboratory data and another complementary modalities such CT to avoid unnecessary procedures and treatment. MRI is very helpful in early stage but lack of specify and must be carefully interpreted.

PO45

Imaging features of Hoffa's fat pad various pathologic entities

I. Bagetakos, A. Neroladaki, A. M. Korchi, M. Sahin, C. Becker, S. Boudabbous; Geneva/CH

Learning Objectives: The infrapatellar Hoffa's fat pad (IFP) is an intracapsular extrasynovial structure that is routinely visualized on magnetic resonance images (MRI) of the knee.

This area is affected by several diseases that are categorized as intrinsic, like Hoffa disease, and extrinsic, mainly due to articular disorders.

Features of these pathologies are various on MRI and the imaging approach is simplified when one is familiar with regional anatomy and possible differential diagnostic considerations.

Background: Retrospective study of MRI and clinical data of 137 patients old from 18 to 82 years old, with IFP reference in a radiological report of our institution during the past 10 years were listed.

Characteristic features on MRI of different pathologic processes were analyzed, classified and pathologic entities were individualized.

Imaging Findings or Procedure Details: Our study showed that 55 patients (40%) were found having a pathologic process of the IFP. Intrinsic IFP pathology present with burning or aching infrapatellar anterior knee pain that can often be reproduced on physical exam.

History of surgery and pattern of fibrotic process on MRI emphasizes fibrosis.

Involvement of IFP from articular disorders including intraarticular nodular fasciitis, arthrosynovial, meniscal and mucoid cysts and localized anterior arthrofibrosis (Cyclops lesion) is well recognized as extrinsic IFP disorders.

Other important pathological entities are well assessed with MRI and include pigmented villonodular synovitis, synovial chondromatosis, extraosseous knee hemangioma, PPP syndrome, patellofemoral friction syndrome.

Histological confirmation was necessary in some cases to confirm these entities.

Conclusion: This article includes a comprehensive educational review of the characteristic MR features of common and uncommon IFP disorders.

PO46

Primary vertebral bone leïomyosarcoma

M. El Issa, A. Soufiane, M. Darouichi; Neuchâtel/CH

Introduction: We report a rare case of primary vertebral bone leïomyosarcoma (PVBL), investigated by CT and MRI. A 80-year-old woman with atrial fibrillation, aortic insufficiency, total right knee replacement, hysterectomy for myoma, partial thyroidectomy presents for low back pain, without triggering factor, appeared 2 month ago and exacerbated when lying down. She mentions paraesthesia in the arms, mainly when she flexes the neck. Neurological examination showed sharp and symmetrical tendon reflexes, no pain during palpation and percussion next to the dorsal and lumbar spine. No lack of sensibility or motricity. Laboratory tests are normal, in particular no inflammation. Mammography, gastroscopy, colonoscopy are normal. Dorsal spine radiographies, total body CT and dorsolumbar MRI are realised.

Imaging: The radiographies show osteolysis of the vertebral body with fuzzy boundaries, and cortical rupture, rare bone sclerosis and calcification. CT shows a destructed vertebral body with invasion of the paravertebral soft tissue by a homogeneous, but ill-defined tissue density. It heterogeneously enhances because of fibrosis. MRI better defined meningeal and medullary infiltration, vascular structures and soft tissues. Signal tumor: iso intense in T1, hyper intense in T2 and heterogeneous enhancement after intravenous Gadolinium injection. Hypo intense signal in T1 and T2 with fibrous tissue. *Differential Diagnosis:* bone metastasis of uterine or gastro intestinal tumors, retroperitoneal leïomyosarcoma, primary bone lymphoma, chondrosarcoma, plasmacytoma, metastasis, and osteogenic osteolytic sarcoma. *Histology:* same to soft tissue leïomyosarcoma. *Immunohistochemistry* is essential for the diagnosis.

Discussion: PVBL is a rare highly malignant mesenchymal tumor, which represent 0.6% of leïomyosarcoma of soft tissues and developed from the smooth muscles cells of the media of bone vessels. It affects older subjects without sex predominance. Predilections are the epiphysis of long bones, especially distal femur and proximal tibia. Spine location is exceptional. First reported in 1944 by Carmody. Since then, a hundred cases have been described. Leïomyosarcoma appellation by OMS in 1993 and 4 histological types are recognized: fusiform,epithelioid, myxoid and pleomorphic. Clinical diagnosis is difficult and late, because of nonspecific semiology. Vertebral pain of varying intensity is the principal symptom. Medullar or radicular symptoms, or pathological fracture may occur. PVBL may be triggered by Paget's disease or prior chemoradiation.

Conclusion: PVBL is a rare, highly aggressive malignant mesenchymal tumor with bad prognostic and difficult diagnosis.

Anatomopathology and immunohistochemistry are essential for the diagnosis. The best treatment is surgery with chemoradiation.

PO47

MR imaging in patients after supraspinatus tendon repair with good clinical outcomes: morphology and signal alterations of the supraspinatus tendon

C. Agten, F. M. Buck, C. W. A. Pfirrmann; Zurich/CH

Purpose: To describe morphology and signal changes in MR imaging in the supraspinatus tendon after surgical tendon repair during a 2-year period in patients with good clinical outcomes.

Methods and Materials: Thirty-three patients (24 men, mean age 59±7 years, 22 right shoulders) with good clinical outcomes (relative Constant-Score >90%) 2 years after surgical repair of a full-thickness supraspinatus tendon tear were prospectively included. MR-arthrography was performed 3 months (n=25), 1 year (n=28) and 2 years (n=27) post-operatively. Morphology of the supraspinatus tendon was assessed by 2 readers as normal, thinning, thickening, or defect – signal intensity as normal, increased, fluid-like, or defect on fluid-sensitive sequences. Descriptive statistics were used.

Results: 5-6/25-28 patients had morphologically normal tendons at all times, 1-3/25-28 tendons were thickened, 12-13/25-28 tendons showed thinning, and 7-8/25-28 tendons were defect. Three months postoperatively no supraspinatus tendon showed normal signal intensity on fluid-sensitive sequences. There was an increase in normal tendon signal intensity after 1 year (2/28 and 6/28 for reader 1 and 2, respectively) and after 2 years (8/27 and 17/27). Tendon defects 3 months and 1 year postoperatively were found in 7/25-28 patients (both readers) and 2 more for reader 1 after 2 years. On fluid-sensitive sequences the proportion of fluid-like/increased signal intensity tendons decreased from 3 months to 2 years from 18/25 to 10/27 for reader 1 (18/25 to 2/27 for reader 2).<

Conclusion: Postoperatively increased tendon signal intensity decreased over time towards normal signal intensity, while no relevant change to the tendon morphology was found.

PO48

Lipoma arborescens

J. Hirsch, L. Alamo, F. Gudinchet, P. Omoumi, I. Letovanec, F. Becce; Lausanne/CH

Learning Objectives: To review the imaging findings, differential diagnosis, and treatment of post-operative follow-up of lipoma arborescens.
Background: Lipoma arborescens in children and young adults is a rare condition affecting synovial linings of the joints and bursae and characterised by villous or polypoid proliferation of the synovial membrane. The knee is the most commonly involved joint, but any joint or bursa may be involved. Patients usually present with chronic pain and swelling, without trauma. It has been hypothesised to be a nonspecific reactive synovial fatty proliferation in response to chronic traumatic or inflammatory stimuli.
Imaging Findings or Procedure Details: A retrospective review in our Hospital revealed 3 patients under 20 years with 5 articulations presenting Lipoma arborescens. MRI is the imaging examination of reference for the diagnosis of lipoma arborescens with conventional sequences (T1-w, T2/PD-w w/wo FS, FS T1-w + contrast) and an additional gradient-echo sequence to rule-out the presence of haemosiderin, which is essential to distinguish it from pigmented villonodular synovitis. Typically, you see a hyperintense fatty infiltration of the synovia on T1-w, and enhancement of the synovial membrane after contrast injection. Articular effusion and synovitis are often observed after contrast injection. The main differential diagnosis include primary synovial (osteo)chondromatosis and synovial haemangioma.
Conclusion: Typical imaging findings at MRI allow the correct identification of lipoma aborescens. Although rare in children and adolescents, lipoma arborescens should be included in the differential diagnosis of patients with chronic nontraumatic swelling of joints, particularly at the knee.

PO49

Hydro-hematocolpos and Hydro-hematometra in pediatric age

V. Ilic[1], C. Lutchmaya-Flick[1], F. Guidinchet[1], S. Hanquinet[2], R. A. Meuli[1], L. Alamo[1]; [1]Lausanne/CH, [2]Geneva/CH

Learning Objectives: The goal of this study is to describe the imaging findings of hydro-hematocolpos and hydro-hematometra in pediatric age.
Background: Hydrohematocolpos / hydrohematometra are rarely observed in children. In most cases, they are related to vaginal obstructions secondary to anomalous embryologic development or acquired pathologies. It is usually diagnosed in neonates or at puberty. In prenatal life, the dilated uterus and/or vagin may compress the adjacent organs, causing hydronephrosis and/or oligohydramnios. At puberty, retention of menstrual blood produces cyclic pain and may cause-pyohematocolpos, pyosalpinx and pelviperitonitis and even long term complications, as endometriosis, pelvic adhesions and decreased fertility.
In neonates, the most often diagnosis are imperforate hymen and cloacae. Unilateral renal agenesis may be associated with congenital genital anomalies. In adolescents, the main pathologies are primary or secondary vaginal obstructions. US is usually the first imaging method performed in these patients, but MRI is increasingly used and allows a complete evaluation of the uro-genital system.
Imaging Findings or Procedure Details: A retrospective review of all the cases of hydro-hematocolpos and hydro-hematometra detected in our Hospital in the last 7 years identified 8 patients with this pathology <15 y.o., 4 of them detected in utero. All patients had abdominal and pelvic US. Additional MRI was performed in 7 cases. The final diagnosis included 4 patients with imperforate hymen; 2 cloacal anomalies; 1 case of Herlyn-Werner-Wunderlich syndrome; and 1 secondary to genital mutilation.
Conclusion: US is the main imaging method for diagnosis of hydro-hematocolpos. MRI is a suitable technique for a complete, non-invasive evaluation of the female pelvic anatomy.

PO50

Imaging of torticollis in children

N. Stahr, I. Scheer, C. J. Kellenberger; Zurich/CH

Learning Objectives: To become familiar with clinical setting, imaging findings and differential diagnosis of Torticollis in children.
To propose an imaging work-up dependant on patient age and clinical setting.
Background: Torticollis is a sign of an underlying congenital or acquired disease process. It can be caused by a malformation in infants but becomes a non-specific sign in older children with a wide differential diagnosis. For imaging evaluation of torticollis the patient's age and associated clinical signs must be taken into consideration.
Imaging Findings or Procedure Details: Differential diagnosis and typical imaging findings of pathologies leading to torticollis will be discussed and illustrated. The use of ultrasound, radiographs, computed tomography and magnetic resonance imaging will be discussed according to clinical signs and patient age.
Conclusion: Radiologists should be familiar with the role of each imaging modality in children with torticollis of various ages and clinical history.

PO51

Inflammatory myofibroblastic tumors as mimickers of malignancy: Are imaging features helpful?

A. A. Youssef, T. Raafat, A. Refaat, M. El-Wakeel, I. Zaki; Cairo/EG

Purpose: Inflammatory myofibroblastic tumor (IMT) is a rare neoplasm of ...

PO52

Evaluation of CT contrast agent contribution in patients dose from PET studies

T. V. M. Lima[1], J. Binder[1], I. Özden[1], K. Strobel[2], S. Matijasevic[2], A. Bopp[1], E. Nitzsche[3], G. Lutters[1]; [1]Aarau/CH, [2]Lucerne/CH, [3]Baden/CH

Purpose: The increased availability of PET-CT devices in addition to the interchange of people and technology between nuclear medicine and radiology explains the increased use of CT techniques like enhanced contrast CT in nuclear medicine. The benefits of the use of contrast agents, especially in terms of the increased accuracy, for enhancing different image modalities are understood and well discussed in the literature. On the other hand, in terms of evaluating the different side effects from the use of these contrast agents only the visible and short-term reactions have been discussed. In respect to studying for a possible increase in dose exposure from the interaction of the radiopharmaceutical radiation with the contrast agent in a contrast enhanced PET-CT study and its effect in the patient radiation exposure is yet to be investigated.
Methods and Materials: This study is aimed to investigate the dose deposition differences with respect to the nuclear medicine isotope radiation interaction with the high density and atomic number of the contrast agent due to increased absorption and scatter of the internal radiation in the patients' tissue. This has been performed with the use of Monte Carlo simulations of 10 patient studies where contrast agent had been used.
Results: Preliminary results show an increase in the dose deposition in the regions enhanced by contrast and its surroundings.
Conclusion: Further quantification of this increased dose deposition in different organs at risk and its estimated effect will be presented.

PO53

Detection rate of underlying malignancy in patients with paraneoplastic syndrome by F18-FDG-PET or PET/CT: A meta-analysis

G. Treglia, B. Muoio, G. Paone, T. Ruberto, M. Raditchkova, L. Ceriani, L. Giovanella; Bellinzona/CH

Purpose: Paraneoplastic syndromes (PNS) are rare manifestations of malignancy unrelated to direct effects of the cancer itself. PNS are associated with significant morbidity influencing patient survival. Because PNS precede direct symptoms of cancer by months to years, timely imaging in PNS may early detect underlying malignancy. Several studies evaluated the detection rate of underlying malignancy in PNS by F18-FDG-PET(/CT). We performed a meta-analysis to assess the diagnostic value of F18-FDG-PET(/CT) in this setting.
Methods and Materials: A literature search of studies published until 11/2014 on F18-FDG-PET(/CT) in PNS was performed. Pooled abnormality rate (AR) and detection rate (DR) of underlying malignancy in suspected PNS were calculated including 95% confidence intervals (95%CI). Pooled sensitivity and positive predictive value (PPV) of F18-FDG-PET(/CT) in diagnosing underlying malignancy in PNS were also assessed. Subgroup analyses based on the device used (PET versus PET/CT) and comparison between F18-FDG-PET and CT findings were carried out.
Results: Thirteen records were selected for the meta-analysis. Pooled AR and DR of underlying malignancy by F18-FDG-PET(/CT) in patients with suspected PNS were 34% (95%CI:25-44%) and 20% (95%CI:13-28%), respectively. Pooled sensitivity and PPV in diagnosing underlying malignancy in PNS were 86% (95%CI:78-92%) and 58% (95%CI:46-69%), respectively. No statistically significant difference between PET/CT and PET findings were found. A trend towards a higher sensitivity and DR of underlying malignancy in PNS was found by using F18-FDG-PET instead of CT.
Conclusion: Due to its high sensitivity, F18-FDG-PET(/CT) may be a very useful tool for detecting underlying malignancy in patients with PNS regardless of the presence of well-characterized paraneoplastic antibodies.

PO54

10 year experience with dual-isotope 99mTc-tetrofosmin and 123I sodium iodide SPECT in hyperparathyroidism

M. Sommerauer, C. Graf, N. Schäfer, G. Huber, P. Schneider, R. Wüthrich, C. Schmid, H. Steinert; Zurich/CH

Purpose: We report about our long-term institutional experience with parathyroid imaging of dual-isotope ^{99m}Tc-tetrofosmin and ^{123}I sodium iodide single-photon-emission-computed-tomography (SPECT) for preoperative detection of hyperactive glands in patients with hyperparathyroidism, and estimated the impact on the surgical procedures and disease outcomes.
Methods and Materials: Dual-isotope SPECT was performed in 70 consecutively patients with primary hyperparathyroidism and in 20 patients with tertiary hyperparathyroidism. Imaging findings were correlated with surgical results. Concomitant thyroid disease, pre- and postoperative laboratory measurements, histopathological results, type and duration of surgery were assessed.
Results: In primary hyperparathyroidism, SPECT had a sensitivity of 80% and a positive predictive value of 93% in patient-based analysis. Specificity was 99% in lesion-based analysis. Patients with positive SPECT elicit higher levels of parathyroid hormone and higher weight of resected parathyroids than SPECT-negative patients. Duration of parathyroid surgery was on average, approximately 40 minutes shorter in SPECT-positive than in SPECT-negative patients (89±46 vs. 129±41 minutes, p=0.006); 86% of SPECT-positive and 50% of SPECT-negative patients had minimal invasive surgery (p=0.021). SPECT had lower sensitivity (60%) in patients with tertiary hyperparathyroidism; however, 90% of these patients had multiple lesions and all of these patients had bilateral lesions.
Conclusion: Dual-isotope SPECT with ^{99m}Tc-tetrofosmin and ^{123}I sodium iodide has a high diagnostic value in patients with primary hyperparathyroidism and allows for saving of operation time. Higher levels of parathyroid hormone and higher glandular weight facilitated detection of parathyroid lesion.

PO55

Renal function measurement in children with transplanted kidney: Value of the accumulation index (AI) measured during dynamic renography (RG)

L. Haefliger, G. Allenbach, H. Chehade, J.-P. Venetz, A. Boubaker; Lausanne/CH

Purpose: To evaluate function of the transplanted kidney measured during RG in children.
Methods and Materials: First RG performed in children with transplanted kidney were reviewed. A 20-min 2-phase dynamic acquisition was started immediately after injection of 0.5 MBq/kg of ^{123}I-hippuran or Tc.99m-MAG3. Absolute single kidney function was measured by an accumulation index (AI) defined as the percent of injected activity (%ID) extracted 30-90 sec after heart-peak activity. Normal AI of a single kidney unit is 11±2 %.
Results: 21 children (10 F, 11 M) aged 2.3-16.4 years (10.0±4.7y) at transplantation had a first RG (17 I-123-hippuran, 4 Tc-99m-MAG3) performed 1day to 3 years (0.4±0.8y) after graft (control (n=15), suspected complication (n=6)). 9 children received a live donor, 12 cadaveric kidney.
AI ranged from 5.3 to 28.0 (13.7±7.0), inferior to normal in 7, normal in 3 and superior to normal in 11 children.AI was lower in children examined for possible complications (9.2±5.8) when compared to baseline control (15.4±6.8) (p=0.05). No difference of AI was noted between hippuran (14.3±7.2) and MAG3 (10.8±6.0 ; p=0.36), nor in cadaveric transplant (13.1±8.5) when compared to live donors (14.4±4.8) (p=0.32). AI in children transplanted before the age of 10 was higher (16.7±6.0) than in older (8.9±4.1; p<0.005).
Conclusion: Initial renal graft function measured with AI was superior to normal upper limit in about half of the children. We found no difference related to radiopharmaceutical and donor (cadaveric or live). Age at transplantation impacted on AI being significantly higher in younger children.

PO56

Meniscal extrusion and meniscal lesions correlate with increased bone tracer uptake in SPECT/CT

A. Hirschmann[1], J. Rechsteiner[2], M. Dordevic[2], A. L. Falkowski[2], M. T. Hirschmann[2]; [1]Basel/CH, [2]Bruderholz/CH

Purpose: To precisely quantify the subchondral bone tracer uptake (BTU) in SPECT/CT of knees with different grades of meniscal lesions.

Methods and Materials: Thirty-four patients (mean age 45.5±11.5 years) with MRI and SPECT/CT were prospectively collected and retrospectively included. Patients with grades 3 and 4 cartilage lesions were excluded. For analysis and comparison of MRI and SPECT/CT a specific localisation scheme was used. Maximum values of each subchondral femorotibial area were quantified and a ratio was calculated in relation to a reference region in the femoral shaft, which represented the BTU background activity. Meniscal lesions were graded (intact/degeneration/tear) using MRI by two musculoskeletal radiologists blinded to the SPECT/CT findings. Extrusion of the meniscus was assessed. To determine a significant difference in BTU between the extruded and non-extruded meniscus an independent t-test was used; for the comparison of meniscal lesions ANOVA ($p<0.05$).

Results: Meniscal degeneration showed a significantly higher mean relative BTU compared to an intact meniscus on the femoral side ($p=0.018$; tibial side $p=0.072$). Meniscal tear showed significantly higher mean relative BTU compared to an intact meniscus ($p<0.01$ femoral and tibial side) as well to degeneration ($p=0.006$, respectively). Meniscal extrusion showed significantly higher mean relative BTU compared to non-extruded meniscus ($p<0.02$).

Conclusion: Subchondral BTU in SPECT/CT of the knee was significantly higher with meniscal degeneration or tear as well as meniscal extrusion. SPECT/CT is able to identify patients with an increased risk for development of osteoarthritis.

PO57

Ultrasound guided ventriculoperitoneal/ventriculoatrial shunt injection

S. Iqbal, M. Iqbal, A. Zuberi, A. Joshi, K. Ali, N. Dobbs; Wichita/US

Learning Objectives: We describe a new technique for performing ...

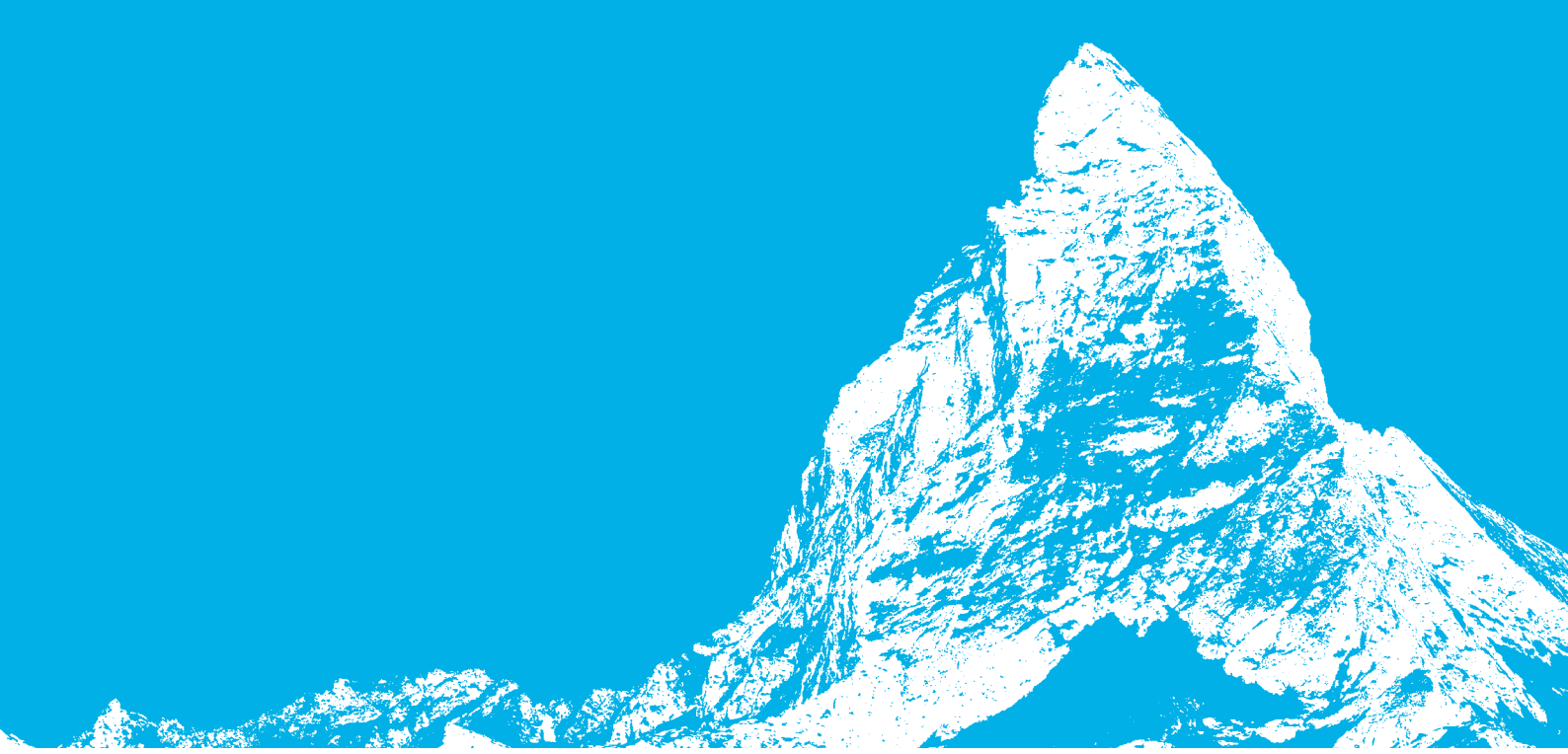

SCR'16 SWISS CONGRESS OF RADIOLOGY

MAY 26–28, 2016 | BERN

SCHWEIZERISCHER RADIOLOGIEKONGRESS
CONGRÈS SUISSE DE RADIOLOGIE

SAVE THE DATE!

SGR SSR
Schweizerische Gesellschaft für Radiologie
Société Suisse de Radiologie
Swiss Society of Radiology

SGNM

SSVIR

SSER

SSSR

www.radiologiekongress.ch